Assessment of Adaptive Radiotherapy Workflows for Head and Neck Cancer

George Antoniou

School of Physical Sciences

March 2022

The University of Adelaide

THE UNIVERSITY of ADELAIDE

Principal Supervisor: A/Prof. Scott Penfold

Co-Supervisor: Dr. Michael Douglass

Table of Contents

Abstract

Inter-fractional anatomical variations of head and neck (H&N) cancer patients can lead to clinically significant dosimetric changes. Adaptive re-planning should thus commence to negate any potential over-dosage to organs-at-risk (OAR), as well as potential under-dosage to target lesions. On-treatment transit dosimetry with an electronic portal imaging device (EPID) may be a useful means of establishing when adaptive re-planning is required for head and neck cancer patients. The aim of this thesis is to a) develop an in-house script to predict transit EPIs with a Varian linear accelerator and the RayStation treatment planning system, and b) apply the script in a treatment simulation environment to explore the correlation between relative change in EPID measured transit dose and relative change in dose volume histogram (DVH) metrics to target and OAR structures over the course of treatment.

The in-house developed script was capable of predicting measured EPIs dose in the setting of pre-treatment quality assurance (i.e. with no patient present), however requires further work to better approximate absolute transit dosimetry.

The transit dosimetry simulation tool was successfully developed and retrospectively applied to 8 head and neck cancer patient data sets. A strong correlation between change in transit fluence and planning target volume (PTV) D98 and a weak correlation with spinal cord D0.03cc was found. A weighted projection mask was developed for PTV and spinal cord structures by considering the intra-angle overlap between fluence and structure contours projected onto the EPID. The sensitivity of the correlation between change in transit fluence with PTV D98 and spinal cord D0.03cc was found to increase by 113% and 196% respectively, with the weighting mask applied. Overall, the simulation toolkit developed in this work provides a useful means to investigate the relationship between change in transit fluence and change in key dosimetric parameters for head and neck cancer patients.

Included Publications

G. Antoniou, and S.N. Penfold, "A novel TPS toolkit to assess correlation between transit fluence dosimetry and DVH metrics for adaptive head and neck radiotherapy", *Physical and Engineering Sciences in Medicine*, vol. 44, pp. 1121 – 1130.

Declaration

I certify that this work contains no material which has been accepted for the award of any other degree or diploma in my name, in any university or other tertiary institution and, to the best of my knowledge and belief, contains no material previously published or written by another person, except where due reference has been made in the text.

In addition, I certify that no part of this work will, in the future, be used in a submission in my name, for any other degree or diploma in any university or other tertiary institution without the prior approval of the University of Adelaide and where applicable, any partner institution responsible for the joint award of this degree.

The author acknowledges that copyright of published works contained within the thesis resides with the copyright holder(s) of those works. I give permission for the digital version of my thesis to be made available on the web, via the University's digital research repository, the Library Search and also through web search engines, unless permission has been granted by the University to restrict access for a period of time.

I acknowledge the support I have received for my research through the provision of an Australian Government Research Training Program Scholarship.

George Antoniou

08/03/2022

Acknowledgements

Firstly, to my principal supervisor Associate Professor Scott Penfold, thank you for your un-rivalled level of support, knowledge, encouragement, and patience over the years. Your supervision and guidance have not only helped me become a better researcher but has also strongly developed my skills as a medical physicist. I wouldn't be the physicist or researcher that I am today without you.

To my co-supervisor, Dr. Michael Douglass, thank you for your assistance throughout the course of my research and for being so humble whilst doing so. It has been a privilege to have you both supervise me, and I look forward to working together again in the future.

Thank you to 'boss man' Kevin Hickson, for your support and patience throughout my final year of research whilst concurrently beginning my journey as a diagnostic imaging medical physics registrar. The mental health support you have provided me, ensuring I maintain a healthy work-life balance, has been immensely helpful.

Special thanks to my DIMP TEAP supervisor Dr. Yuri Matyagin, Chris Boyd, and the rest of the Medical Physics & Radiation Safety group at SA Medical Imaging for your guidance, patience, and encouragement throughout this period too.

To my parents, John and Vicki, you have both done everything you can to give me and my sister Daniele everything in life. I truly owe all of my accomplishments to you both and will be forever grateful. To my sister Dan, thank you for always listening to (and pretending to care about) what I learnt throughout my degree, and for being such a strong role model and paving the way for me.

Finally, to my fiancé Sandra, thank you for being so encouraging, motivating, loving, supportive and calming. You have given me never-ending support without hesitation and have helped me enormously throughout my degree.

1. Introduction

From 1982 to 2017, the number of Australians diagnosed with cancer has increased from 383 to 470 cases per 100,000 people [1]. This increase in diagnosis can be partially attributed to an ageing population, as well as more advanced technologies and screenings in being able to identify the presence of such cancers. The mortality rate of Australians with cancer, however, has decreased from 209 to 161 cases per 100,000 people in the same time frame [1]. Thus, cancer research over the past 40 years can be deemed effective, where future research and improvements to treatments should continue to further benefit the increasing number of people diagnosed. Currently, there are three main methods of treatment available for cancer patients in Australia, being chemotherapy; surgery; and radiation therapy.

One major advancement in radiotherapy treatment delivery was the development of volumetric modulated arc therapy (VMAT), enabling more optimised treatment plans to deliver a suitable dose to the target, whilst keeping doses to organs at risk (OARs) as low as reasonably achievable. Radiotherapy treatment plans have developed from being generic with minimal patient-to-patient variation, to fully personalised treatment plans which vary in complexity depending on the type, location, stage, and size of the diagnosed tumour. The increased complexity and conformity of modern radiotherapy treatment plans makes it essential to monitor for dosimetric changes over the course of treatment, arising most commonly from a change in patient anatomy. Altering the treatment plan during the treatment course to maintain desirable dosimetry is known as adaptive radiotherapy.

Adaptive radiotherapy is however both time and resource intensive, noticeably increasing the workload of the clinical team. The implementation of an adaptive radiotherapy workflow should thus be optimised to balance the clinical benefit with this additional workload. An automated, quantitative trigger for determining when plan adaptation is required would thus reduce the clinical workload of the team significantly. Several commercial transit dosimetry verification tools have been developed for this purpose.

Commercial transit dosimetry verification software solutions, such as PerFRACTION™ by Sun Nuclear Corporation, aim to verify delivery of complex radiotherapy treatment plans both pre-treatment (fraction 0) and during the treatment schedule (fraction n). This allows the clinical team to assess if

dosimetric changes are occurring over the treatment course, helping to decide if plan adaptation is required. The sensitivity and specificity of commercial transit dosimetry solutions to changes in dose-volume treatment plan metrics, upon which clinical assessment is based, must first be well characterised.

The research presented in this thesis had two objectives. Firstly, to develop an in-house script for generating predicted transit EPIs of VMAT treatment plans for H&N cancer patients, and secondly, to use this script to investigate the correlation between change in transit fluence and change in dose-volume metrics inside the patient. Chapter 2 of this thesis presents a general background on the topic of radiotherapy delivery for H&N cancer patients, highlighting the need for adaptive radiotherapy and how this can be achieved through the use of an EPID. Chapter 3 presents a literature review on the different approaches to treatment verification using transit dosimetry for VMAT treatment plans. Chapter 4 explores an *absolute* transit dosimetry approach to treatment verification of H&N VMAT plans, and Chapter 5 explores the correlation between *change* in transit fluence and *change* in dosimetric quantities. Finally, conclusions and future work are summarised in Chapter 6.

2. Background

2.1. Radiation Therapy

Since the discovery of x-rays in 1895, the use of ionising radiation for therapeutic and diagnostic applications has widely been applied. X-rays, neutrons, electrons, gamma rays, protons, and heavy ions have all been utilised to form effective therapeutics against cancerous cells. The main aim of radiation therapy is to maximise radiation dosage to target lesions whilst minimising dose to healthy tissue and organs, in other words maximising the therapeutic ratio. Palmer et al. [2] exemplifies the advancements in technology regarding the delivery of the radiation dose to lung cancer and head & neck (H&N) cancer patients, comparing x-ray dose distributions of such patients from the 1980's to a more advanced proton treatment plan in 2017. A 56% and 67% decrease in radiation dose to the lung and heart, respectively, were observed when comparing the treatment plans for lung cancer patients – showcasing the drastic improvements in radiation therapy over the last 40 years. These improvements are attributed to advancements in treatment delivery technologies and treatment planning system (TPS) software, global collaboration in developing guidelines for treatment, and verification of treatment plans through quality control measures.

2.2. Treatment Delivery

Advancements in treatment delivery include the development of more advanced medical linear accelerators (linac's), used to conform external radiation beams to particular shapes for more targeted treatment. Linac's are used in what is known as external beam radiation therapy (EBRT), giving rise to many treatment techniques such as 3-D Conformal Radiotherapy (3DCRT); Intensity Modulated Radiotherapy (IMRT); and Volumetric Modulated Arc Therapy (VMAT) - all utilising x-ray photons and multi-leaf collimators (MLC's).

Complex beam shapes are able to be constructed through the use of beamline components which act to accelerate, bend, shape, and block particular regions of the beam. An outline of photon production from a linac is as follows: Electrons are first accelerated and focussed upon a tungsten target via the use of an accelerating waveguide and bending magnets. Upon interacting with the tungsten target,

electromagnetic radiation is emitted primarily in the form of x-ray photons through a process named bremsstrahlung. The photons produced are then constrained in the forward direction and subsequently flattened out through the use of a primary collimator and flattening filter, providing a uniform field at depth. The photon beam is then further shaped through the use of a secondary collimator, or jaws, which block out any unwanted radiation and thus produce rectangular fields. Finally, the rectangular beam then passes through a series of multi-leaf collimators – which shape the beam to best match the tumour.

2.2.1. 3D-CRT

3-Dimensional conformal radiation therapy makes use of the linac MLC's at different gantry angles to give a conformal radiation dose to the tumour. The arrangement of the MLC's is fixed for a given gantry angle, with the patient being irradiated at a number of different beam angles. This method of treatment delivery is more commonly used for palliative treatments and tangential breast cancer treatments nowadays after having been phased out by the more conformal delivery techniques outlined below.

2.2.2. IMRT

Intensity modulated radiation therapy modulates the intensity of the beam at each gantry angle, in order to provide a more conformal dose to the tumour. Intensity modulation is achieved by attenuating different areas of the beam to a different degree with the MLC's while at a given gantry angle. This attenuation can be performed via segmented MLC delivery (SMLC), in which the MLC's do not move when the beam is on, or dynamic MLC delivery (DMLC), in which the MLC's are constantly moving.

2.2.3. VMAT

The next step in dose delivery complexity is volumetric modulated arc therapy. VMAT combines a continuously rotating gantry with continuously moving MLCs to optimize the radiation fluence to the target, whilst providing minimal dose to healthy tissue. VMAT delivery is typically conducted in only a few minutes – a major advantage over IMRT.

2.3. Treatment Planning

Advancements in treatment planning systems have also contributed to improved treatments. The role of the TPS is to optimise the treatment to maximise the therapeutic ratio, via an inverse optimisation approach in which clinical goals and thresholds are pre-defined and a mathematical procedure is followed to determine the radiation fluence required to achieve these clinical goals [3].

A typical treatment plan for EBRT generally begins with obtaining a radiotherapy computed tomography simulation (CT-Sim) scan of the patient. Previously acquired diagnostic imaging modalities such as Magnetic Resonance Imaging (MRI) or Positron Emission Tomography (PET) can also be used to assist in target volume definition. The clinical team then contour target volumes and organs-at-risk (OAR's), and select beam angles for the treatment. The TPS then optimises the radiation fluence to achieve the patient specific dose constraints. The treatment plan ultimately determines the treatment machine parameters which are utilised at the time of treatment.

2.3.1. Treatment Delivery Quality Assurance

Ongoing patient specific quality assurance (PSQA) is necessary to ensure patients are receiving the approved planned dose. While treatment delivery techniques are constantly evolving, allowing for more conformal dose delivery, they are also increasingly complex. These considerations have led to an increase in PSQA workloads [4]. PSQA can be classified as pre-treatment, in which the ability of the treatment unit to deliver the planned radiation fluence is verified, or on-treatment, in which the delivered dose to the patient on a given fraction is verified. The objective of pre-treatment quality assurance is to identify:

- errors in machine parameter transfer from the treatment planning system to the linac
- errors in linac calibration
- limitations in TPS beam modelling for a particular treatment plan

This can be done through the use of ionisation chambers or radiographic films in measuring dose delivered to a phantom object, measuring dose delivered to a 2D detector array [5], [6], and, for the first dot point above, through the analysis of treatment plan delivery log files [7].

PSQA can also be conducted during a treatment course. This form of PSQA has the potential to identify errors in patient positioning and machine delivery errors, but is perhaps most useful in

monitoring the effect of systematic changes in patient anatomy. Electronic portal imaging devices (EPID) attached to a medical linac have become a popular tool for on-treatment PSQA, due to the ability to obtain dosimetric information [8], [9] in an efficient manner.

2.4. Electronic Portal Imaging Device (EPID)

The electronic portal imaging device (EPID) attached to a medical linac is able to utilise the transmitted high energy photons (MeV) from treatment deliveries to provide information about dose delivered to the patient. The original purpose of the EPID when first integrated with the linac was verifying a patient's position before treatment commences. More recently, EPIDs have been utilized for pre-treatment dose delivery verification and on-treatment transit dosimetry monitoring. EPIDs are typically amorphous silicon detectors, which convert the incident radiation into visible light via a gadolinium oxide scintillation layer followed by subsequent detection of the light by the amorphous silicon photodiodes, as shown in **Fig. *1***. In this work, the sensitive area of the photodiode array, which gives rise to the pixel array, is a 40.0 x 40.0 cm grid with a pixel size of 0.336 mm. The EPID is positioned at a specified source-to-detector distance (SDD) via a mechanical arm, which is mounted under the EPID and onto the linac. When acquiring images from the EPID, it is important to consider any processing done by the EPID software prior to the image export, as well as any imaging artefacts present.

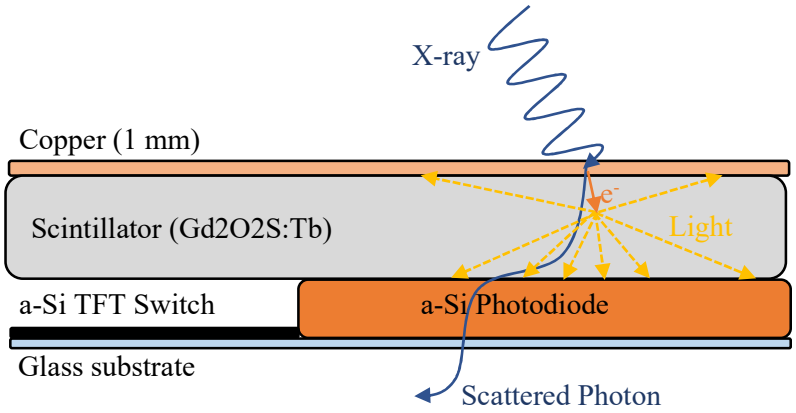

Fig. 1 Generic sketch of indirect-type digital detector, analogous to an aS1200 EPID.

Image processing done by the EPID software prior to image export involves a dark field correction, pixel sensitivity correction, and, when operated in the portal dosimetry mode, a beam profile correction [10]. The dark field correction is applied through obtaining an electronic portal image (EPI) with no linac output. This represents the background electronic noise present in the EPID hardware and

is subtracted from acquired EPIs. A pixel sensitivity correction, also known as a flood field correction, is derived in order to account for individual pixel sensitivities [11]. The pixel sensitivity correction is applied via dividing the acquired image on a pixel-by-pixel basis by a reference 40x40 cm field – which encompasses the entire pixel-array of the EPID. If the EPID is being used in portal dosimetry mode, a beam profile correction, or horn correction, is then necessary in order to reintroduce the shape of the beam that was removed by the normalization of the flood field correction. The resulting EPI can be exported in Digital Imaging and Communications in Medicine (DICOM) format for further analysis.

Additional processing to the EPIs obtained can be conducted in order to further diminish any artefacts present in the dataset. Two common sources of artefacts include any backscatter from the EPID positioning arm and pixel ghosting as a result of any memory effects [12]. The Varian aS1200 EPID used in this work accounts for the arm backscatter through additional shielding material attached to the underside of the panel [13], where backscatter can be deemed to be negligible (<0.5%) and independent of field size [14].

2.5. Adaptive Radiotherapy

Anatomical variations in H&N cancer patients can lead to clinically significant plan deterioration and adaptive radiotherapy (ART) may be required to restore the desired dose distribution [15]. Past literature has explored the benefits of implementing ART workflows within a clinic for H&N cancer and has mostly been focused on improving dosimetry in parotid glands, which is crucial when lowering risk of xerostomia [15-16]. Monitoring the dose delivered to the spinal cord, via evaluation of kV cone-beam computed tomography (CBCT), has also shown to be beneficial in answering the golden question: *when* should we replan? [17]

Traditional methods to implement ART into the clinic are associated with a significant increase in the clinical workload to the radiotherapy department as a whole. As a result, there has been a recent push to develop an accessible and automated quantitative trigger for ART, with one common method being transit dosimetry with an EPID [18]. This can be done through considering gradual changes in the transit dosimetry EPI relative to the first fraction/session, or by considering absolute changes between the transit dosimetry EPI obtained during the treatment versus that predicted.

Using absolute transit dosimetry, one can calculate the expected EPI resulting from each treatment fraction and compare it to that clinically obtained. Changes in patient anatomy could result in gradual deviation from the predicted EPI, where large abrupt changes between the predicted and measured EPIs could be a result of a positional error. Difficulties arise, however, in attempting to accurately calculate the predicted EPI, where a large number of corrections must be applied as previously discussed. Similarly, using relative EPID transit dosimetry, one can explore the gradual change in transit fluence over the course of treatment without necessarily needing to rely on the absolute precision and accuracy of the images themselves.

Assuming linac output remains relatively constant over the course of treatment, change in measured transit fluence is theoretically correlated with anatomical variations and patient setup errors. While a change in transit dosimetry indicates that something has changed, it is typically ambiguous as to how this change translates to dose-volume metrics inside the patient. Several groups have attempted to correlate dosimetric impacts with change in transit fluence, where 2D relative gamma analysis is commonly utilised [19]–[22]. Through conducting gamma analysis on the transit EPIs acquired over the course of treatment, a variety of parameters can be extracted to help quantify change in dose to the patient.

3. Literature Review

Quality assurance is a major aspect of modern-day radiation therapy, where the use of EPID dosimetry has been explored over the past 20 years. Verification processes are typically classified as either being 'pre-treatment verifications', without the patient in the beam, or 'on-treatment verifications', with the patient in the beam. Transit dosimetry involves the verification of dose within a patient by measurement of the radiation field after passing through the patient. Transit dosimetry has been applied to VMAT treatment deliveries via back- and forward-projection techniques as shown in Fig. 2. The following literature review is specific to the topic of transit dosimetry for H&N cancer treatment deliveries utilising the VMAT technique.

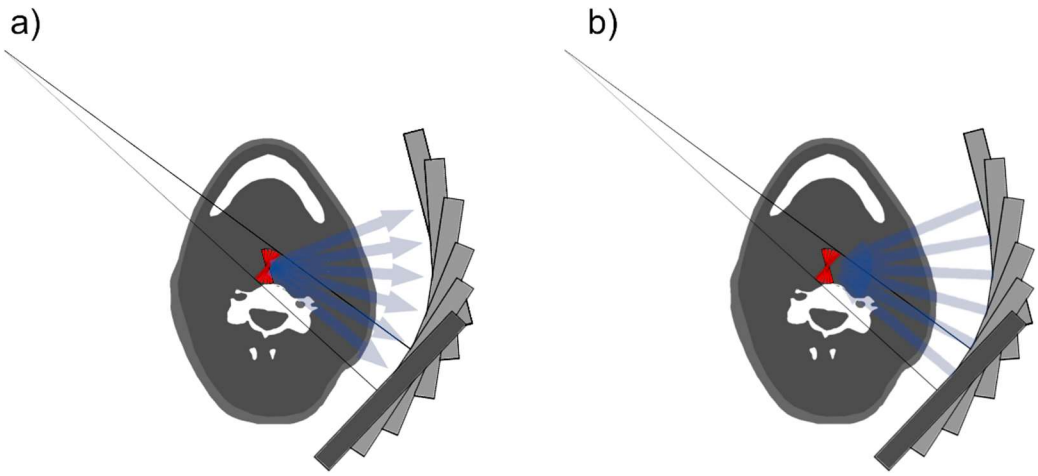

Fig. 2 Schematic of transit dosimetry using a) forward- and b) back-projection techniques.

3.1. Reconstruction of Internal Doses (Back-projection)

Back-projecting the integrated signal at the EPID into the patient, at each angle, allows for the comparison between planned and delivered dose in VMAT treatment deliveries at the level of the patient. The result is a 3D dose distribution displayed inside the patient, which is more easily interpreted in comparison to a difference in EPI signal (i.e., as in forward projection) [23]. There have been multiple algorithms developed for *in vivo* EPID dosimetry via back-projection for VMAT treatment deliveries such as the commercial package iViewDose (Elekta) which is based on the work of Wendling *et al*. and Mans *et al*. [23-25]. As visualised in **Fig. *3***, a pixel-by-pixel sensitivity correction is first applied to

determine the dose at the EPID plane. A de-convolution algorithm is then applied to the image to subtract the scatter originating within the EPID, followed by a beam profile correction, to give the primary portal dose at the EPID plane. Scatter originating from within the patient is then subtracted based on the integrated value of the primary fluence at the EPID plane. At this stage of the processing the EPI represents dose at the EPID due to primary photons only. This primary fluence is then projected back to the plane of the patient using the inverse square law and corrected for attenuation using the primary portal dose image with and without the patient, as well as the planning CT contours. The patient-specific scatter component of the primary dose can then be reintroduced based on field size and patient thickness to give the dose within a patient along a 2D plane. This process can then be repeated over each control point in a VMAT plan to determine the 3D dose distribution within the patient.

Clinical implementation of this methodology has previously been found to be successful in the ability to detect change in patient anatomy due to weight loss, atelectasis, and patient contour change [26]. Other treatment errors were also detectable using the back-projection method such as flawed plans during transfer from the TPS, fine-tuning of TPS parameters, and accidentally modified plans. Significant assumptions regarding patient scatter and attenuation are however made, as this methodology is typically based on the patient anatomy at the time of planning via the planning CT.

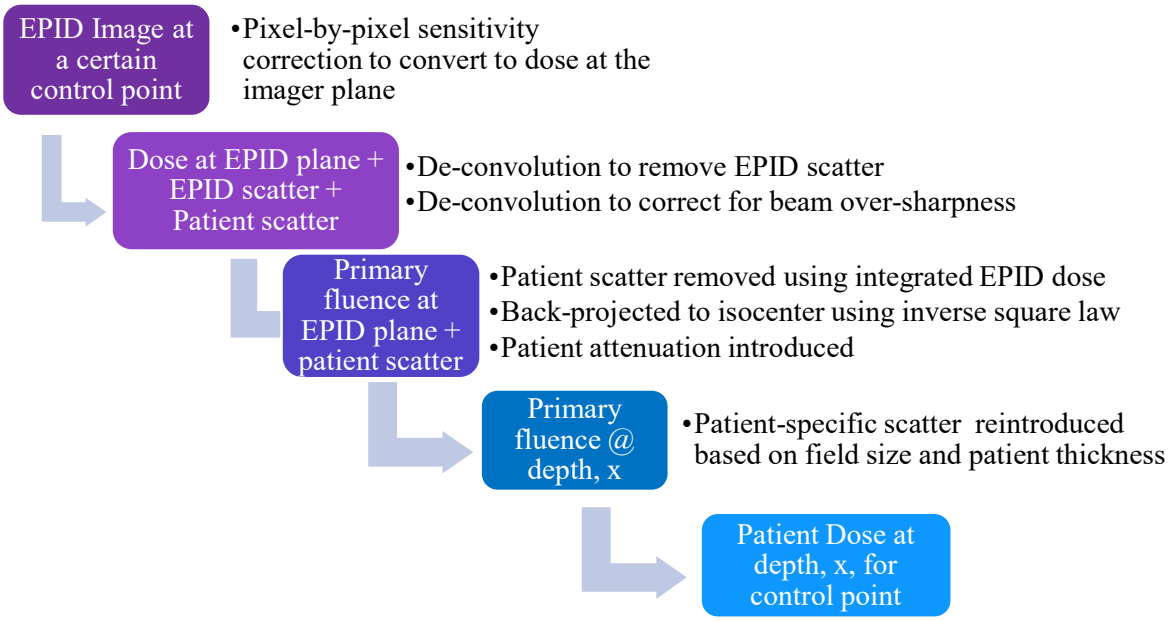

Fig. 3 Schematic of back-projection methodology described by Wendling *et al.* and Mans *et al.* [24-25]

3.2. Comparison of Integral Planar Images (Forward-projection)

3.2.1. Comparison with Prediction

Rather than back-projecting measured EPI data to the plane of the *patient* and verifying dose, the forward-projection methodology aims to verify treatment plans at the plane of the *EPID*. Bedford et al. [23] compared forward- and back-projection techniques for VMAT treatment of the prostate, where it was found that the two methods provided similar results between calculated and reconstructed patient dose (back-projected) and calculated and measured EPI fluence (forward projected). Here, the percent gamma pass rate, mean gamma values, and percentage CAX dose differences were all clustered around the line of equality between the two methods. Both methods have advantages and disadvantages. The advantage of the back projection method lies in its ease of interpretation, as it is much simpler to interpret a difference in a 3D dose grid at the plane of patient rather than an integrated EPI. The disadvantage is that to perform the reconstruction of dose, the algorithm assumes the patient anatomy is unchanged from the planning CT, even though this is one of the primary changes attempting to be detected. Advantages of the forward projection method are i) the direct nature of the comparison (i.e. fewer assumptions about patient anatomy are required) and ii) the possibility of conducting real-time verification using the EPID's *cine* mode. The work presented in this thesis is based on the forward-projection technique of EPID *in vivo* dosimetry, as it relies less on measured data and makes use of a calibrated TPS wherever possible.

The prediction of portal dose images using a TPS by modelling the EPID into the planning CT scan has been previously explored [28–30]. In order to predict the scatter and attenuation by the patient, the planning CT can be imported in the TPS, where the extent of these contributions to the EPI can then be calculated. The amount of scatter from the patient to the EPID has previously been accounted for using a superposition of patient scatter kernels, generated using Monte Carlo simulations [31]. In addition to attenuation, the scattered dose to the EPID arising from the patient can be calculated independently, as previously done with BEAMnrc [31], and added onto the EPID pre-treatment prediction model to predict EPIs more accurately.

One main method of implementing forward-projected transit dosimetry verification of VMAT plans utilises the predicted dose in the isocentre plane of the patient along each control point. Bedford et al. [32] describes the methodology used by the AutoBeam inverse treatment planning system, where an in-field and out-of-field portal image intensity at each pixel on the EPID is calculated for each control point. The in-field portal image intensity predicts the primary beam contribution to the image, accounting for attenuation, and the out-of-field portal intensity predicts the patient scatter contribution to the image. The two contributions are then combined with a kernel to model scatter originating within the EPID to give the final predicted portal image at a given control point. These images can then be compared to the measured EPIs either in 'continuous' mode or summed together and compared to the 'integrated' EPI. The accuracy and precision of VMAT verification using this methodology gave a mean gamma pass rate of 93.7% as achieved with a 3.0 %, 3.0 mm gamma analysis threshold. Alternatively, the primary fluence calculated by the TPS can be forward projected to the EPID plane to improve the predicted EPI.

Recent work by Nilsson [33] has developed a treatment verification algorithm for EPID dosimetry, implemented in the RayStation TPS. Here the predicted EPI is an extension of the pre-treatment prediction algorithm, in which patient scatter and attenuation of the primary beam by the patient is modelled in the TPS. Scatter projected onto the EPID from the patient was calculated through the use of modelling the EPID in the TPS as a 5 cm thick water slab. The dose from scatter was calculated in the plane of the EPID after projection through a patient CT, whilst setting the Total Energy Released per unit Mass (TERMA) within the EPID to zero. This adjustment ensures that the energy from the primary fluence reaching the EPID does not generate scattered dose from within the EPID. Instead, only the scattered dose from the patient will be extracted, and subsequently added to the predicted primary fluence image to give a complete predicted image. Nilsson also accounted for the linear attenuation of the beam from the patient through considering the primary fluence. The fluence intensity reaching the EPID (I) was derived by starting with the pre-treatment prediction (I_0) and correcting for any attenuation (μ) from the patient, as well as beam hardening (σ) introduced at a specified off-axis distance (r) and radiological depth (d_r) using the Beer-Lambert law, where $I =$

$I_0 . e^{-\mu(r) d_r + \sigma d_r^2}$. The coefficients used for this correction were derived with the aid of measured transit and non-transit EPIs. The advantage of this approach is that the scatter originating in the EPID does not need to be modelled directly but is included via the pre-treatment measurement. The disadvantage of this approach is that any errors in pre-treatment delivery are propagated through the subsequent predicted EPIs.

A similar approach to Nilsson has been adopted in the current work by modelling the EPID in the RayStation TPS. In contrast to Nilsson's methodology, however, we seek to generate predicted EPIs purely through TPS modelling of the patient and EPID panel.

3.2.2. Comparison for Constancy

Through comparing the change in EPIs relative to the first or previous fraction, one can measure the constancy of a treatment delivery. The main benefit of comparing EPIs in this regard is that one does need to accurately model scatter and optical process of the EPID hardware or mimic the post-processing of the measured data performed by the EPID software. This approach was adopted by Piron et al. [20] who recorded change in transit fluence for 50 H&N cancer patients. Through utilising the mean gamma value, γ_{mean}, from a 2D 3%/3mm relative gamma analysis test on whole EPIs, they concluded that change in transit fluence could be used as a predictor for plan deterioration as a result of anatomical variations. Utilising the whole EPI, however, could result in misleading mean gamma values. If only a small area of pixels included large deviations, the EPI as a whole may still be similar to the baseline EPI and thus result in a score that is below the trigger threshold, ultimately decreasing sensitivity. By considering projections of regions of interest onto the EPIs, the sensitivity of the analysis may be improved.

By projecting planning target volume's (PTV's) onto EPIs obtained every fraction and correlating $\gamma_{mean}$with dosimetric changes (V95%), Piron et al. [21] found that projecting PTVs onto the EPIs and then conducting gamma analysis improved sensitivity to anatomical changes. However, projecting OARs onto the EPIs were not considered.

The same group then went on to establish an action threshold for H&N ART, and proposed a threshold of $\gamma_{mean} > 0.42$, as evaluated using the whole EPI [22]. By considering a dosimetric

threshold of V100% < 90% the group was able to analyse the sensitivity and specificity of the threshold proposed. Moreover, the group also explored the correlation between mean dosimetric differences of PTV and OARs with mean gamma values of the whole EPI for patients that did reach the action threshold, as well as patients that did not. A strong correlation between change in spinal cord dose and γ_{mean} was not observed, likely due to the inherent nature of the gamma analysis test conducted on whole EPIs - being more sensitive in high dose regions, such as PTVs, than lower dose regions, such as OARs.

Lim et al. [34] explored the correlation between change in transit fluence, in a generalised rectangular region surrounding the neck, and volumetric change of a ROI (ΔV_{ROI}) spanning from the Condyloid process (jaw) to C6 of the spinal cord. Volumetric change, which is a good predictor for grade 2 xerostomia [35], was found to be strongly correlated with change in transit fluence ($R = -0.776, p < 0.001$). A 5% threshold in ΔV_{ROI} could be used as a trigger for ART, where the area under the receiver-operating characteristic curve (ROC) was determined to be 0.88. This study did not investigate the potential improvement in sensitivity by projecting the ROI onto the EPID.

3.3. Current Work in the Context of Previous Studies

Past literature has explored the use of EPIDs for transit dosimetry quality assurance, via a wide variety of approaches as previously discussed. Limited research has utilised Varian's relatively new aS1200 EPID as well as the TPS RayStation by RaySearch Laboratories with VMAT treatment delivery. The capability of the TPS to predict the improved dosimetric images obtained by the aS1200 EPID, both pre-treatment and in transit dosimetry for H&N VMAT treatment plans has been investigated in the current work.

Once validated to predict change in transit fluence, the EPI prediction model was then extended to explore any correlation between change in transit fluence and change in DVH metrics for H&N cancer VMAT treatment plans. When utilising linac-measured EPIs for comparison of constancy with relative gamma analysis, one of the largest sources of systematic error in these types of studies include the accuracy of the first fraction EPI. The results of these studies all rely on the assumption that the patient anatomy at the time of the first fraction EPI is representative of the patient anatomy at the time

of the planning CT (pCT). A poor baseline could be misleading and yield results with γ_{mean} values significantly lower than actually representative of the change since obtaining the pCT. The research presented in the second portion of this work differs from previous studies by predicting transit EPIs using an in-house script developed in the RayStation treatment planning system (TPS) by RaySearch Laboratories, rather than analysing linac-measured EPIs. The advantage of this approach is in the removal of any patient set-up errors, as well as any anatomical variation in the patient between obtaining the pCT and first fraction baseline EPI. Rather than using weekly CBCTs over the course of treatment, this work will also only consider the pCT and a rescan CT (rCT) to avoid any uncertainties associated with deformable image registration of the pCT's to CBCT's, or dose calculation uncertainty on CBCT. Considering these factors, the developed tool allows for the investigation of correlation between change in transit fluence and change in patient DVH metrics in a more controlled environment.

4. Development of an In-house Toolkit for EPID-based Non-transit and Transit Dosimetry with a Varian Linac and RayStation Treatment Planning System

4.1. Introduction

As discussed in Chapter 2, EPID-based patient specific quality assurance (PSQA) may be divided into pre-treatment (non-transit) dosimetry and on-treatment (transit) dosimetry. The application of EPID-based PSQA to head and neck radiotherapy was described in Chapter 3. In this chapter, the development of an in-house toolkit to perform EPID-based non-transit and transit PSQA with a Varian aS1200 EPID and the RayStation treatment planning system (TPS) is described. While commercial software systems are available for this purpose, the powerful scripting application programming interface (API) of the RayStation TPS means an in-house solution may be achievable which can be adapted towards a departments specific requirements. Furthermore, by utilizing the primary TPS for this purpose, a more direct quality assurance of the clinical treatment plan is performed when compared to incorporating a third party system for calculation of expected EPID results. In this Chapter the development of a Varian EPID model within the RayStation TPS is described, in addition to methodology and results for validating the model. Testing of the TPS EPID model was performed for non-transit and transit dosimetry conditions.

4.2. Methods

4.2.1. EPID Measured Data

The structure and functioning of the Varian aS1200 EPID attached to a Varian TrueBeam Linac was discussed in Section 2.4. All measured EPIs in this work were exported via the PortalDosimetry software. PortalDosimetry was calibrated by the physics team at the Royal Adelaide Hospital via the following steps to give the signal in each pixel in ‘calibration units’ (CU).

1. A dark field is applied to the EPID, obtained through acquiring an image with no output from the beam. This represents the background electronic noise in the EPID hardware.

2. A flood field is then applied to account for individual pixel sensitivities. This is done through acquiring a reference 40 x 40 cm field, spanning across the entire EPID.
3. A beam profile correction is then applied to re-introduce characteristic profile shapes removed via Step 2. The beam profile corresponded to a radial beam profile acquired in a water tank at 3.6 cm depth in a 40 cm × 40 cm.
4. Dose normalisation then links the imager response of a 10 cm x 10 cm field with 100 MU at 100 cm SID to correspond to 100 CU.

In this work, we aimed to predict EPIs for 6 MV photon beams. Data acquired on the EPID to validate the TPS EPID model were square fields with side lengths of 2, 3, 4, 5, 10, and 20 cm, as well as 5 cm × 10 cm, 5 cm × 20 cm, 10 cm × 5 cm, and 20 cm × 5 cm rectangular fields. These fields were defined at isocenter (100 cm), with the EPID positioned at a source to image receptor distance (SID) of 100 cm and 150 cm. In the latter scenario, the couch was placed in the beam, and transit dosimetry was also investigated utilising 1, 2, 3, 5, 10, and 20 cm thick PMMA slabs positioned with the centre of the phantom at isocenter.

4.2.2. EPID Model

Modelling the EPID in the TPS and extracting a dose plane utilises the TPS dose calculation algorithm when considering the effects of patient attenuation, patient scatter, and any scatter from within the EPID itself. The production of the EPID image involves the conversion of X-rays to visible light and subsequent collection of optical photons with silicon photodiodes. This process cannot be simulated in commercial radiotherapy TPS's and therefore approximations of the image generation process must be made, as described by various authors [29-30, 33].

The RayStation TPS allows the user to define geometrical structures within the dose calculation environment. These geometrical structures can also be assigned a material which includes density and chemical composition. In this work the TPS EPID model was defined as layers of rectangular volumes on a RayStation Research v10a server. The thickness and composition of each layer of the TPS EPID model was varied to reproduce the central axis dose and relative beam profile of EPID-measured rectangular fields exported from PortalDosimetry. The extraction plane of the TPS EPID model in this

work was positioned at 100 cm SID for non-transit dosimetry, and 150 cm SID for transit dosimetry. The DICOM header within the measured EPI was also utilised to convert the 2D fluence map into a pseudo 2D dose map ('calibration units') via the "Rescale Intercept" (0028, 1052) and "Rescale Slope" (0028, 1053) tags.

4.2.3. TPS Dose Plane Calculation

The predicted EPIs were calculated for non-transit and transit dosimetry set-ups, as described in **Fig. 4**.

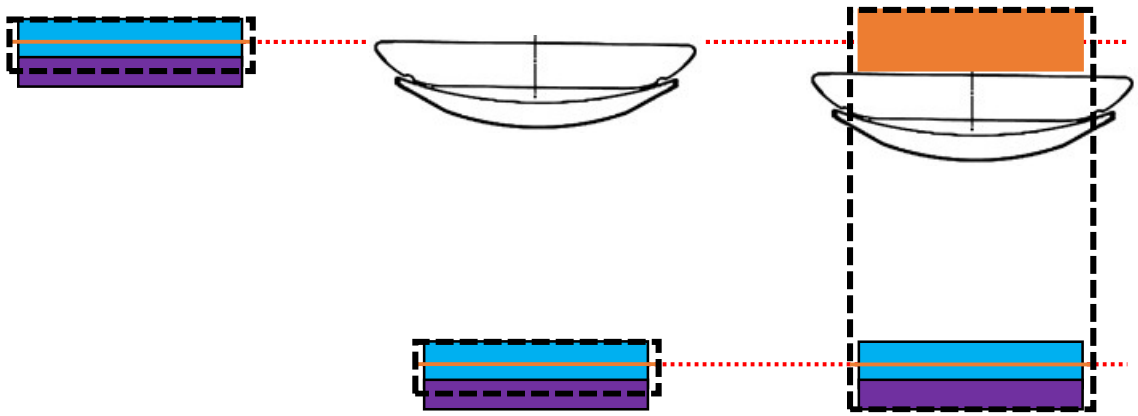

Fig. 4 EPID model setup for non-transit dosimetry at 100 cm SID (left), non-transit dosimetry at 150 cm SID (middle), and transit dosimetry at 150 cm SID (right) with dose grids shown in black (dashed).

4.2.3.1. Non-transit calculation

In the case of non-transit dosimetry, the dose grid spanned across 40 cm x 40 cm, in the x- and y-axis respectively, using 1 x 1 mm^2 pixels and an extraction depth of 3.6 cm in the model. The extraction depth of 3.6 cm was chosen by comparing central axis (CAX) dose in the TPS to that of measured data at 100 cm SID on the EPID.

To help verify if the model is capable of transit dosimetry, non-transit dosimetry was also conducted at 150 cm SID, with the couch in the beam. Here, the dose grid spanned across the entire surface of the EPID model, resulting in a 40 x 40 x 6 cm^3 dose grid with 1 x 1 x 1 mm^3 voxels. A volumetric dose grid was exported in this scenario to explore the effects of varying extraction depth on beam shape. The dose grids were then subsequently exported as DICOM RT Dose files, where dose planes could be extracted, post-processed, and compared to corresponding linac-obtained EPIs.

4.2.3.2. Transit calculation

For transit dosimetry, the TPS dose grid was extended to include the phantom in order for RayStation to consider the attenuation and scatter properties of these materials. The voxel size was increased to 2 mm^3 to help reduce calculation time and file size, whilst still retaining enough spatial resolution to accurately define the penumbra of the beam profiles. The dose grids were then subsequently exported as DICOM RT Dose files, where dose planes could be extracted, post-processed, and compared to corresponding linac-obtained EPIs.

4.2.4. TPS Dose Plane Post-processing

Once the dose plane has been extracted from the TPS, post-processing steps were required to better approximate the signal received by the EPID. All post-processing steps described in this work were applied solely to the calculated EPIs, rather than those measured, as this allows for treatment validation to be conducted at the time of acquisition. As a result, all post-processing can be applied to the prediction *prior* to acquisition on the linac.

4.2.4.1. Non-transit dosimetry

The EPID model developed for non-transit dosimetry at 100 cm SID corresponds to the dose deposition of 6 MV beams at a given depth in a given material. Post-processing is thus required, to match the signal being readout by the EPID software. The corrections applied were aimed towards mimicking the processing performed by the EPID software, namely a flood field correction and a beam profile correction.

To account for the varying pixel sensitivity across the EPID panel, the EPID software divides each measured EPI by a normalised reference 40 x 40 cm square (flood) field on a pixel-by-pixel basis. To mimic this processing, a 40 x 40 cm square field was calculated with the EPID model in the TPS. Each raw predicted EPI is then subsequently divided through by this normalised reference image on a pixel-by-pixel basis. The second correction applied is a beam profile correction. This beam profile correction is applied due to the flood-field correction removing the radial dependence of the measured

dose within a beam profile, also known as the "horns". Overall, the corrected TPS calculated EPI is related to the TPS calculated EPI as shown in Equation 1.

$$\Phi^{*}_{pred} = \frac{(\Phi_{pred} \times BPC)}{\Phi_{FF,pred}} \quad (1)$$

Where Φ_{pred} is the TPS calculated EPI, Φ^{*}_{pred} is the corrected TPS calculated EPI, BPC is the radial beam profile correction measured at 3.6 cm deep in a water tank, and $\Phi_{FF,pred}$ is the normalised TPS calculated 40 x 40 flood field. This correction process can be compared to that done in the PortalDosimetry software, which is summarised in Equation 2.

$$\phi^{*}_{meas} = \frac{(\phi_{meas} - \phi_{DF}) \times BPC}{\phi_{FF,meas}} \quad (2)$$

Each parameter follows a similar definition to that above, however applying to measured EPIs instead. The PortalDosimetry software has an added step in which the dark field is subtracted from the measured field prior to any subsequent processing. A side-by-side comparison of the post-processing steps conducted by the PortalDosimetry software and that applied to the TPS calculated EPIs is summarised in **Fig. *5***.

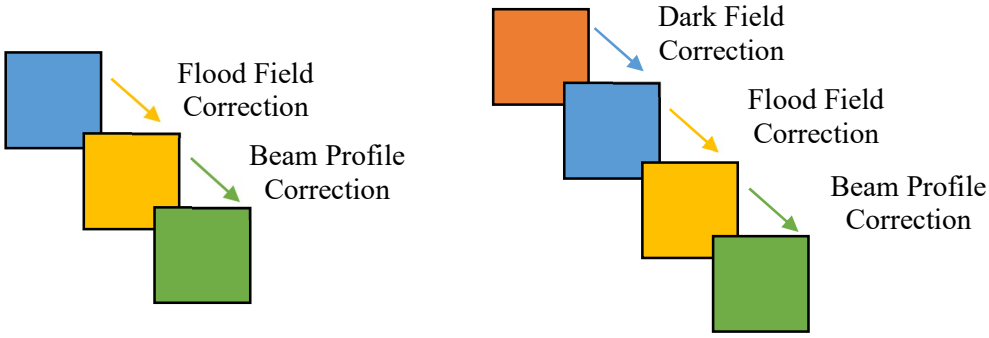

Fig. 5 Schematic of corrections applied to the TPS EPID (left) model and EPID (right).

4.2.4.2. Transit dosimetry

EPID calibration post-processing done by the PortalDosimetry software is applicable at 100 cm SID. To obtain quantitative EPIs at 150 cm SID, an extended SID correction is required. This was obtained by acquiring a 27 x 27 cm open field EPI at 100 cm SID, applying an inverse square law and magnification correction to 150 cm SID, and taking the ratio of the same open field EPI with the EPID positioned at 150 cm SID. Note that a 27 x 27 cm field was chosen as this corresponds to a flood 40 x

40 cm EPI at 150 cm SID. Post-processing applied to predicted EPIs were thus extended to the new SID through applying this SID correction factor, extending Equation 1 as follows:

$$SID\ Correction(r) = \frac{\phi_{meas_{150}}(r)}{\phi_{meas_{100\rightarrow150}}(r)} \tag{3}$$

$$\Phi^{*}_{\mathrm{pre}\ \ 150} = \Phi_{pred_{150}} \times \frac{(SID\ Correction \times BPC_{100\rightarrow150})}{\Phi_{\mathrm{FF,pred}_{100\rightarrow150}}} \tag{4}$$

4.2.5. Comparative Analysis

Comparative analysis between the TPS predicted and measured EPIs was done via comparison of the CAX dose and output factors, comparison of beam profile shape, and 2D comparison using the gamma analysis test.

Central axis dose was utilised to better optimise the extraction depth within the EPID model, as well as the composition of materials within the model. All corrections applied to the predicted EPIs were normalised to the CAX and thus the CAX dose is unaffected by any corrections applied. Comparison of CAX dose was simply made through considering the percentage difference along the CAX for varying square field sizes.

Comparison of output factors was done by dividing the CAX doses through by that for the 10 cm × 10 cm field. This allowed iterative adjustment of the materials used in the EPID model to be made, as different materials and material thicknesses will affect the model's response to varying field size and scatter.

Once the extraction depth and foundation of the model was decided upon, the corrections described above resulted in better agreement in the beam profile between measured and computed data. Comparison of beam profiles was thus conducted to observe the effects of any corrections applied, as well as explore any additional corrections required. Comparison of beam profiles was completed through calculating the 2D percentage difference between measured and predicted EPIs and exploring the radial response.

The most widely utilized comparative analysis tool for 2D dose maps, such as EPIs, is the gamma analysis test [36], which considers both the dose difference between two distributions, as well as the

distance-to-agreement (DTA) of the two distributions. The dose difference is useful in quantifying significant differences in regions of low dose gradient, where the DTA is useful in regions of high dose gradient. The dose criteria in a gamma evaluation are typically relative to some global or local dose maximum in a reference distribution, where typical clinical gamma criteria include a 2% dose difference with a max DTA of 2 mm (i.e., 2%, 2mm), or a 3% dose difference with a max DTA of 3 mm (i.e., 3%, 3mm). Values of gamma can be calculated as follows, where points with $\gamma < 1$ corresponds to points that meet the gamma test criteria (i.e., DTA and percentage dose difference) and thus indicate a pass and points with $\gamma > 1$ corresponds to points that do not meet the gamma test criteria and thus indicate a fail:

$$\Gamma(r_r, r_e) = \sqrt{\left(\frac{r}{\Delta d}\right)^2 + \left(\frac{\delta}{\Delta D}\right)^2} \tag{5}$$

Where $r = |r_r - r_e|$ is the distance between the evaluated and reference points, and $\delta = D_r(r_r) - D_e(r_e)$ is the dose difference between the evaluated and reference points, for DTA threshold Δd and dose threshold ΔD. The value of gamma for a given reference point is thus given as $\gamma(r_r) = \min(\Gamma(r_r, r_e))$.

The percentage of points that pass the gamma evaluation criteria (i.e., the gamma pass rate) can thus be used as a quantitative approach in determining how similar the two dose distributions are. In this work, the gamma function in the open-source library PyMedPhys was used to conduct the gamma analysis.

4.2.6. Change in Dosimetry

In the clinical scenario, one could also utilise the *change* in transit dosimetry at a given treatment fraction relative to some baseline fraction, to assess whether adaptive radiotherapy should be considered. To verify if the model is able to assess change in transit dosimetry, the change in measured EPIs were compared against change in predicted EPIs for one extreme case and two moderate cases:

1) Extreme Case: Phantom thickness reducing from 10 cm to 5 cm
2) Moderate Case 1: Phantom thickness reducing from 5 cm to 3 cm
3) Moderate Case 2: Phantom thickness reducing from 3 cm to 1 cm

Predicted and measured change was assessed as a percentage difference between the two 'fractions' (ΔEPI), relative to the maximum value of the first 'fraction' where:

$$\Delta EPI_{(i,j)}\,[\%] = \frac{EPI_{1_{(i,j)}} - EPI_{0_{(i,j)}}}{\max(EPI_0)} \times 100 \quad (6)$$

The change in transit fluence between the two 'fractions' for the measured and calculated data was then compared to each other through a raw percentage difference, where $\%diff = \Delta EPI_{TPS_{(i,j)}} - \Delta EPI_{linac_{(i,j)}}$.

4.3. Results

4.3.1. EPID Model

The EPID was first modelled based on non-transit EPIs obtained at 100 cm SID, using 2.5 cm slabs of various materials. Initially, cork and water were explored. The overall shape of the beam profile was better matched to measurements when using the water slab, where the CAX dose was only very slightly better matched with the water slab. Utilising a 5 cm thick water slab allowed for a dose plane to be extracted deeper within the EPID model – reducing the CAX dose significantly to better match that of the measured EPI as shown in **Fig. *6***. The addition of a 5 cm thick lead backing was included to further improve the output factors of the larger square fields, where adding dense material is expected to affect the larger fields more than the smaller fields due to the higher probability of backscatter. A 3.6 cm extraction depth was thus chosen as this optimised the CAX dose and output factors (See **Fig. 7**).

Once validated at 100 cm SID, the model was then further altered to better approximate CAX doses at 150 cm SID. Through assessment of the beam profiles and CAX doses, the 5 cm lead backing was altered to a 4 cm lead backing as it was noted the predicted output factors were previously, on average, ~1.0% higher than that measured. Output factors measured at 150 cm SID with the updated model are shown in **Fig. 8**, noting a maximum percentage difference in CAX dose of 1.02% and an average of 0.43%.

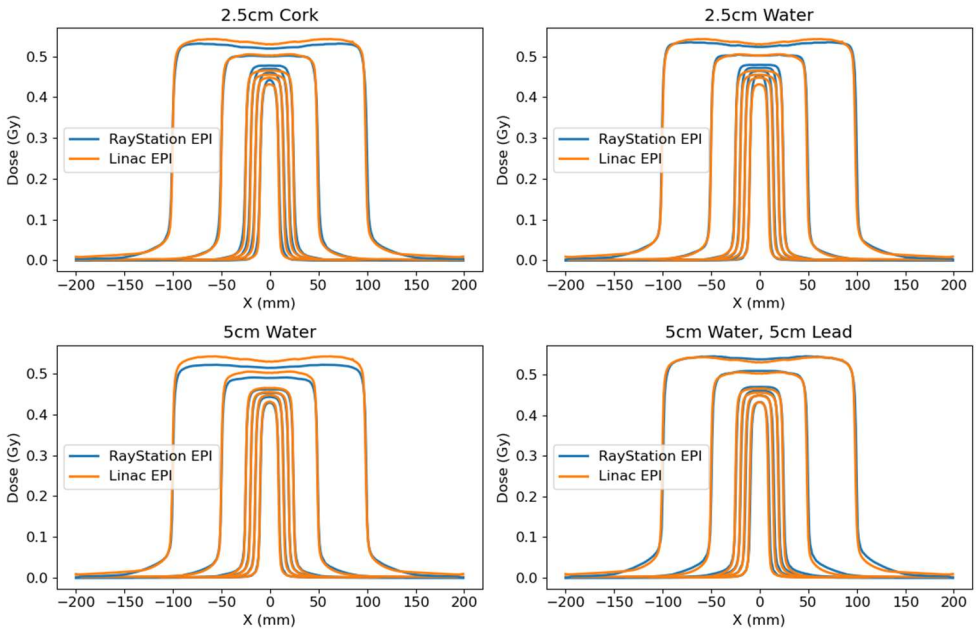

Fig. 6 Raw x-axis beam profiles using various EPID models and depth of extraction planes.

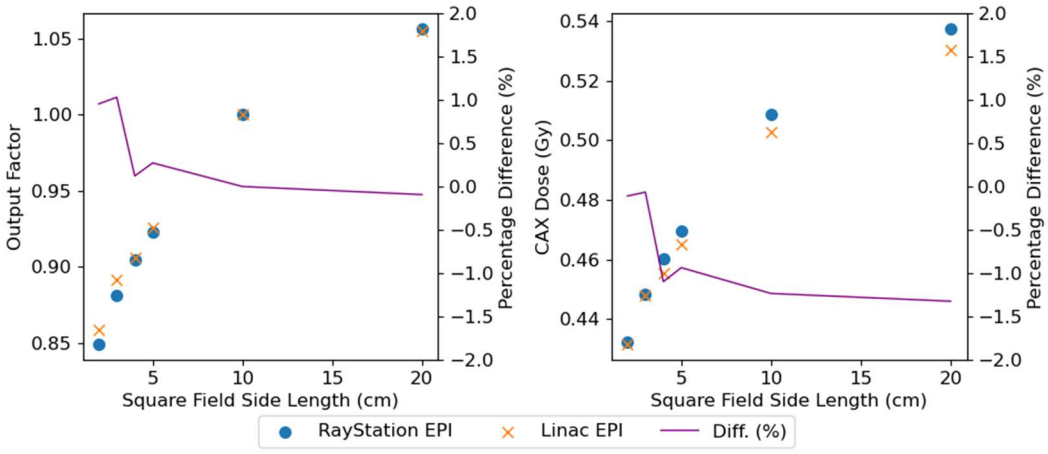

Fig. 7 Output factors and CAX dose, using the 5cm water 5cm lead EPID model in comparison with the measured EPI.

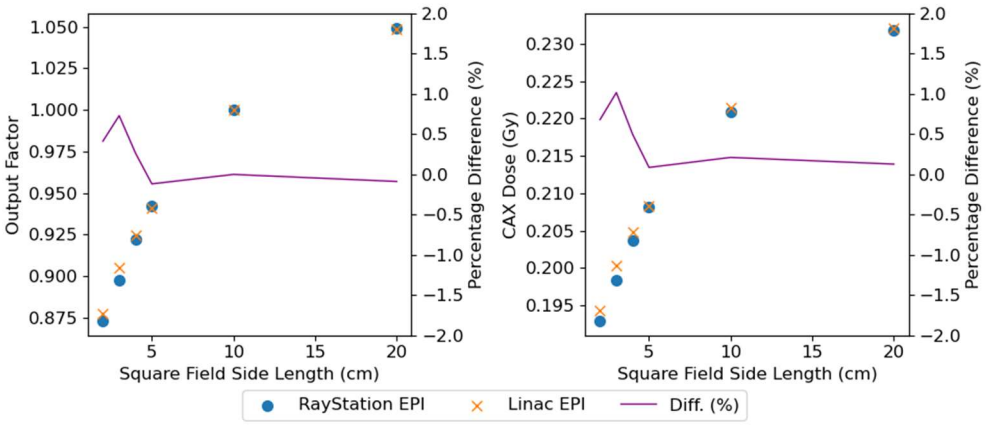

Fig. 8 Output factors and CAX dose for updated 5 cm water, 4 cm lead model at 150 cm SID.

4.3.2. Non-transit dosimetry

The EPID model developed for the purpose of non-transit dosimetry proved to be reliable when considering the CAX dose and output factors, yielding a maximum percentage difference in CAX dose of 1.02% at 150 cm SID. Additional corrections, however, were required to further correct the overall beam shape via mimicking the additional processing done by the PortalDosimetry software. Namely, the application of a flood field, and subsequent beam profile correction.

The progressive change in beam profile shape in going from the raw TPS output to the flattened flood field data, to the final beam profile corrected data is shown in **Fig. *9***, with non-normalised diagonal profiles and percentage differences shown in **Fig. *10***.

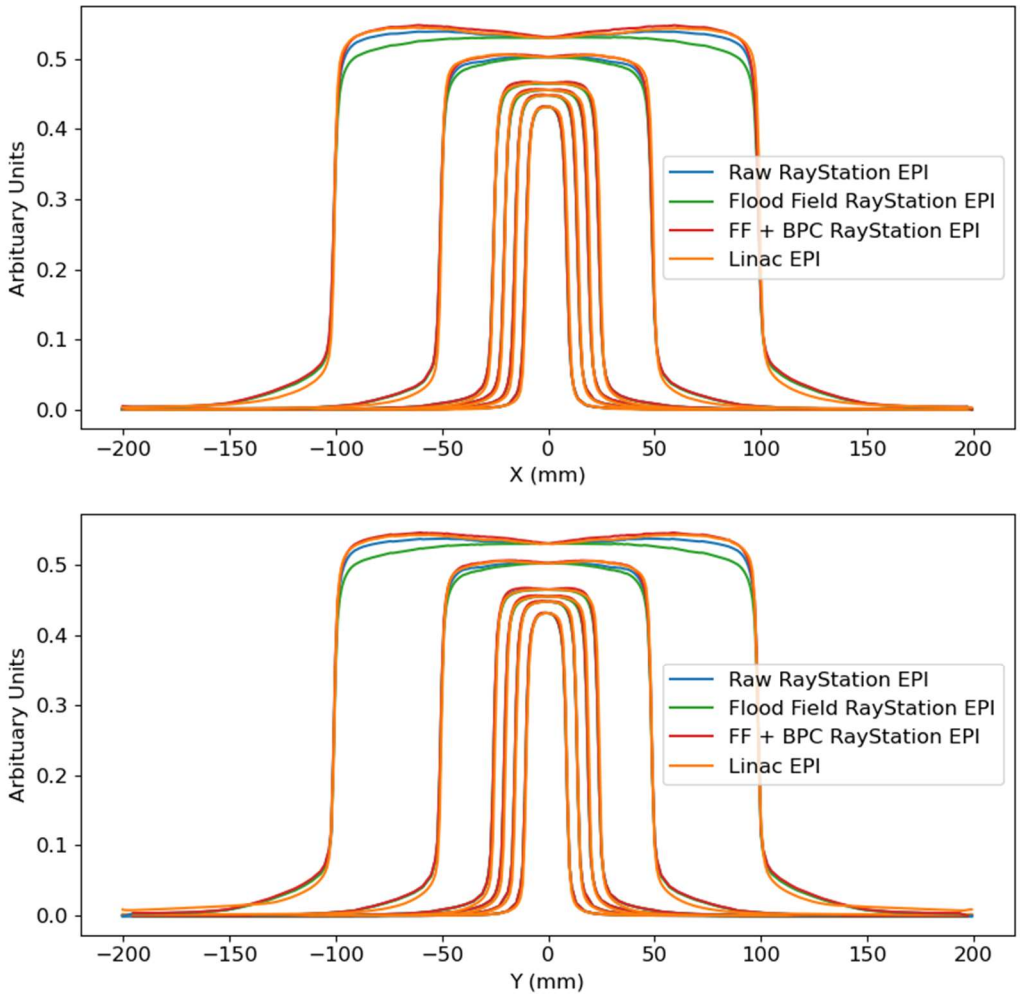

Fig. 9 X- and y-profiles normalised to CAX for various square fields, showing progression of beam profile shape at each image processing stage. Each profile has been offset in height for ease of viewing.

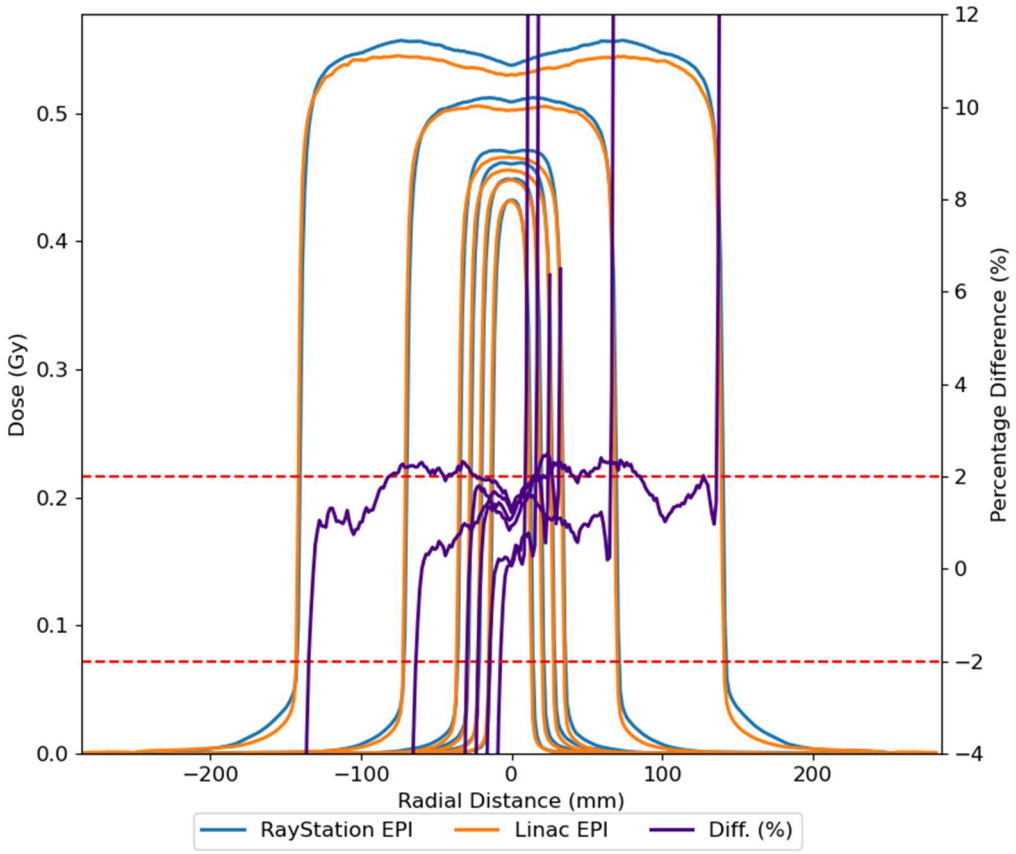

Fig. 10 Non-normalised, non-transit diagonal profiles and percentage differences for various square fields at 100 cm SID.

Overall, the agreement between predicted and measured beam profiles at 100 cm SID was validated when using the 5 cm water + 5 cm lead EPID model. At 150 cm SID, the EPID model was updated to 5 cm water and 4 cm lead, with square field beam profiles shown in Fig. ***11***.

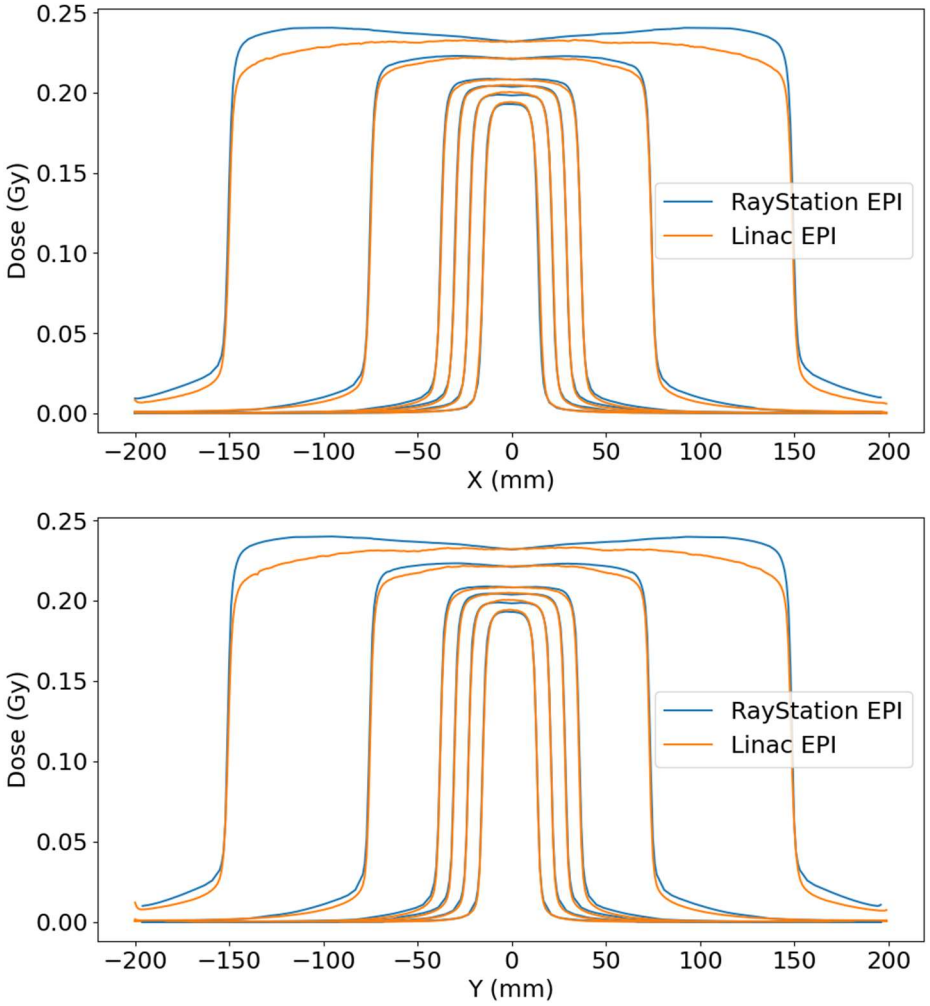

Fig. 11 Raw x-profiles of predicted and measured EPIs at 150 cm SID using the 5cm water and 4 cm lead EPID model.

To account for the significant difference in beam profile shape at 150 cm SID, the additional SID correction factor described in section 4.2.4.2, as shown in Fig. ***12***, was applied. Any deviation from the inverse square law, as shown by the red horizontal line in Fig. ***12***, is likely due to a differing amount of scatter reaching the EPID. This distribution of scatter suggests that scattered photons overlap more-so towards the centre of the EPID. Moreover, scattered photons will have less energy than those in the primary beam. The EPID is known to display an energy dependence, due to the attenuation coefficient relationship with energy of materials within the EPID design, as shown in Fig. ***13***. This energy dependence may also contribute to the reduction in intensity relative to the inverse square law, as the EPID would under-respond at 150 cm SID compared to 100 cm SID due to the smaller scatter-to-primary (SPR) beam ratio.

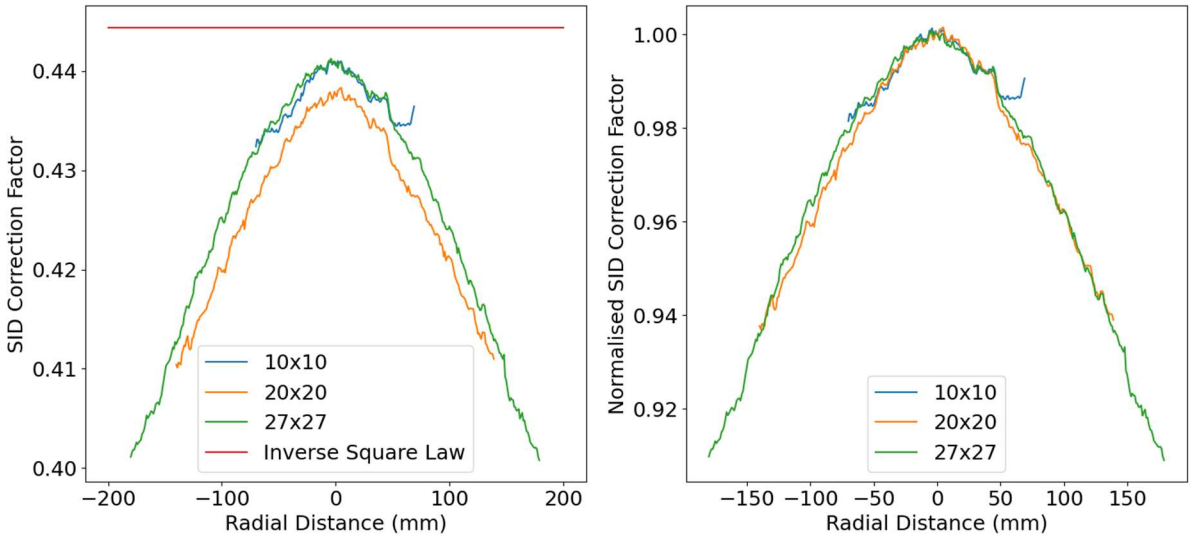

Fig. 12 SID correction factors for change in SID, showing negligible dependence upon field size when normalised.

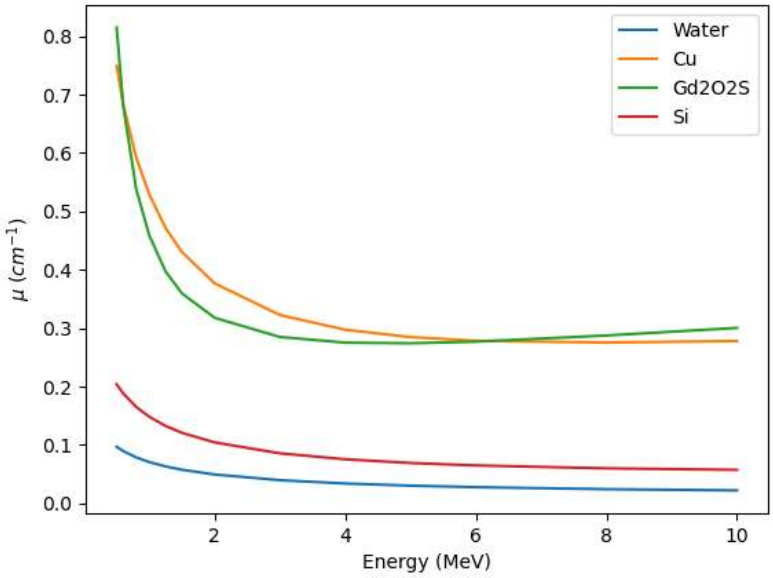

Fig. 13 Linear Attenuation coefficient relationship with energy for water and materials found within the aS1200 EPID.

Applying the extended SID factor to the predicted EPIs significantly improves the overall shape of the beam profiles at 150 cm SID, as shown in **Fig.** ***14*** for a 20x20 cm square field. Diagonal profiles of each square field, with percentage differences, are shown below in Fig. ***15*** for non-transit EPIs at 150 cm SID.

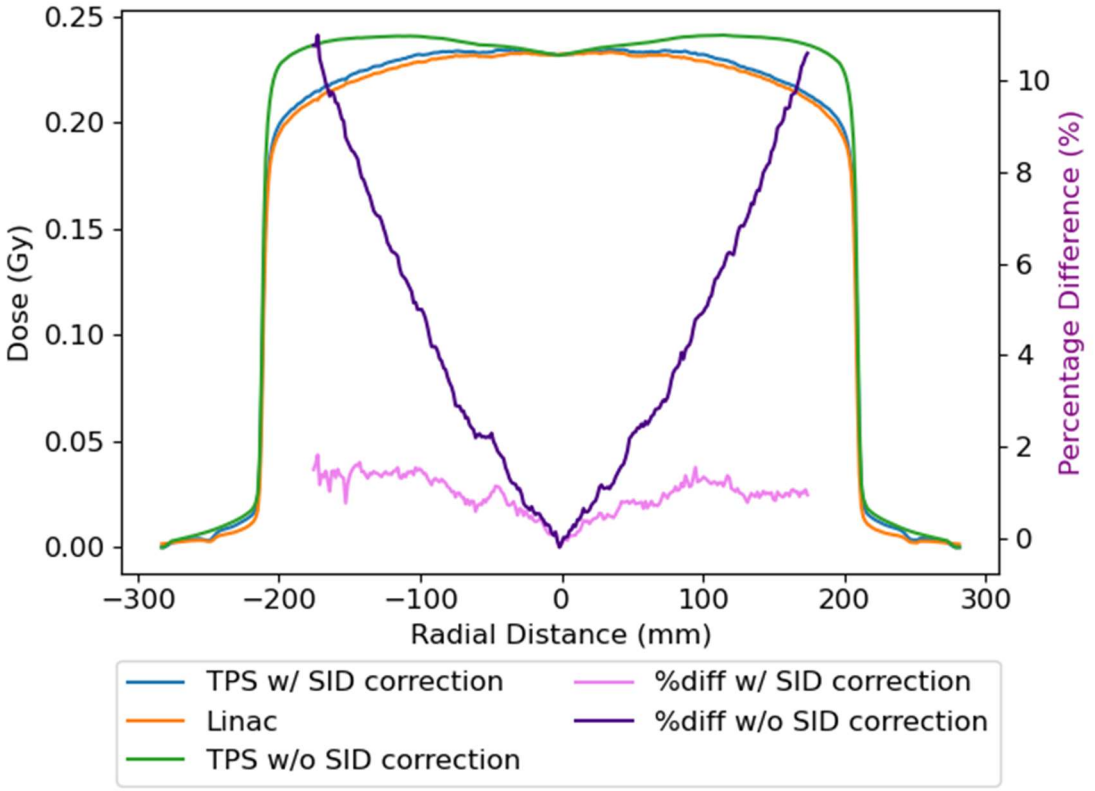

Fig. 14 Diagonal profile comparison when scaling the corrections to 150cm SID, *with* (blue) and without (green) the SID correction factor applied.

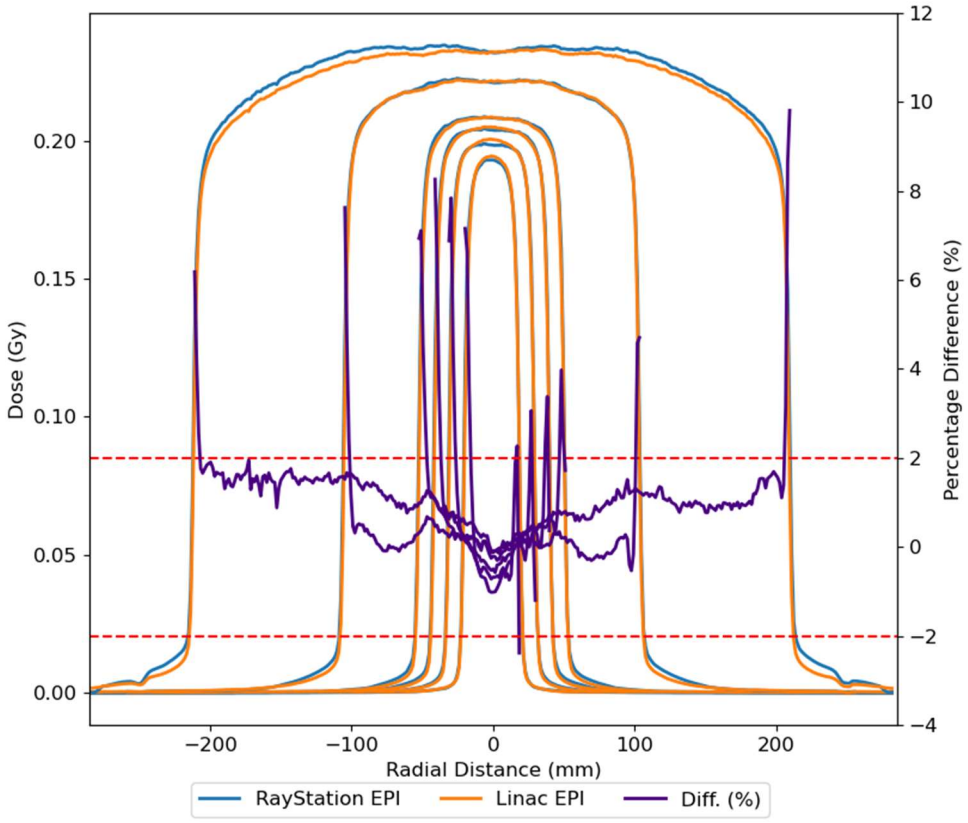

Fig. 15 Non-transit diagonal beam profiles and percentage differences for various square fields.

4.3.2.1. *Gamma Analysis at 100 cm SID*

A 2D gamma analysis with an acceptance criteria of 2.0 % dose difference and 2.0 mm DTA was conducted between normalised predicted and measured EPIs for square fields with side lengths of 2 cm, 3 cm, 4 cm, 5 cm, 10 cm, and 20 cm, and rectangular fields of size 10 x 5 cm, 5 x 10 cm, 20 x 5 cm, and 5 x 20 cm as shown in **Fig. *16***. The percentage gamma pass rate, excluding doses less than 10.0% of the global maximum, was calculated as well as the mean percentage difference within the fields.

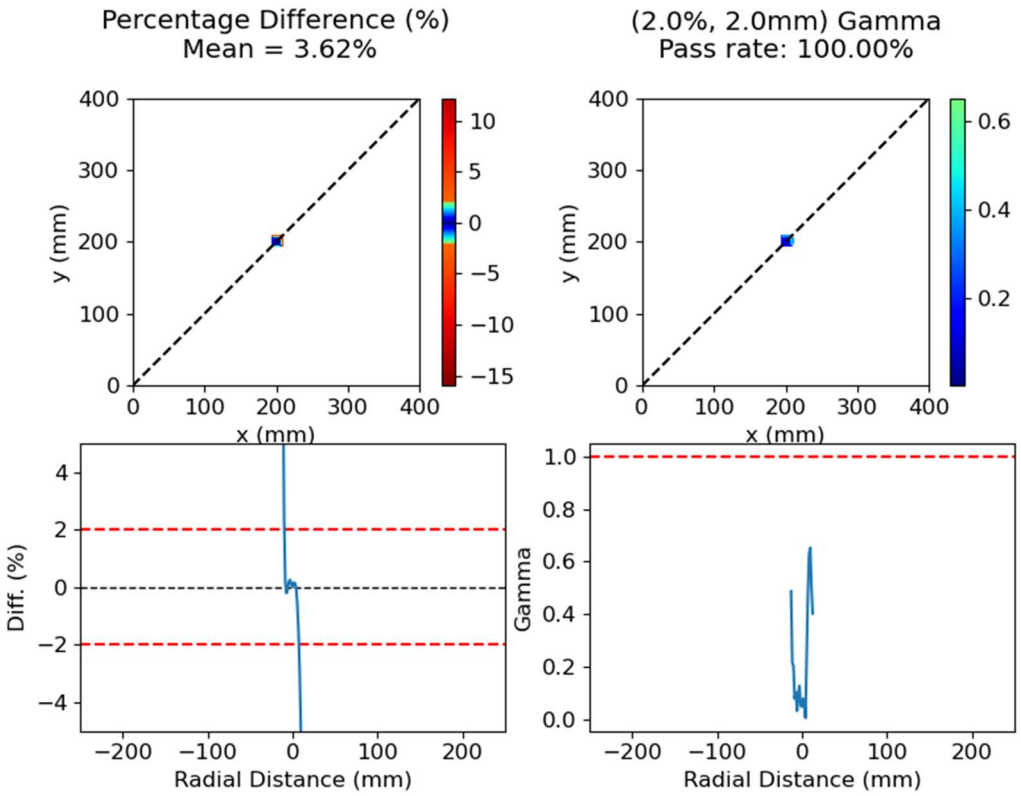

Fig. 16-1 (2.0 %, 2.0 mm) Gamma analysis for a 2.0 x 2.0 cm normalised field using the 5cm Water + 5cm Lead EPID model, with extraction at 3.6 cm.

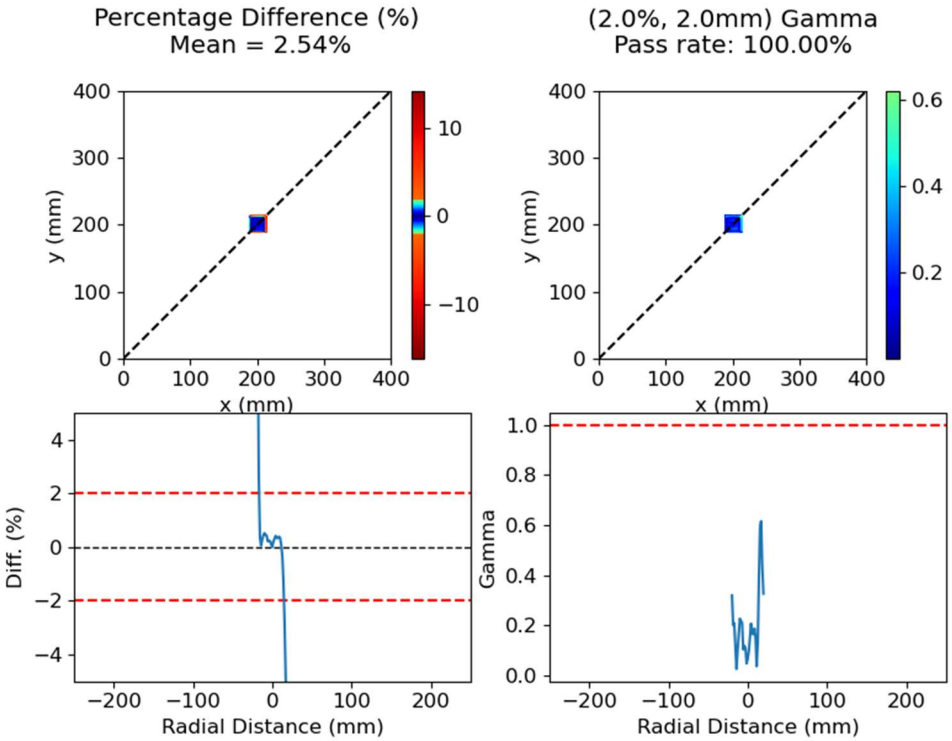

Fig. 16-2 (2.0 %, 2.0 mm) Gamma analysis for a 3.0 x 3.0 cm normalised field using the 5cm Water + 5cm Lead EPID model, with extraction at 3.6 cm.

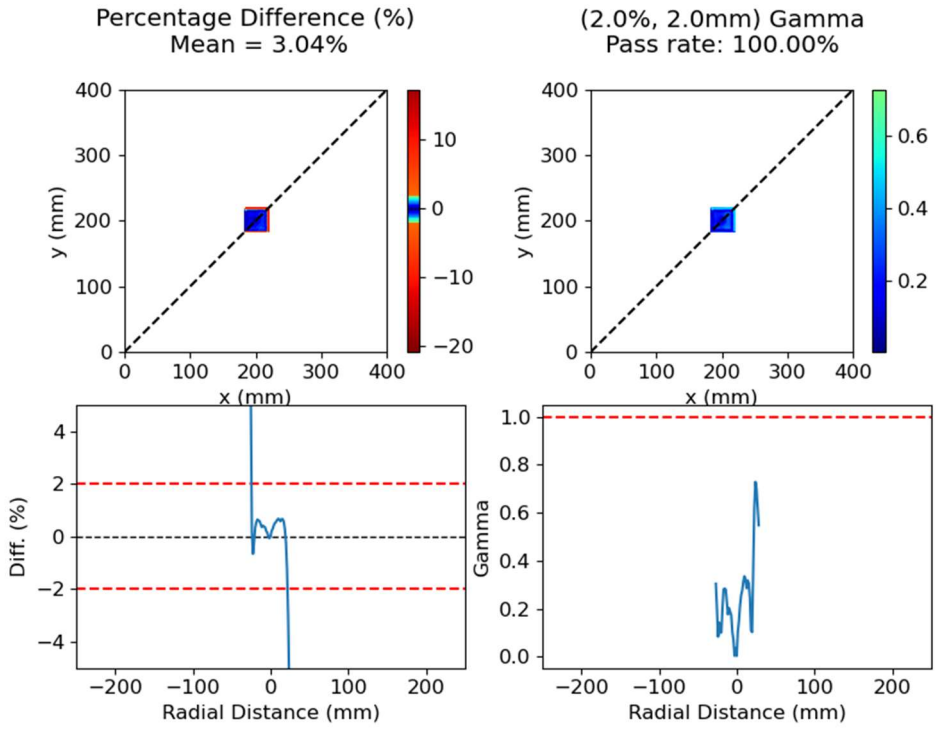

Fig. 16-3 (2.0 %, 2.0 mm) Gamma analysis for a 4.0 x 4.0 cm normalised field using the 5cm Water + 5cm Lead EPID model, with extraction at 3.6 cm.

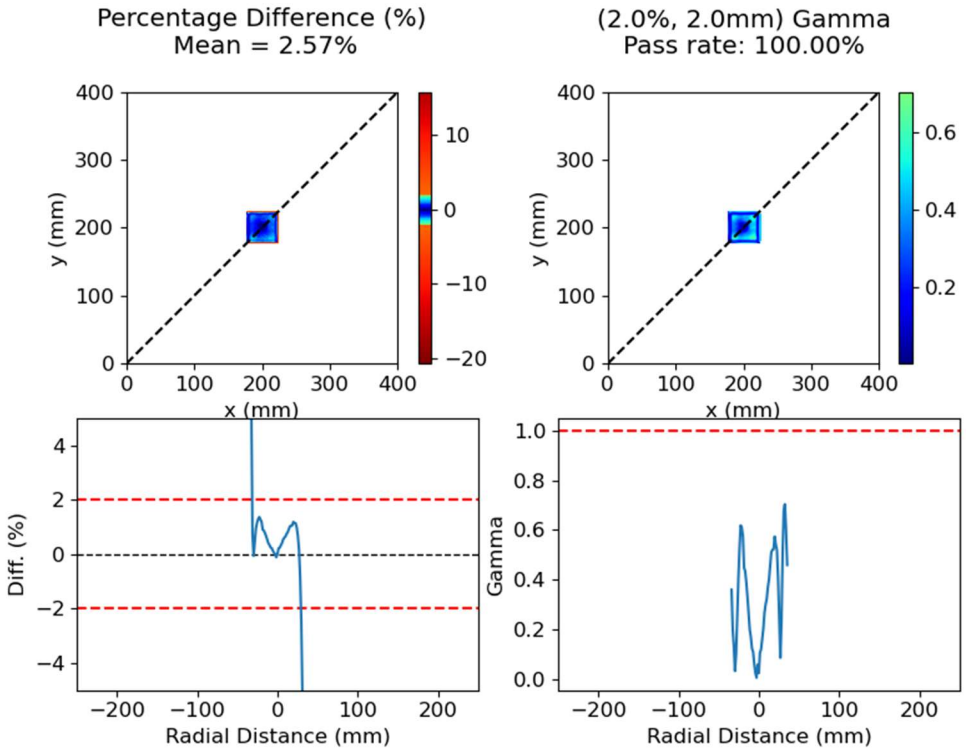

Fig. 16-4 (2.0 %, 2.0 mm) Gamma analysis for a 5.0 x 5.0 cm normalised field using the 5cm Water + 5cm Lead EPID model, with extraction at 3.6 cm.

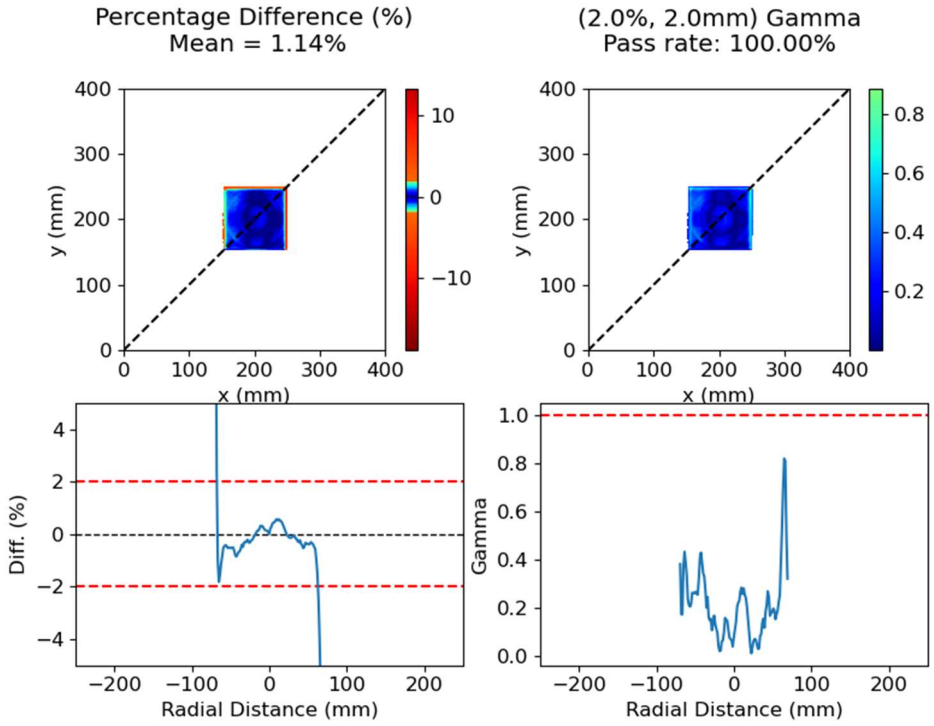

Fig. 16-5 (2.0 %, 2.0 mm) Gamma analysis for a 10.0 x 10.0 cm normalised field using the 5cm Water + 5cm Lead EPID model, with extraction at 3.6 cm.

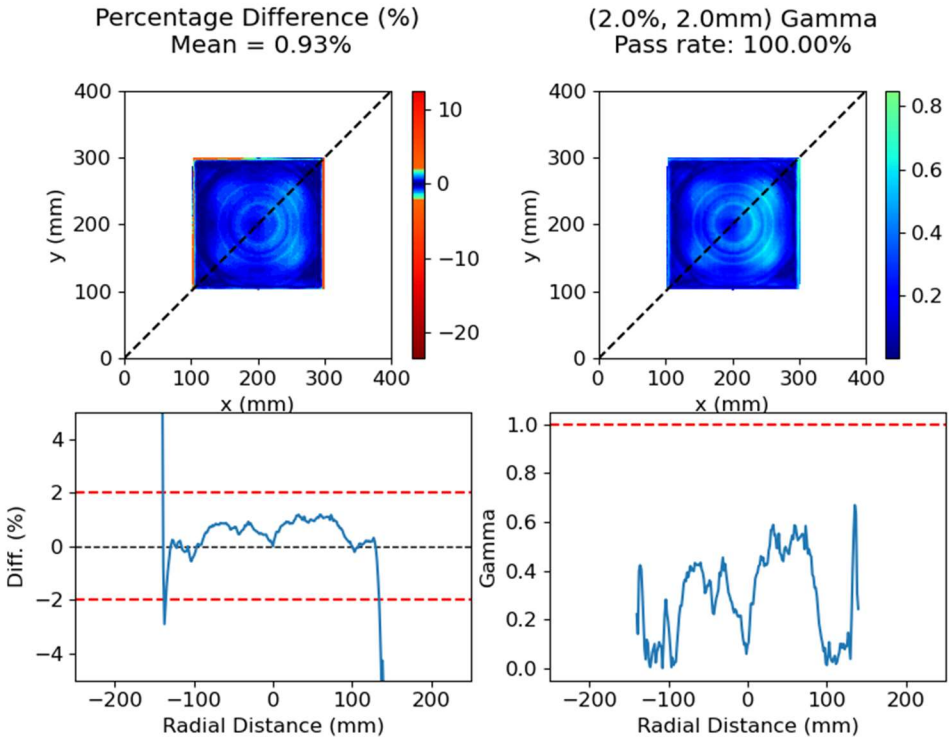

Fig. 16-6 (2.0 %, 2.0 mm) Gamma analysis for a 20.0 x 20.0 cm normalised field using the 5cm Water + 5cm Lead EPID model, with extraction at 3.6 cm.

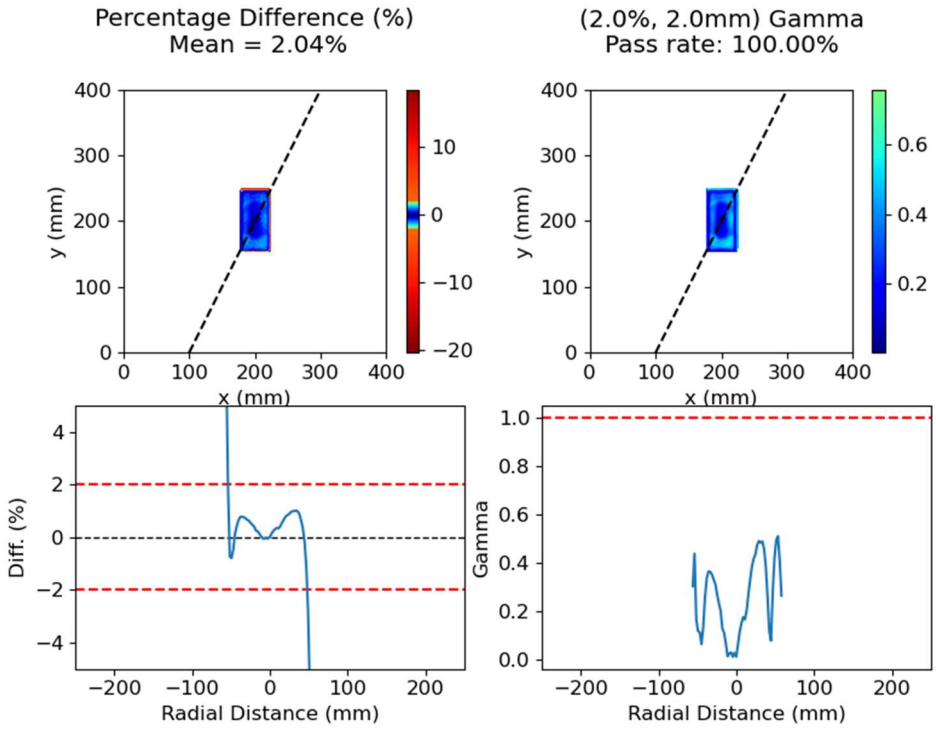

Fig. 16-7 (2.0 %, 2.0 mm) Gamma analysis for a 5.0 x 10.0 cm normalised field using the 5cm Water + 5cm Lead EPID model, with extraction at 3.6 cm.

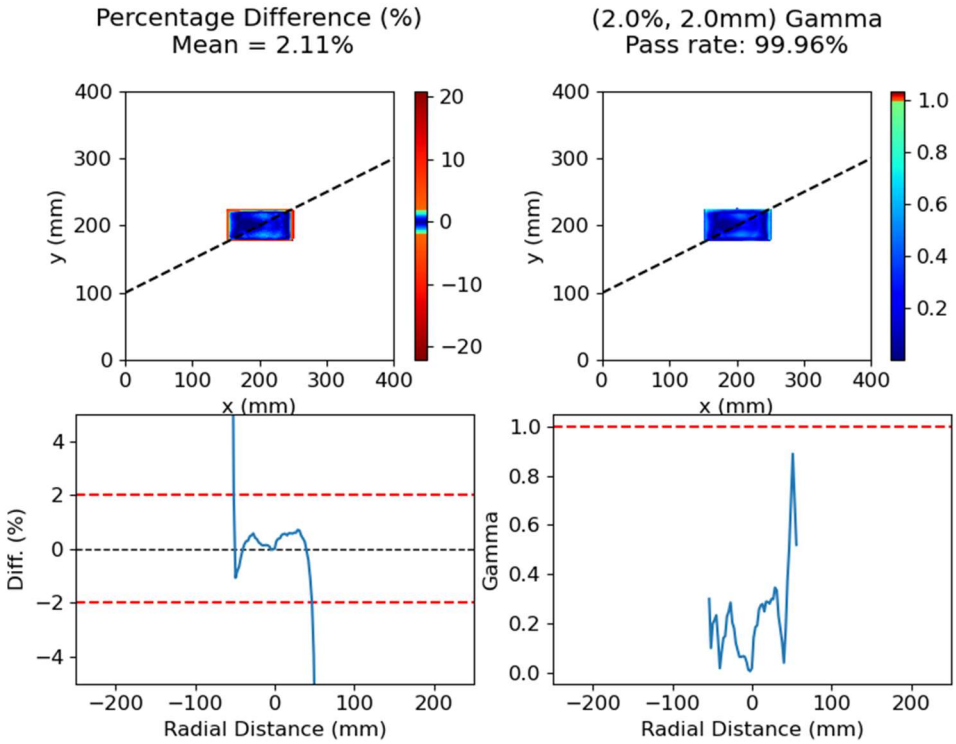

Fig. 16-8 (2.0 %, 2.0 mm) Gamma analysis for a 10.0 x 5.0 cm normalised field using the 5cm Water + 5cm Lead EPID model, with extraction at 3.6 cm.

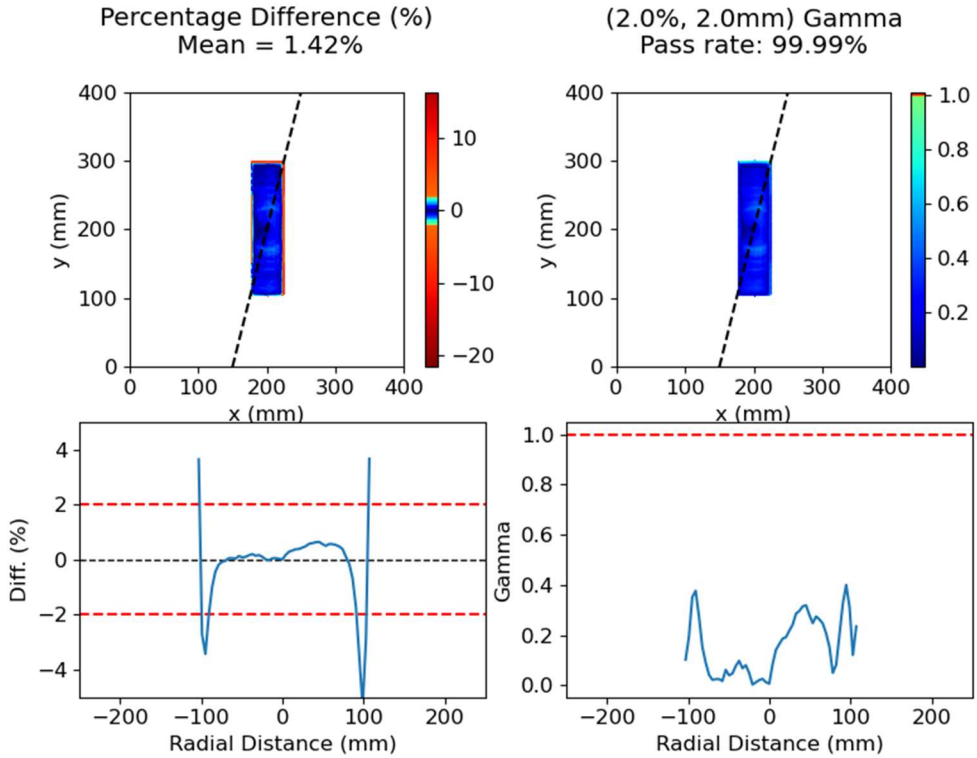

Fig. 16-9 (2.0 %, 2.0 mm) Gamma analysis for a 5.0 x 20.0 cm normalised field using the 5cm Water + 5cm Lead EPID model, with extraction at 3.6 cm.

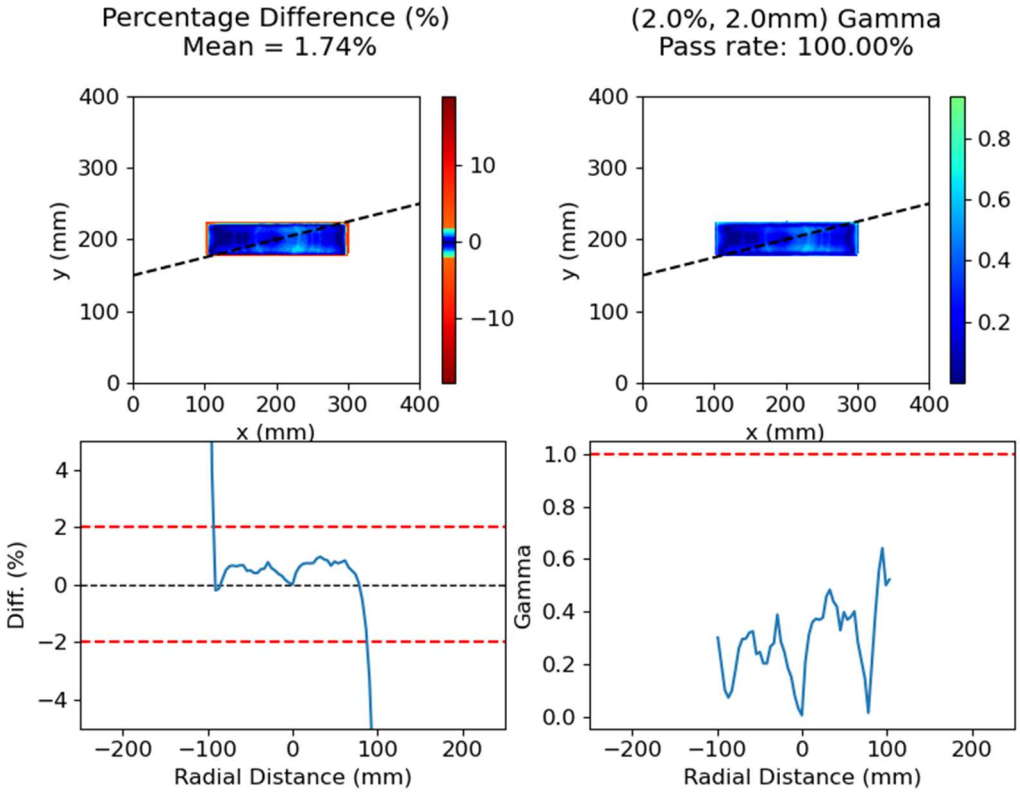

Fig. 16-10 (2.0 %, 2.0 mm) Gamma analysis for a 20.0 x 5.0 cm normalised field using the 5cm Water + 5cm Lead EPID model, with extraction at 3.6 cm.

The 2D gamma analysis shown in **Fig. *16*** demonstrates the model's ability to predict non-transit EPIs at 100cm SID. Similar pass rates were achieved for transposed rectangular fields, suggesting no backscatter correction factor needs to be applied to account for field asymmetry. The percentage difference maps show a 'ringing' pattern, likely due to the assumption that the radial beam profile correction obtained has no angular dependence.

4.3.2.2. Gamma Analysis at 150 cm SID

A non-transit (2.0 %, 2.0 mm) gamma analysis test was also conducted on the corrected dataset at 150 cm SID, as shown in **Fig. 17**. The percentage gamma pass rate, excluding doses less than 10.0% of the global maximum, was calculated as well as the mean percentage difference within the fields. The model proved to be reliable when used for non-transit dosimetry at 150 cm SID, yielding gamma pass rates of 100% for all square and rectangle fields, excluding the 20 x 20 cm field (99.98%).

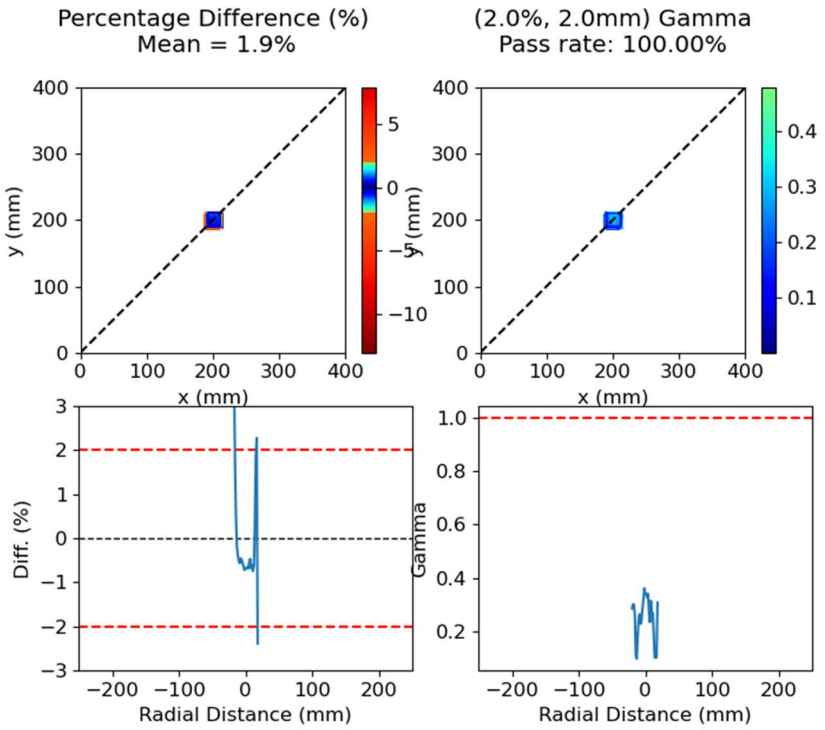

Fig. 17-1 Non-transit (2.0 %, 2.0 mm) Gamma analysis for a 2.0 x 2.0 cm, non-normalised, field using the 5cm Water + 4cm Lead EPID model at 150 cm SID

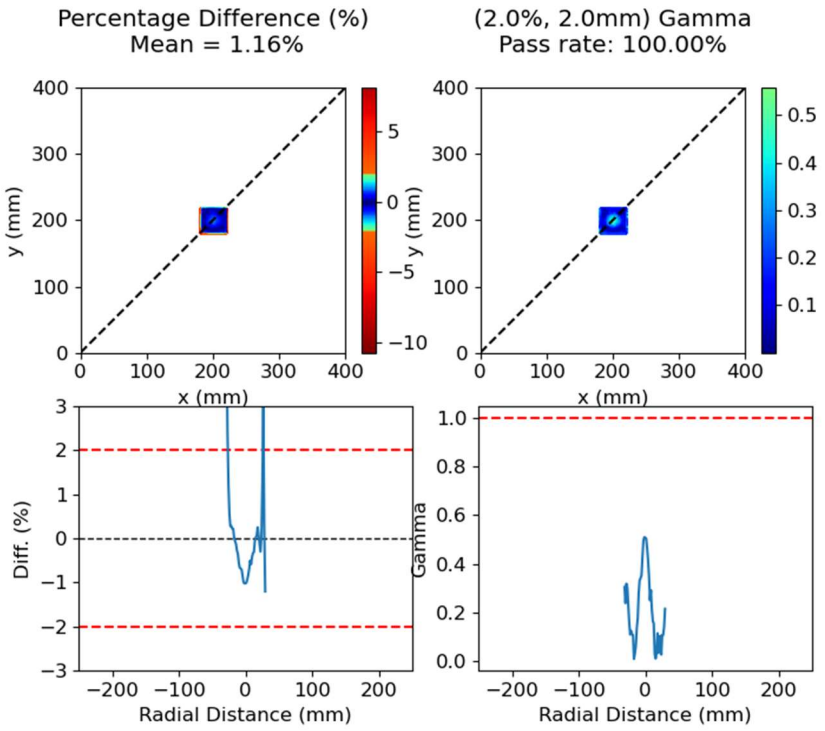

Fig. 17-2 Non-transit (2.0 %, 2.0 mm) Gamma analysis for a 3.0 x 3.0 cm, non-normalised, field using the 5cm Water + 4cm Lead EPID model at 150 cm SID

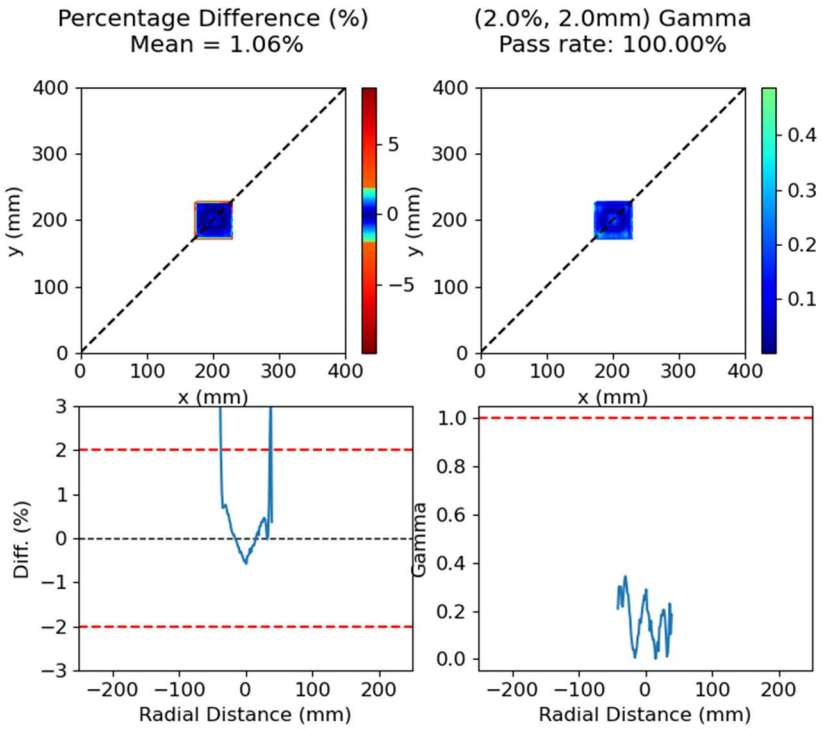

Fig. 17-3 Non-transit (2.0 %, 2.0 mm) Gamma analysis for a 4.0 x 4.0 cm, non-normalised, field using the 5cm Water + 4cm Lead EPID model at 150 cm SID

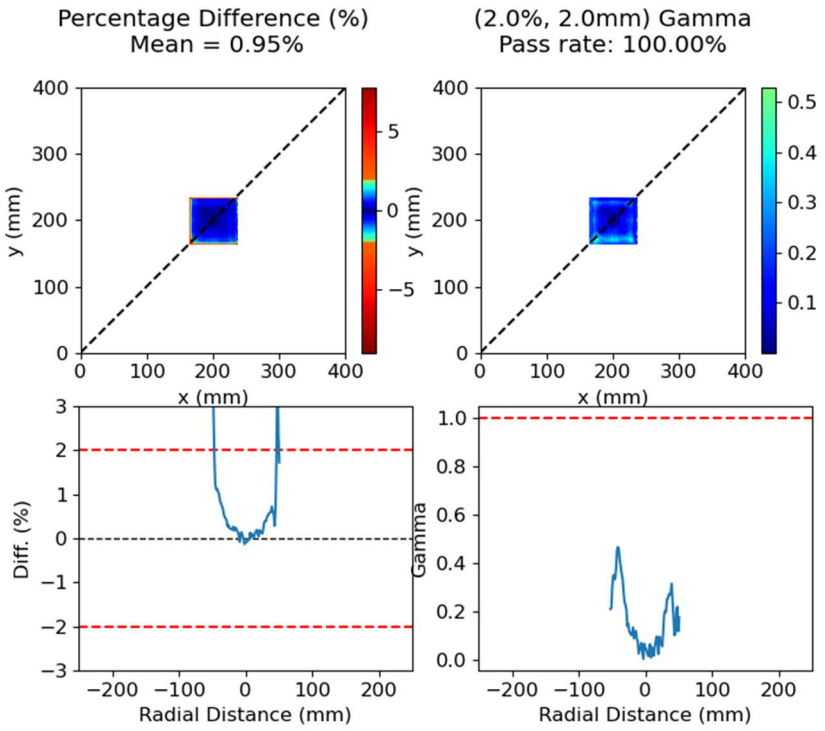

Fig. 17-4 Non-transit (2.0 %, 2.0 mm) Gamma analysis for a 5.0 x 5.0 cm, non-normalised, field using the 5cm Water + 4cm Lead EPID model at 150 cm SID

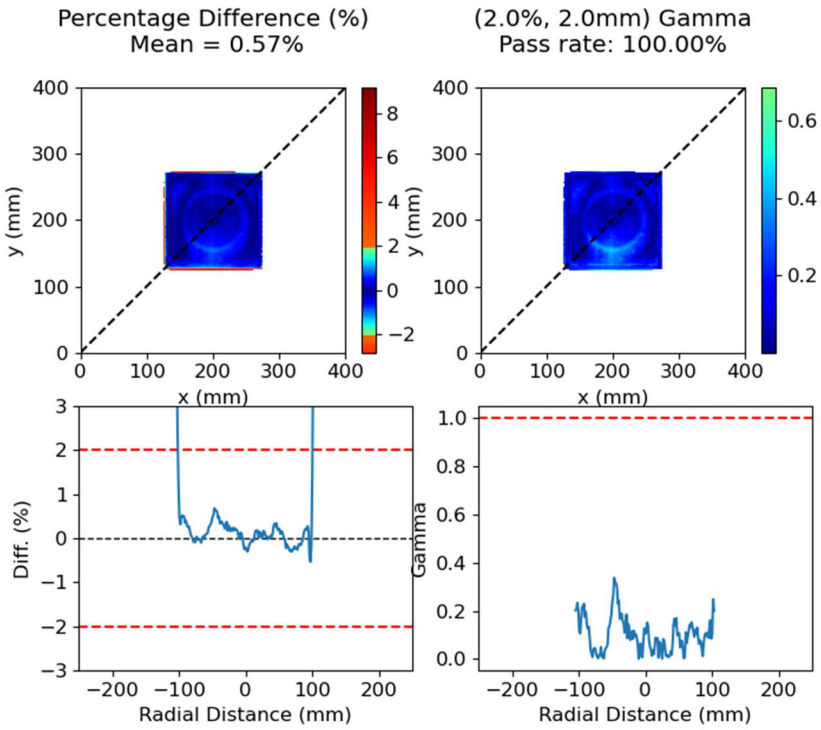

Fig. 17-5 Non-transit (2.0 %, 2.0 mm) Gamma analysis for a 10.0 x 10.0 cm, non-normalised, field using the 5cm Water + 4cm Lead EPID model at 150 cm SID

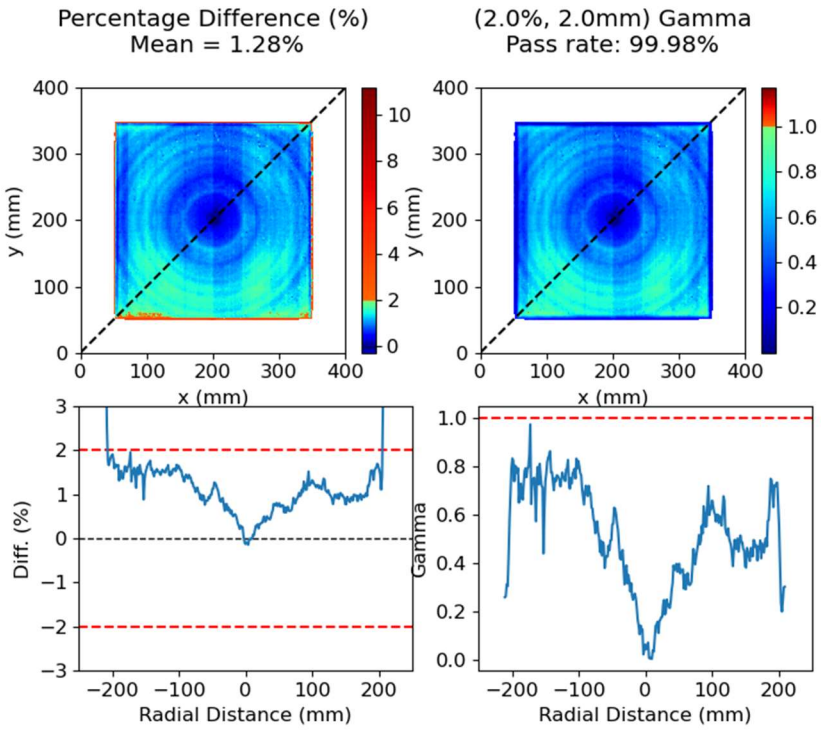

Fig. 17-6 Non-transit (2.0 %, 2.0 mm) Gamma analysis for a 20.0 x 20.0 cm, non-normalised, field using the 5cm Water + 4cm Lead EPID model at 150 cm SID

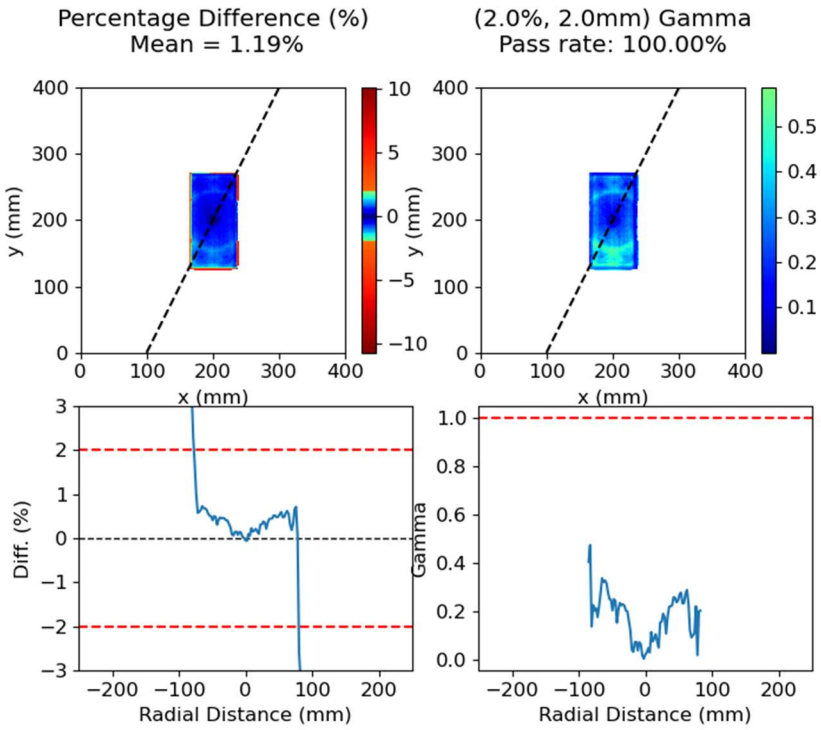

Fig. 17-7 Non-transit (2.0 %, 2.0 mm) Gamma analysis for a 5.0 x 10.0 cm, non-normalised, field using the 5cm Water + 4cm Lead EPID model at 150 cm SID

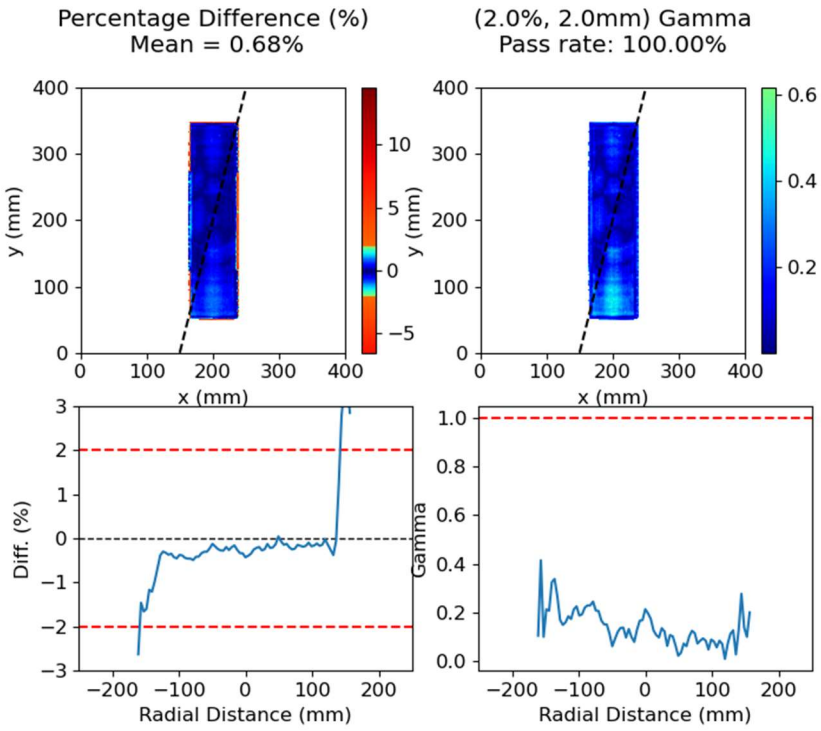

Fig. 17-8 Non-transit (2.0 %, 2.0 mm) Gamma analysis for a 5.0 x 20.0 cm, non-normalised, field using the 5cm Water + 4cm Lead EPID model at 150 cm SID

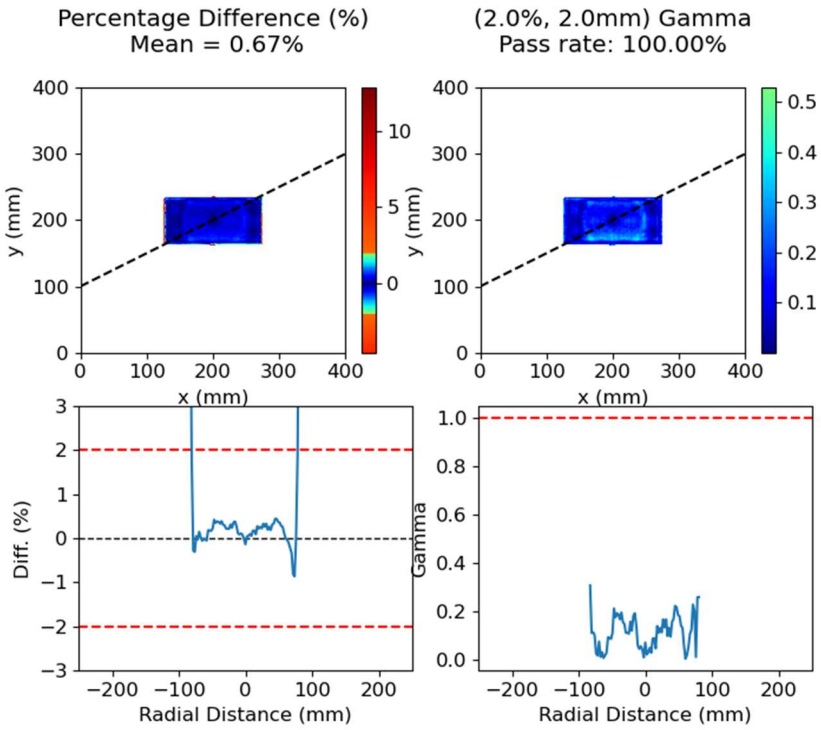

Fig. 17-9 Non-transit (2.0 %, 2.0 mm) Gamma analysis for a 10.0 x 5.0 cm, non-normalised, field using the 5cm Water + 4cm Lead EPID model at 150 cm SID

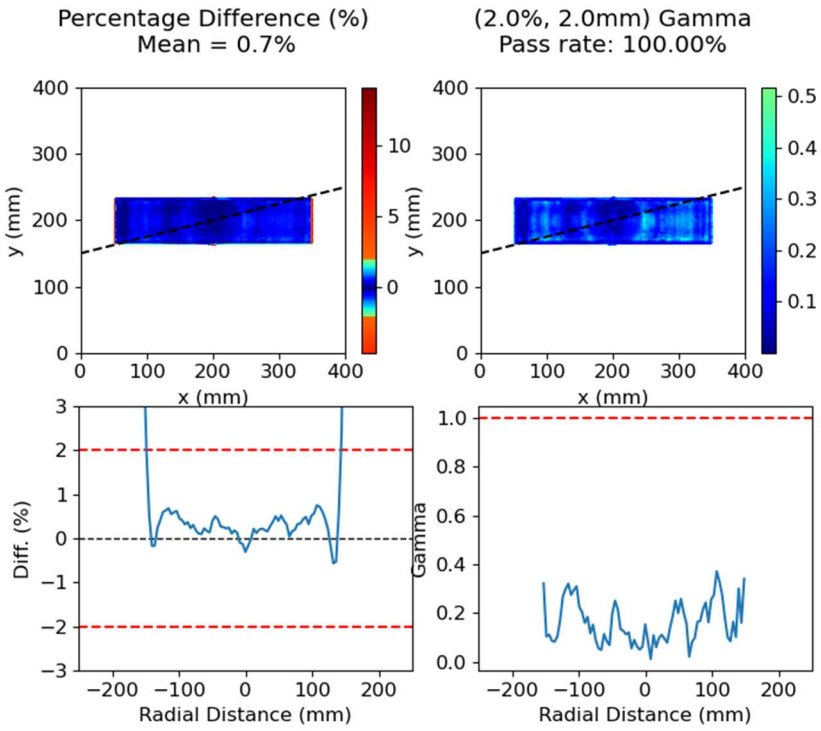

Fig. 17-10 Non-transit (2.0 %, 2.0 mm) Gamma analysis for a 20.0 x 5.0 cm, non-normalised, field using the 5cm Water + 4cm Lead EPID model at 150 cm SID

4.3.3. Transit Dosimetry

The TPS model's ability to predict measured transit EPIs was then investigated by introducing a 10 cm thick slab of solid water at isocentre. Output factors and CAX doses are shown below in

Fig. **18**. Significant differences in CAX dose of up to -9.5% were observed, indicating that the TPS algorithm systematically over-estimated the measured signal.

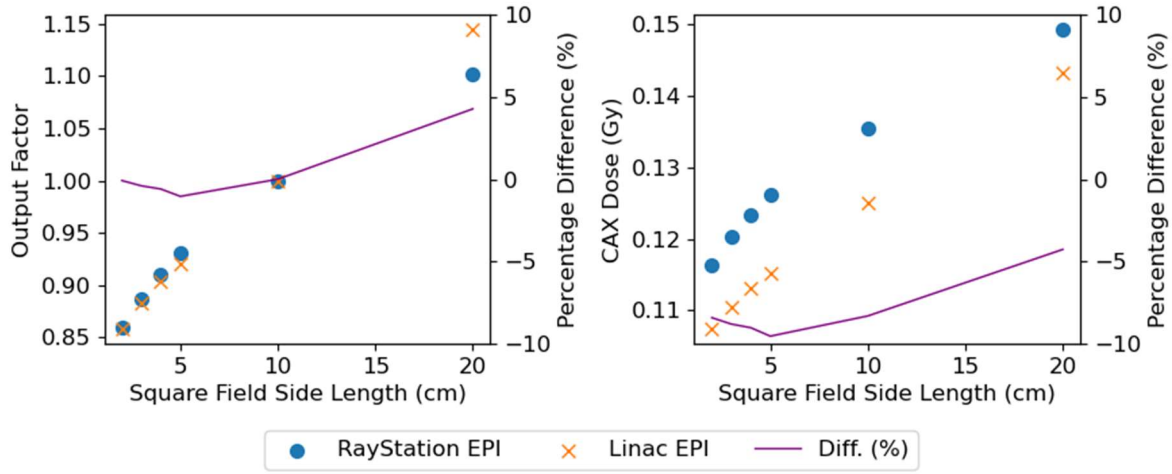

Fig. 18 Output factors and CAX dose for predictions at 150 cm SID with 10 cm PMMA phantom

In addition to poor agreement of output factors when introducing a 10 cm phantom to the beam, **Fig. *19*** also shows that the overall shape of the beam profiles was not in agreement. This is likely due to the model's response to scattered radiation, as the TPS has not been commissioned to predict exit dose at a distance of 150 cm from the source. Measured EPIs are much less uniform across the square fields and decrease radially beyond ~2.5 cm from the isocenter.

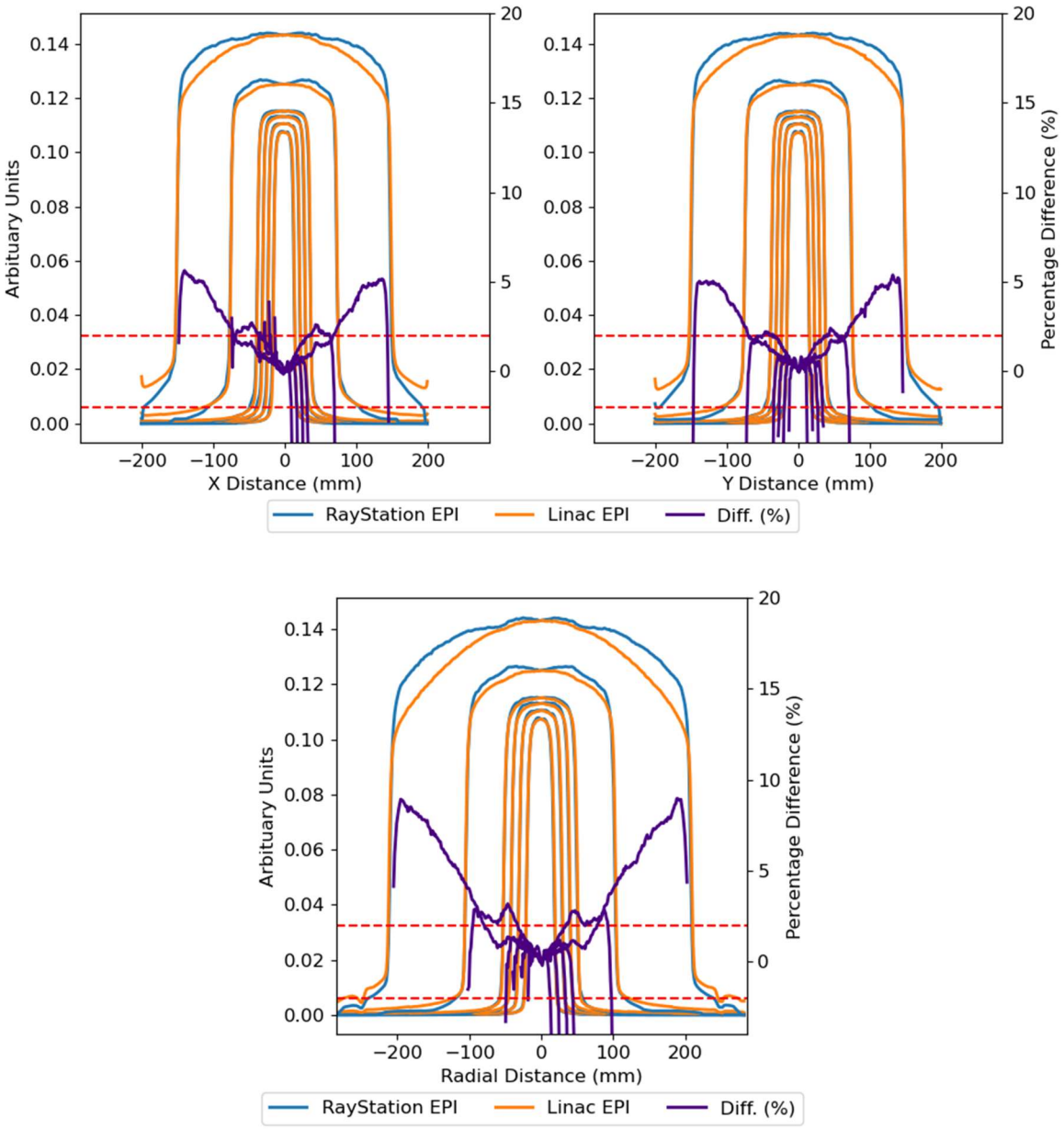

Fig. 19 Normalised beam profiles for transit dosimetry setup with a 10 cm phantom.

To further explore the significant decrease in agreement in transit beam setups, a wider range of PMMA slab thicknesses were utilised. **Fig. *20*** shows the percentage difference along the central axis of various square fields, with varying PMMA slab thicknesses. The agreement in CAX dose progressively worsens for both increasing field size as well as increasing phantom thickness, with the exception of the 10 x 10 and 20 x 20 square fields with a 20 cm phantom. This indicates that the model needs further corrections to account for scattered photons, as the amount of scatter also increases with field size and phantom thickness.

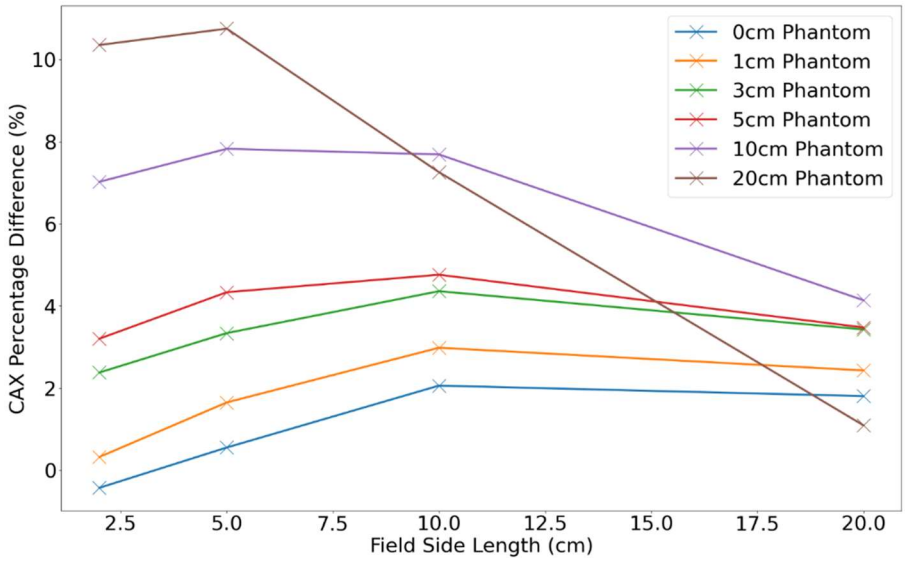

Fig. 20 Percentage difference between measured and calculated CAX dose vs square field sizes for various PMMA slab thicknesses.

4.3.3.1. Gamma Analysis at 150 cm SID

A normalised (2.0 %, 2.0 mm) gamma analysis was conducted on the corrected transit dataset, as shown in **Fig. *21***. The percentage gamma pass rate, excluding doses less than 10.0% of the global maximum, was calculated as well as the mean percentage difference within the fields. The model proved to be reliable when used for non-transit dosimetry at 150 cm SID with smaller fields (i.e., <5 cm side length) however begins to deteriorate with increasing field size.

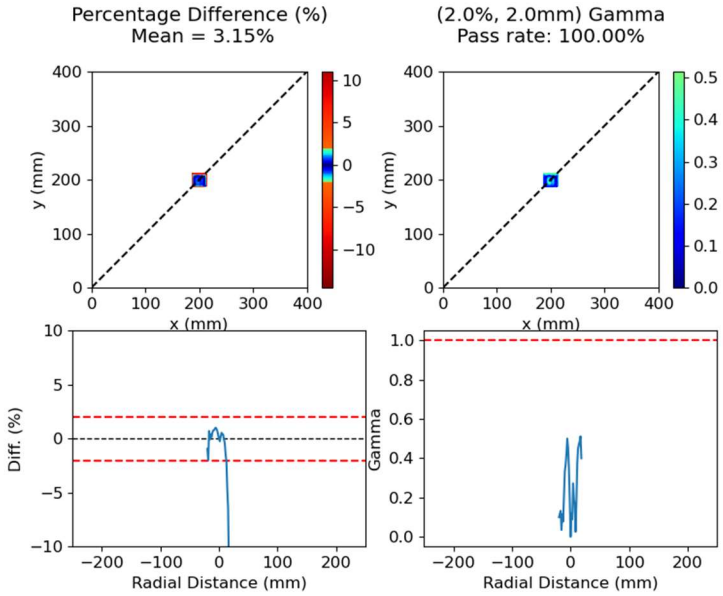

Fig. 21-1 Normalised (2.0 %, 2.0 mm) gamma analysis test for a 2.0 x 2.0 cm field, with a 150 cm SID and a 10 cm PMMA slab at 95 cm SSD.

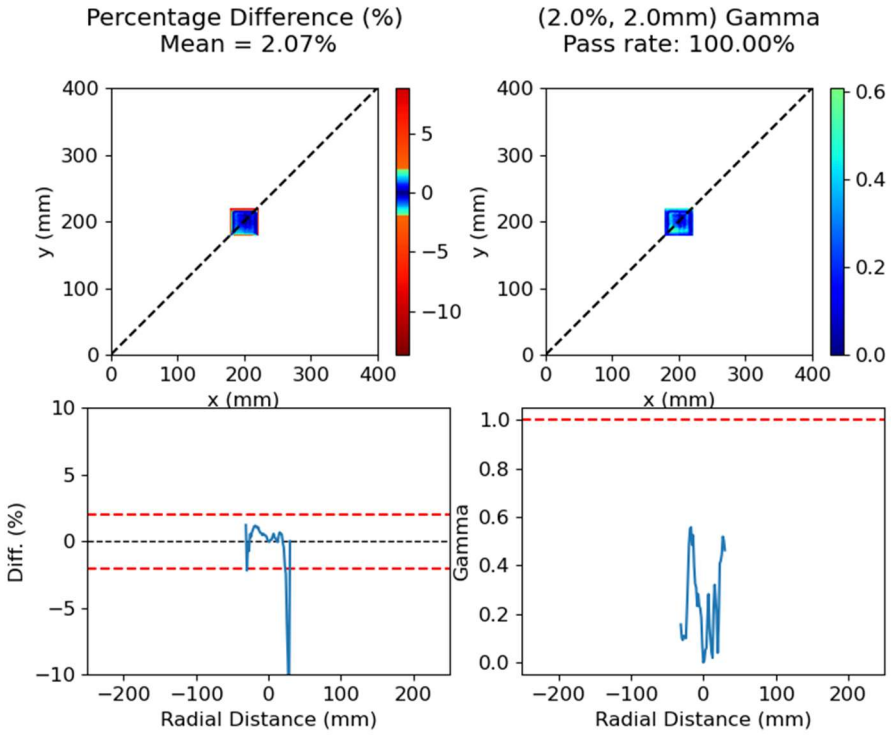

Fig. 21-2 Normalised (2.0 %, 2.0 mm) gamma analysis test for a 3.0 x 3.0 cm field, with a 150 cm SID and a 10 cm PMMA slab at 95 cm SSD.

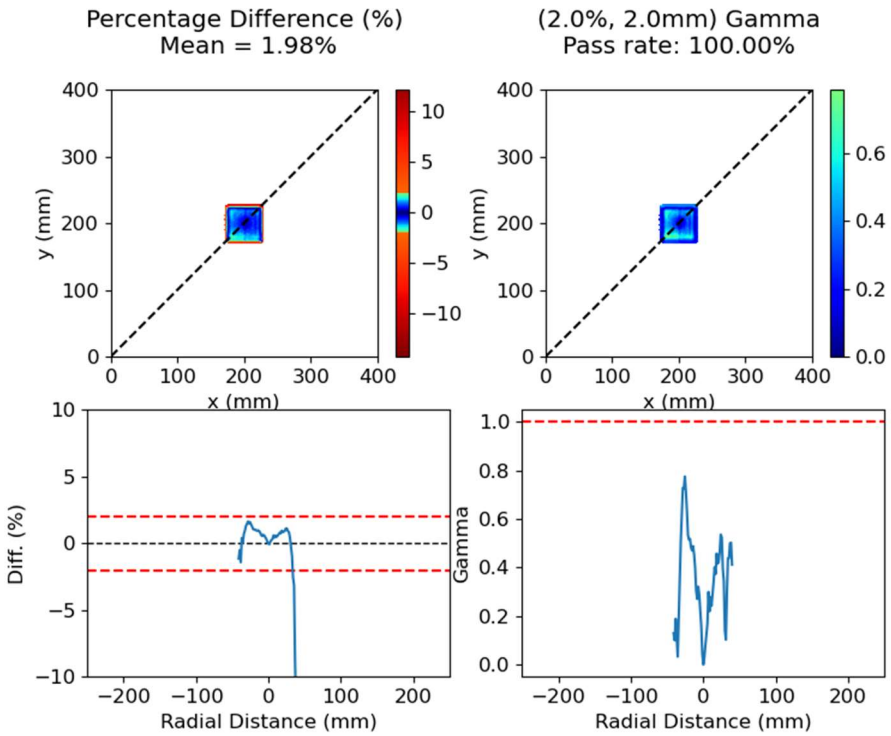

Fig. 21-3 Normalised (2.0 %, 2.0 mm) gamma analysis test for a 4.0 x 4.0 cm field, with a 150 cm SID and a 10 cm PMMA slab at 95 cm SSD.

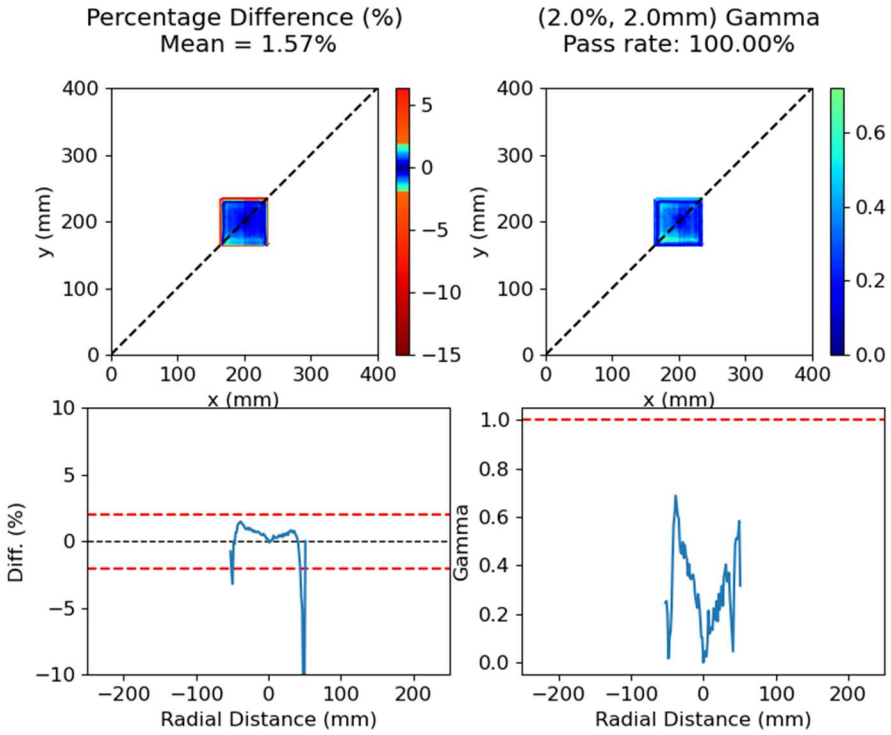

Fig. 21-4 Normalised (2.0 %, 2.0 mm) gamma analysis test for a 5.0 x 5.0 cm field, with a 150 cm SID and a 10 cm PMMA slab at 95 cm SSD.

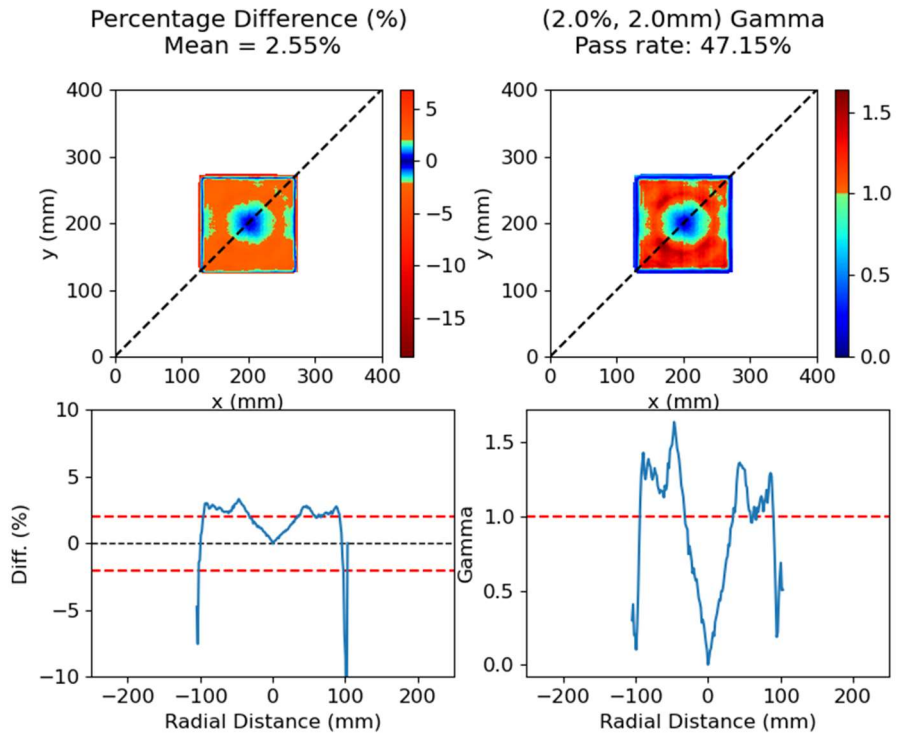

Fig. 21-5 Normalised (2.0 %, 2.0 mm) gamma analysis test for a 10.0 x 10.0 cm field, with a 150 cm SID and a 10 cm PMMA slab at 95 cm SSD.

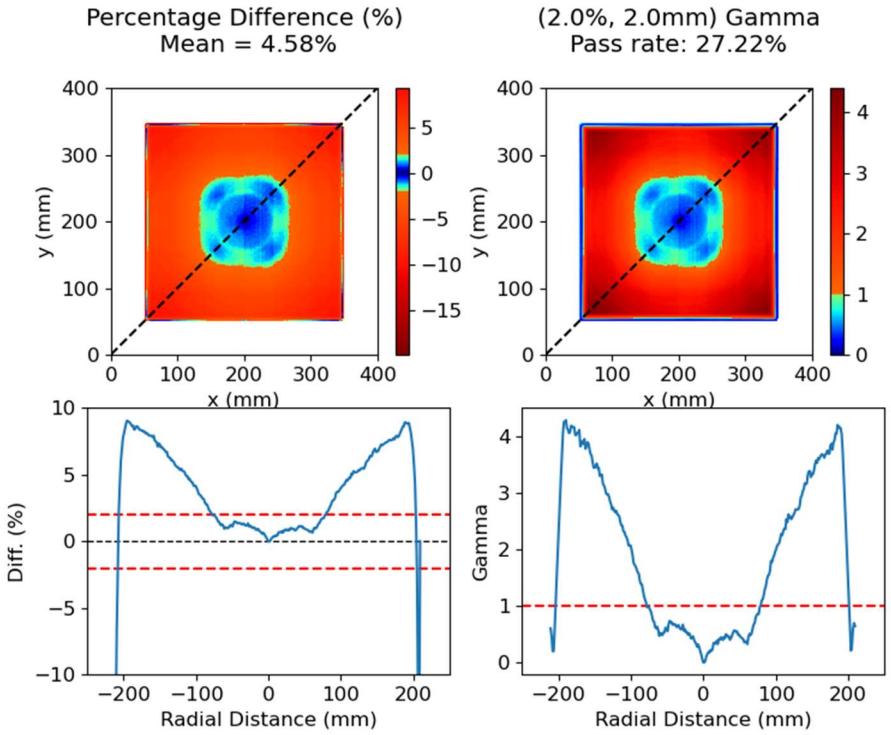

Fig. 21-6 Normalised (2.0 %, 2.0 mm) gamma analysis test for a 20.0 x 20.0 cm field, with a 150 cm SID and a 10 cm PMMA slab at 95 cm SSD.

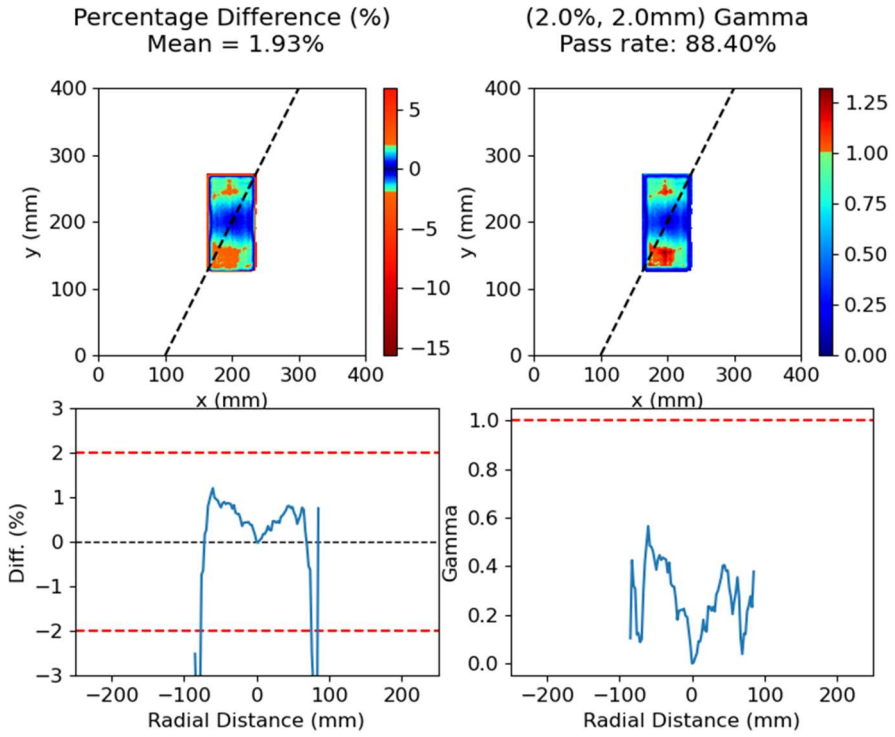

Fig. 21-7 Normalised (2.0 %, 2.0 mm) gamma analysis test for a 5.0 x 10.0 cm field, with a 150 cm SID and a 10 cm PMMA slab at 95 cm SSD.

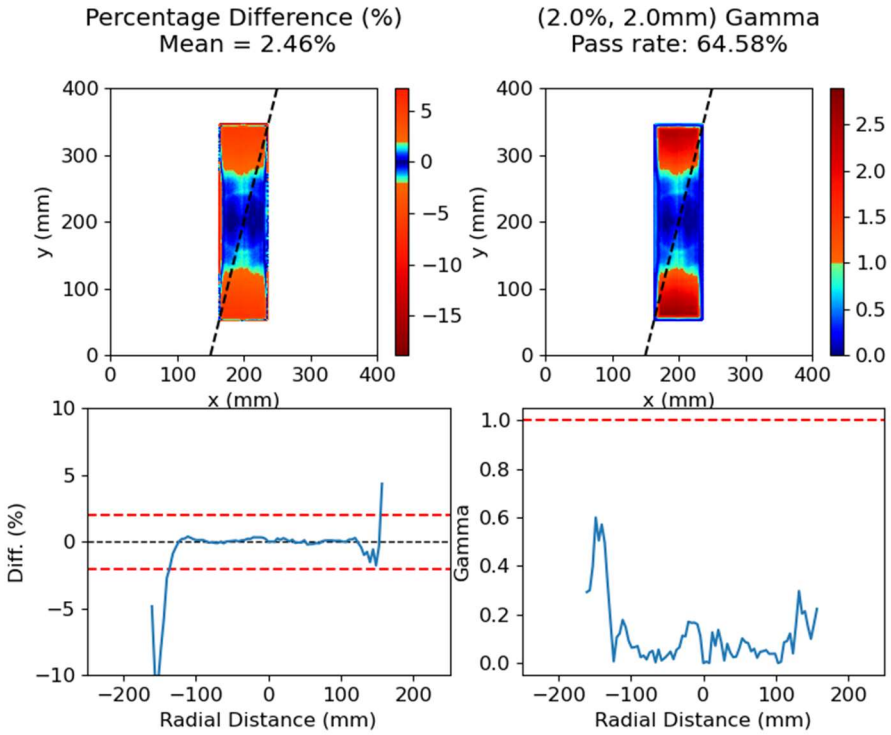

Fig. 21-8 Normalised (2.0 %, 2.0 mm) gamma analysis test for a 5.0 x 20.0 cm field, with a 150 cm SID and a 10 cm PMMA slab at 95 cm SSD.

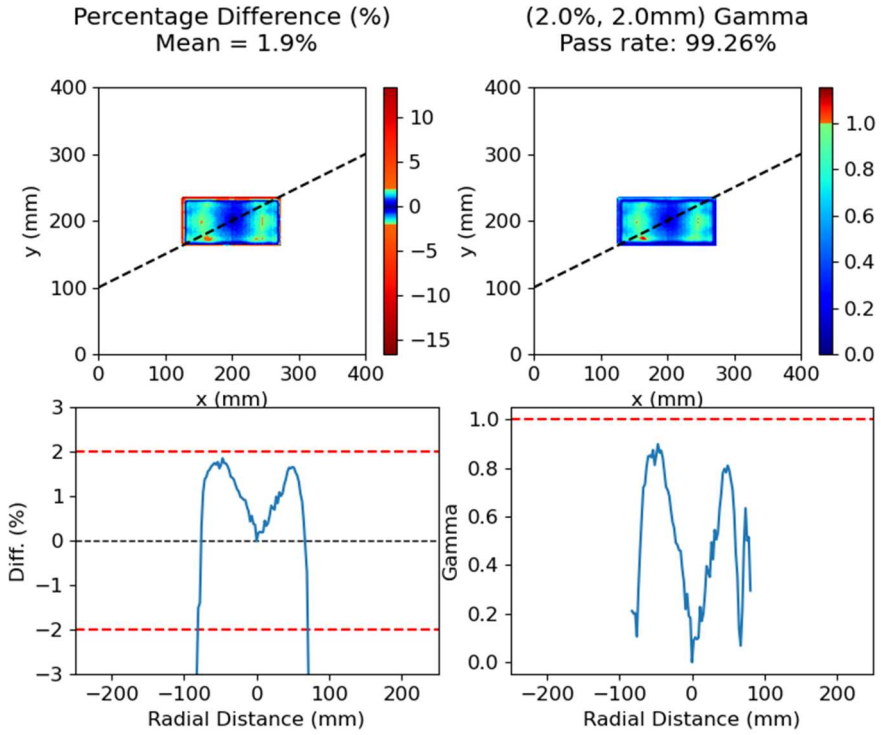

Fig. 21-9 Normalised (2.0 %, 2.0 mm) gamma analysis test for a 10.0 x 5.0 cm field, with a 150 cm SID and a 10 cm PMMA slab at 95 cm SSD.

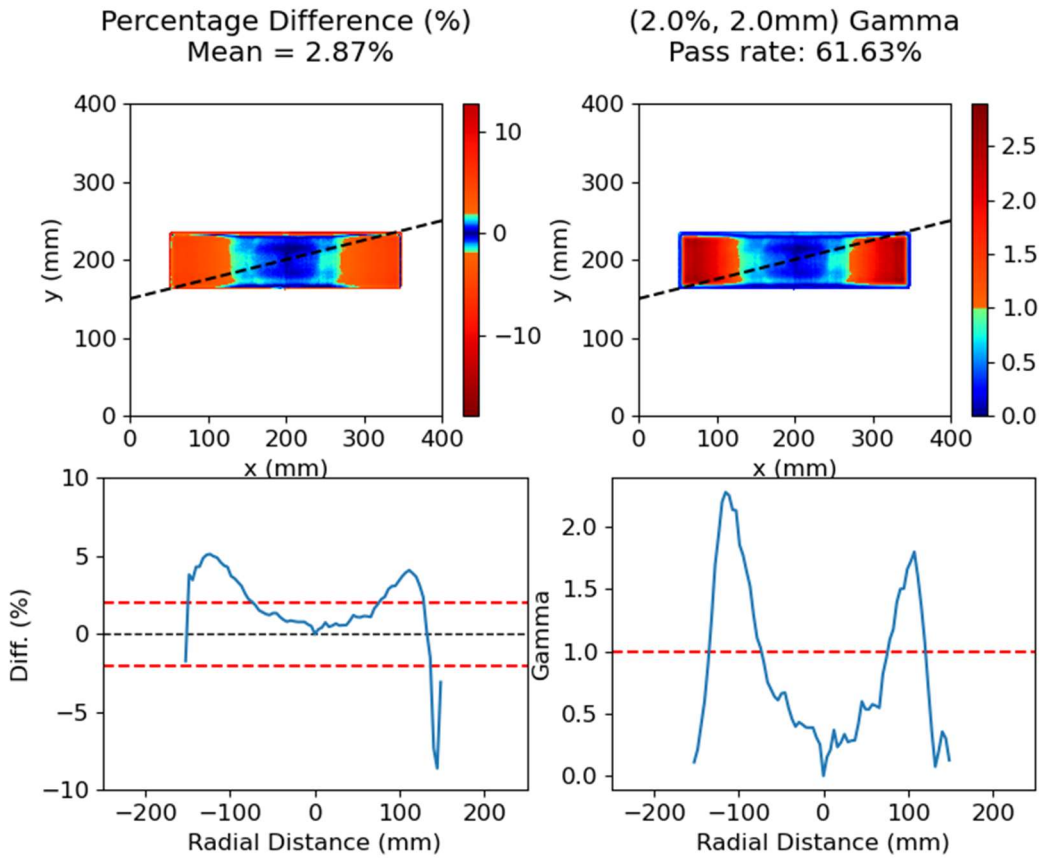

Fig. 21-10 Normalised (2.0 %, 2.0 mm) gamma analysis test for a 20.0 x 5.0 cm field, with a 150 cm SID and a 10 cm PMMA slab at 95 cm SSD.

Normalised gamma pass rates of 100 % were achieved for all square fields below 5 cm in side length, however upon closer inspection it was noted that a steep, undesirable, 'V-shaped' diagonal profile of percentage difference and gamma values were present.

As expected, the non-normalised data combines the lack of agreement in CAX dose with the lack of agreement in beam profile shape and thus also yields poor gamma analysis results, as summarised in **Fig. *22***.

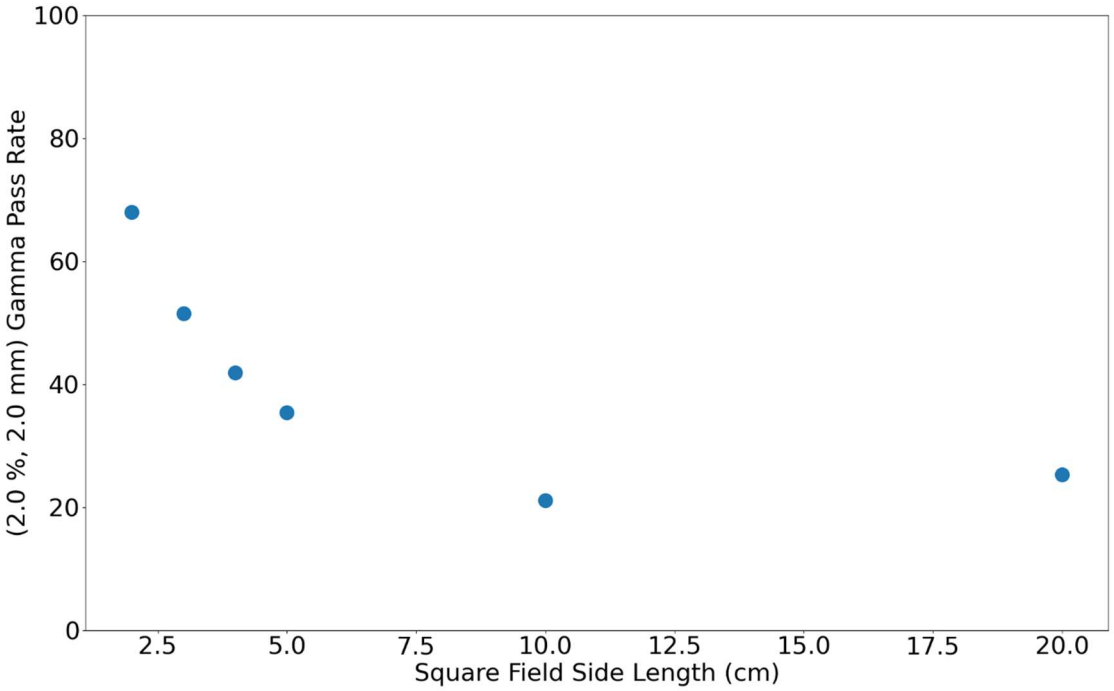

Fig. 22 (2.0 %, 2.0 mm) Gamma analysis pass rates for a non-normalised transit dosimetry setup

Table 1: Summary of all (2.0 %, 2.0 mm) gamma pass rates

Field Size (cm x cm)	Normalised, non-transit pass rate (%) at 100 cm SID	Non-transit pass rate (%) at 150cm SID	Normalised transit pass rate (%) at 150cm SID	Transit pass rate (%) at 150cm SID
2x2	100	100	100	61.28
3x3	100	100	100	43.96
4x4	100	100	100	34.29
5x5	100	100	100	27.44
10x10	100	100	47.15	15.97
20x20	100	99.98	27.22	8.37
5x10	100	100	88.40	22.77
10x5	99.96	100	99.26	21.35
5x20	99.99	100	64.58	19.09
20x5	100	100	61.63	17.59

4.3.4. Change in Dosimetry Validation

Change in transit dosimetry for three clinically relevant scenarios was further explored to validate the model's capability of predicting *change* in transit EPIs, relative to a baseline treatment fraction.

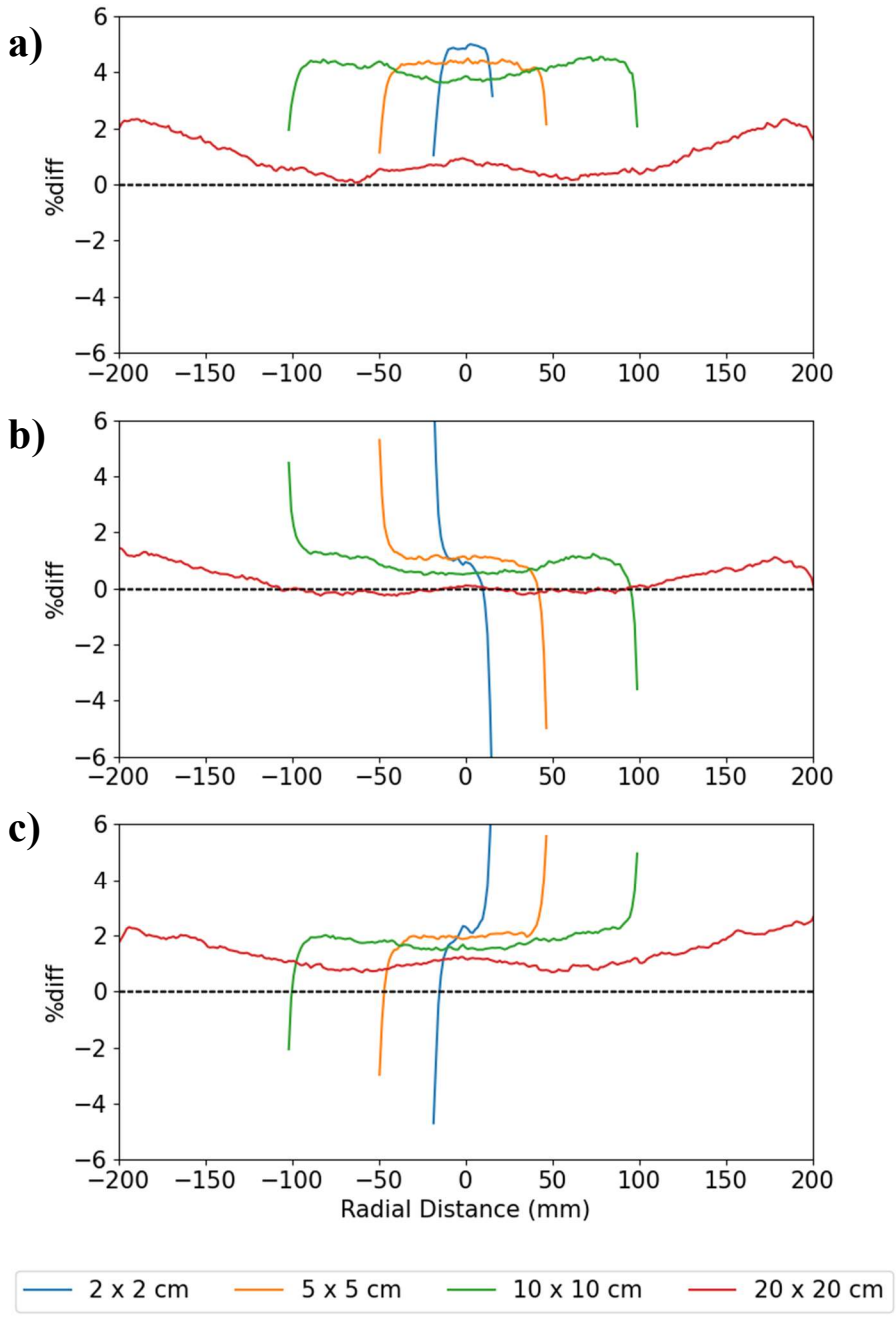

Fig. 23 Percentage difference between change in predicted and calculated EPIs for various square fields to assess validation of change in transit dosimetry for three cases: a) Extreme (10 to 5 cm), b) Moderate (5 to 3 cm), c) Moderate (3 to 1 cm).

Within the field, the percentage differences were <5% for all square field sizes for the extreme case (5 cm reduction), and <2% for both moderate cases (2 cm reduction), as shown in **Fig. 23**. It is noted that the raw percentage difference values are typically greater than zero, indicating that the model over-estimates change in EPIs between two fractions. This indicates that either the model will have a lower specificity in comparison to measured EPIs, or that change in measured EPIs may have a lower sensitivity than change in predicted EPIs. Nonetheless, the model will be more prone to fail a gamma analysis between two predicted fractions compared to those measured and can thus be used as a useful tool for early detection of change. Moreover, the agreement between change in measured and change in predicted EPIs was shown to improve with increasing field size. It can also be noted that there is a sharp increase in percentage difference towards the edge of the fields in **Fig. 23** b) and c) due to a misalignment between the fields with varying phantom thicknesses. This error could not be resolved as the misalignment was less than the resolution of the exported EPI.

Overall, the model has shown to be useful in predicting *change* in EPIs for even large changes in phantom thicknesses between 40 and 67%. This is further investigated in Chapter 5.

4.4. Discussion

The in-house toolkit developed for non-transit dosimetry at 100 and 150 cm SID was validated through the comparative analysis detailed in section 4.3. The (2.0 %, 2.0 mm) gamma pass rates were all above 99.96% at 100 cm SID and 99.98% at 150 cm SID.

When validating the model for transit dosimetry, however, the model's agreement worsened significantly, generating non-normalised gamma pass rates as low as 8.37%, with an average of 27.2% for all square and rectangular fields. In the transit dosimetry beam setup, the non-normalised predicted EPIs had a significantly sharper penumbra than those measured, with typical variations within the umbral region of ~8% as opposed to ~13% respectively. Moreover, CAX doses varied by up to -9.5% although improved with increasing field size. Analysis of the output factors showed fields smaller than 10 x 10 were being over-approximated relative to the 10 x 10 field, whereas the 20 x 20 field was under-approximated. This agrees with the hypothesis that the EPID panel tends to over-respond to lower energy, scattered photons.

The methodology described by Nilsson et al. [33] showed promising transit results with a 10 cm phantom, giving mean absolute percentage differences of 0.26%, 0.54%, and 1.04% for square fields with side lengths of 5, 10, and 20 cm respectively. When compared to measured EPIs by Nilsson et al., the normalised predicted x-profiles in this work yielded mean absolute percentage differences of 0.66%, and 0.88% for square fields of side length 10 and 20 cm respectively. Contrastingly, when compared to normalised measured x-profiles in this work, mean absolute percentage differences of 1.69 %, and 2.71% were obtained. This indicates that the predicted EPIs may be better matched to the measured EPIs taken by Nilsson et al. [33] as opposed to those in this work. This may be due to the different construction of EPIDs between that in this work and Nilsson et al.'s. Further work could thus be taken to better tailor the prediction algorithm to specific devices, potentially utilising a correction factor characteristic to a treatment suite's EPID. This could include device-specific output-factor correction or optimised detector kernel convolution as described in Nilsson et al.'s work [33].

As briefly discussed in 4.3.2, the aS1200 EPID installed has an inherent energy dependence, and will tend to over-respond to lower energies [8, 37-39]. This is particularly problematic for transit dosimetry as scattered photons will have lower energy than the primary beam and will thus lead to a wider range of photon energy reaching the panel [40]. An additional correction factor could thus be developed to help simulate this energy dependence into the EPID model in the future. One method for this correction could include obtaining a 2D distribution of effective energy reaching each pixel within the EPID and applying a corresponding correction factor to the signal intensity for the given energy. Applying this correction in the clinic, however, may have unintended consequences due to the significant difference between a non-homogenous patient and a slab of PMMA. Photons delivered via a 6 MV treatment plan are expected to predominantly interact through Compton scatter. This interaction pathway is highly dependent on geometry and thus applying any correction factor based on the intensity of these photons should ideally be obtained in the clinical setup, utilising *a priori* patient thicknesses and densities via planning CT or on-the-day CBCT scans.

Finally, a graphical user interface (GUI) was also developed to allow for efficient comparison between predicted and measured EPIs in the clinic, without the need for background knowledge in programming. The GUI was written using the programming language Python v3.8, utilising the PyQt5

framework, and allows the user to observe EPIs via 2D dose distribution maps and beam profiles, as well as conduct gamma analysis to assess the pass rate, and view trends of these gamma parameters over time. Further details of the GUI developed can be found in Appendix A.

Overall, although further work is required to better validate the model's ability to predict absolute transit dosimetry, the model showed improvements in its ability of predicting *change* in transit dosimetry relative to some baseline. In the context of the clinic, this could very well still provide a useful means to prompt the user to consider an adaptive replan of a specific patient's treatment. The following chapter, and published manuscript, thus aims to explore the correlation between this predicted change in transit fluence with some change in dose volume histogram metrics relating to patient specific dosimetry.

5. Relative Transit Dosimetry in the Context of Dosimetry

The following manuscript was published in the Physical and Engineering Science in Medicine (PESM) Journal:

G. Antoniou, and S.N. Penfold, "A novel TPS toolkit to assess correlation between transit fluence dosimetry and DVH metrics for adaptive head and neck radiotherapy", *Physical and Engineering Sciences in Medicine*, vol. 44, pp. 1121 – 1130.

5.1. Contextual Statement

This manuscript details the development of a tool used to explore the correlation between transit fluence, as measured at an electronic portal imaging device (EPID), and dose volume histogram (DVH) metrics to target and organs-at-risk (OAR) structures in a simulated environment for VMAT treatment plans of H&N cancers. Other work conducted on assessing if transit dosimetry is viable as a trigger for adaptive radiotherapy were briefly discussed in the introduction of the manuscript. A novel fluence projection mask was also developed to assess change in transit dosimetry, however no statistical difference in the correlation coefficient were identified when this mask was applied. Strong correlations were observed with planning target volume (PTV) data, whereas only weak correlations were observed for the spinal cord data. Future directions of this work include conducting analysis on weekly CBCT scans to obtain progressive data and thus determine a suitable mean percentage difference action limit, as well as conducting analysis on EPIs obtained in *cine* mode rather than on a single integrated image.

5.2. Statement of Authorship

5.2.1. Conceptualisation

The idea to move towards a *relative* transit dosimetry simulation tool originated from A/Prof. Scott Penfold. The idea of creating a fluence projection mask originated from A/Prof. Scott Penfold. The tool and its methods were conceived by George Antoniou under supervision of A/Prof. Scott Penfold.

5.2.2. Realisation

George Antoniou, under the supervision of A/Prof. Scott Penfold, developed the tool. This included writing the code for extracting transit fluence from the treatment planning system, writing the code for creating an intra-angle fluence projection mask, analysed the data, and visualised the data in the form of regression plots.

5.2.3. Documentation

The manuscript was written by George Antoniou, as well as the figures submitted. A/Prof. Scott Penfold reviewed the manuscript on multiple occasions providing feedback and revisions where needed.

Statement of Authorship

Title of Paper	A Novel TPS Toolkit to Assess Correlation between Transit Fluence Dosimetry and DVH Metrics for Adaptive Head and Neck Radiotherapy
Publication Status	☒ Published ☐ Accepted for Publication ☐ Submitted for Publication ☐ Unpublished and Unsubmitted w ork w ritten in manuscript style
Publication Details	Antoniou, G & Penfold, S.N. 2021, 'A novel TPS toolkit to assess correlation between transit fluence dosimetry and DVH metrics for adaptive head and neck radiotherapy', Physical and Engineering Sciences in Medicine, vol. 44, pp. 1121 - 1130.

Principal Author

Name of Principal Author (Candidate)	George Antoniou		
Contribution to the Paper	Tool and method conceived and developed by George Antoniou under the supervision of A/Prof. Scott Penfold. This included writing the code for extracting transit fluence from the TPS, writing the code for creating an intra-angle fluence projection mask, analysed the data, and visualised the data in the form of regression plots. Manuscript written by George Antoniou as well as figures submitted.		
Overall percentage (%)	70%		
Certification:	This paper reports on original research I conducted during the period of my Higher Degree by Research candidature and is not subject to any obligations or contractual agreements with a third party that would constrain its inclusion in this thesis. I am the primary author of this paper.		
Signature		Date	23/02/2022

Co-Author Contributions

By signing the Statement of Authorship, each author certifies that:

i. the candidate's stated contribution to the publication is accurate (as detailed above);

ii. permission is granted for the candidate in include the publication in the thesis; and

iii. the sum of all co-author contributions is equal to 100% less the candidate's stated contribution.

Name of Co-Author	A/Prof. Scott Penfold		
Contribution to the Paper	Initial idea, supervision and guidance, review of manuscript. 30%		
Signature		Date	9/3/22

Name of Co-Author			
Contribution to the Paper			
Signature		Date	

Please cut and paste additional co-author panels here as required.

Physical and Engineering Sciences in Medicine (2021) 44:1121–1130
https://doi.org/10.1007/s13246-021-01048-5

SCIENTIFIC PAPER

A novel TPS toolkit to assess correlation between transit fluence dosimetry and DVH metrics for adaptive head and neck radiotherapy

George Antoniou[1,2] · Scott N. Penfold[1,3,4]

Received: 18 May 2021 / Accepted: 13 August 2021 / Published online: 31 August 2021
© Crown 2021

Abstract

Inter-fractional anatomical variations in head and neck (H&N) cancer patients can lead to clinically significant dosimetric changes. Adaptive re-planning should thus commence to negate any potential over-dosage to organs-at-risk (OAR), as well as potential under-dosage to target lesions. The aim of this study is to explore the correlation between transit fluence, as measured at an electronic portal imaging device (EPID), and dose volume histogram (DVH) metrics to target and OAR structures in a simulated environment. Planning data of eight patients that have previously undergone adaptive radiotherapy for H&N cancer using volumetric modulated arc therapy (VMAT) at the Royal Adelaide Hospital were selected for this study. Through delivering the original treatment plan to both the planning and rescan CTs of these eight patients, predicted electronic portal images (EPIs) and DVH metrics corresponding to each data set were extracted using a novel RayStation script. A weighted projection mask was developed for target and OAR structures through considering the intra-angle overlap between fluence and structure contours projected onto the EPIs. The correlation between change in transit fluence and planning target volume (PTV) D98 and spinal cord D0.03cc with and without the weighting mask applied was investigated. PTV D98 was strongly correlated with mean fluence percentage difference both with and without the weighting mask applied ($R_{Mask} = 0.69$, $R_{No\ Mask} = 0.79$, $N = 14$, $p < 0.05$), where spinal cord D0.03cc exhibited a weak correlation ($R_{Mask} = 0.35$, $R_{No\ Mask} = 0.53$, $N = 7$, $p > 0.05$) however this result was not statistically significant. The simulation toolkit developed in this work provided a useful means to investigate the relationship between change in transit fluence and change in key dosimetric parameters for H&N cancer patients.

Keywords Adaptive radiotherapy · Volumetric modulated arc therapy (VMAT) · Transit dosimetry · RayStation scripting

Introduction

Anatomical variations in head and neck (H&N) cancer patients can lead to clinically significant plan deterioration and adaptive radiotherapy (ART) may be required to restore an optimal dose distribution [1]. Past literature has explored the benefits of implementing ART workflows within a clinic for H&N cancer and has mostly been focused on improving dosimetry in parotid glands, which is crucial when lowering risk of xerostomia [1, 2]. Monitoring the dose delivered to the spinal cord, via evaluation of kV cone-beam computed tomography (CBCT), has also shown to be beneficial in answering the golden question: *when* should we replan? [3]

Traditional methods to implement ART into the clinic are associated with a significant increase in the clinical workload to the radiotherapy department as a whole. As a result, there has been a recent push to develop an accessible and automated quantitative trigger for ART, with one common method being transit dosimetry with an electronic portal imaging device, EPID [4]. Using relative EPID dosimetry, one can explore the gradual change in transit fluence over the course of treatment without necessarily needing to rely on the absolute precision and accuracy of the images themselves. Change in transit fluence is expected to be correlated with anatomical variations and patient setup errors, which

✉ George Antoniou
george.antoniou@sa.gov.au

1 Department of Physics, The University of Adelaide, Adelaide, SA 5005, Australia

2 Medical Physics & Radiation Safety, South Australia Medical Imaging, Adelaide, SA, Australia

3 Department of Radiation Oncology, Royal Adelaide Hospital, Adelaide, SA 5000, Australia

4 Department of Physics, Australian Bragg Centre for Proton Therapy and Research, Adelaide, SA 5000, Australia

has thus far been the main focus of research on this topic. Several groups have tried to correlate dosimetric impacts with change in transit fluence, where 2D relative gamma analysis is commonly utilized [5–8]. Through conducting gamma analysis on the transit EPID images acquired over the course of treatment, a variety of parameters can be extracted to help quantify change in dose to the patient.

Through utilising the mean gamma value, γ_{mean}, from a 2D 3%/3 mm relative gamma analysis test on whole electronic portal images (EPIs), Piron et al. [5] concluded that change in transit fluence could be used as a predictor for plan deterioration for H&N cancer patients as a result of anatomical variations. Utilising the whole EPI, however, could result in misleading mean gamma values. If only a small area of pixels included large deviations, the EPI as a whole may still be similar to the baseline EPI and thus result in a score that is below the trigger threshold, ultimately decreasing sensitivity. By considering projections of regions of interest onto the EPIs, the sensitivity of the analysis may be improved.

By projecting planning target volume's (PTV's) onto EPIs obtained every fraction and correlating γ_{mean} with dosimetric changes (V95%), Piron et al. [6] found that projecting PTVs onto the EPIs and then conducting gamma analysis improved sensitivity to anatomical changes. However, projecting organs-at-risk (OARs) onto the EPIs were not considered.

The same group then went on to establish an action threshold for H&N ART, and proposed a threshold of $\gamma_{mean} > 0.42$, as evaluated using the whole EPI [7]. By considering a dosimetric threshold of V100% < 90% the group was able to analyse the sensitivity and specificity of the threshold proposed. Moreover, the group also explored the correlation between mean dosimetric differences of PTV and OARs with mean gamma values of the whole EPI for patients that did reach the action threshold, as well as patients that did not. A strong correlation between change in spinal cord dose and γ_{mean} was not observed, likely due to the inherent nature of the gamma analysis test conducted on whole EPIs—being more sensitive in high dose regions, such as PTVs, than lower dose regions, such as OARs.

Lim et al. [9] explored the correlation between change in transit fluence, in a generalised rectangular region surrounding the neck, and volumetric change of a ROI (ΔV_{ROI}) spanning from the Condyloid process (jaw) to C6 of the spinal cord. Volumetric change, which is a good predictor for grade 2 xerostomia [10], was found to be strongly correlated with change in transit fluence ($R = -0.776, p < 0.001$). A 5% threshold in ΔV_{ROI} could be used as a trigger for ART, where the area under the receiver-operating characteristic curve (ROC) was determined to be 0.88. This study did not investigate the potential improvement in sensitivity by projecting the ROI onto the EPID.

When utilising Linac-measured EPIs for relative gamma analysis, one of the largest sources of systematic error in these types of studies include the accuracy of the first fraction EPI. The results of these studies all rely on the assumption that the patient anatomy at the time of the first fraction EPI is representative of the patient anatomy at the time of the planning CT (pCT). A poor baseline could be misleading and yield results with γ_{mean} values significantly lower than actually representative of the change since pCT. The research presented in this study differs from previous studies by predicting transit EPIs using an in-house script developed in the RayStation treatment planning system (TPS) by RaySearch Laboratories, rather than analysing Linac-measured EPIs. The advantage of this approach is in the removal of any patient set-up errors, as well as any anatomical variation in the patient between obtaining the pCT and first fraction baseline EPI. Rather than using weekly CBCTs to obtain multiple EPIs over the course of treatment, this study will also only consider the pCT and rescan CT (rCT) to avoid any uncertainties associated with deformable image registration of the pCT's to CBCT's, or dose calculation uncertainty on CBCT. Considering these factors, the developed tool allows for the investigation of correlation between change in transit fluence and change in patient DVH metrics in a more controlled environment. Moreover, current triggers for ART at the Royal Adelaide Hospital are based on visual assessment of tightness of mask fit and contour change on set-up images by treating radiation therapists. This method is both highly subjective and has poor specificity. The developed tool is useful in assessing sensitivity and specificity of transit dosimetry as a quantitative trigger for ART.

Methods

Patient selection

Human research ethics and research governance approval was obtained for the study. The radiotherapy datasets (treatment plans, planning CTs and RT structure sets) of eight patients previously having undergone ART for H&N cancer at the RAH were collected and anonymized. Each patient consented to their data being used for research purposes and had at least 1 rescan CT acquired over the course of treatment.

EPI prediction in RayStation

EPID model

The EPID model developed in this work was generated to represent EPI's measured with a Varian TrueBeam aS1200 MV imager in Portal Dosimetry mode. Square field Portal Dosimetry images were collected to provide beam profiles

and output factors with and without solid water in place and the EPID at 150 cm source to detector distance (SDD).

A simple EPID model was constructed in RayStation (8B) to model the Varian TrueBeam aS1200 MV imager operating in Portal Dosimetry mode. The model consisted of a 40 cm × 40 cm × 5 cm water slab atop a 40 cm × 40 cm × 4 cm lead slab. Dose planes were extracted at 3.6 cm depth in the water slab. The selected water slab thickness and extraction depth were guided by Varian Portal Dosimetry calibration settings. The thickness of the lead slab was selected based on a comparison of measured and computed output factors. Calculated EPIs simulated in RayStation at 150 cm SDD were first downscaled to 100 cm SDD, where flood field and beam profile corrections were applied, and subsequently scaled back to 150 cm SDD. The flood field correction was obtained by dividing all calculated EPID dose planes by an open field calculation that covered the EPID dose plane area. This simulates the flood field correction of the actual EPID. The beam profile correction was obtained by multiplying the flood field corrected array with a 40 cm × 40 cm^2 radial beam profile measured at 3.6 cm in water. This again simulates the beam profile correction applied by the Varian Portal Dosimetry software. This was done to mimic the major corrections applied in forming an EPI in portal dosimetry mode on the Linac.

EPI extraction

The RayStation EPID template model was imported as regions of interest into the original treatment plan of a given patient within RayStation. By utilising a number of functions within the RayStation python scripting environment, an automated sequence of steps was programmed to rotate the EPID model around isocenter for each control point of a VMAT plan as outlined in Fig. 1. The EPID model was first positioned to have the 3.6 cm extraction depth positioned 50.0 cm below the origin. This was followed by rotation to a given control point, and subsequent translation to be centred at the isocenter. Once positioned appropriately, the dose for that VMAT control point was calculated. The dose delivered to the extraction plane within the EPID model was then stored into a 200 × 200 pixel array, with a pixel size of 2.0 mm, and subsequently integrated over every control point of the VMAT plan. To help optimise the time required to extract the EPIs from *n* beams, the dose from all beams at a given gantry angle was calculated via a collapsed cone algorithm, rather than rotating the model around the patient *n* times. Thus, the generated image is a sum of all beams in a fraction, rather than per-beam images. Once the original treatment plan had been simulated using the pCT, the process was repeated using the rCT to obtain a second EPI.

VMAT script validation

To validate our model, a 20.0 × 20.0 × 10.0 cm thick solid water slab was positioned at 90.0 cm SSD on a Varian TrueBeam Linac, with the EPID positioned at 150.0 cm SDD. A VMAT treatment plan was then delivered, and a baseline EPI was extracted. To simulate change in patient anatomy, 2.0 cm of the solid water slab was removed anteriorly and the same VMAT treatment plan was delivered to extract a second fraction EPI. The change between the second EPI and the baseline was then calculated as a 2D percentage difference map, relative to dose maximum of the baseline. This process was then repeated using the simulation toolkit developed in RayStation to obtain a predicted 2D percentage difference map.

ROI projection mask

Past research has shown that projecting ROI's onto the EPIs can lead to improved sensitivity in using change in transit fluence as a quantitative trigger for ART. The contours of the spinal cord and PTV's for each patient included in the study, at time of planning, were thus extracted through utilising DICOM RT structure files. These contours could then be

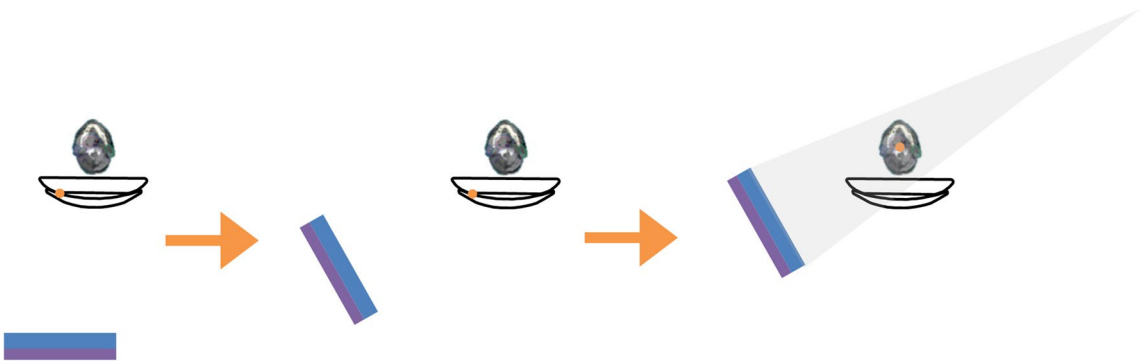

Fig. 1 EPID extraction process repeated along every control point for both the pCT and rCT. EPID first positioned 50.0 cm below origin, then rotated to a given control point angle, and translated to 50.0 cm from isocenter

projected onto the extraction plane of the EPI with the use of modules within the dicompyler-core Python package [11]. A ROI projection mask was then created, taking the thickness of the structure in the beam's-eye-view into consideration to weight the mask by the path length through the structure as shown in Fig. 2a.

In this work, the spinal cord was chosen as a significant ROI alongside the PTV's as plan adaption for H&N patients at the Royal Adelaide Hospital is often triggered by the monitoring of spinal cord doses during on-course plan dosimetry assessment. However, the methods outlined in this work can still be applied to a variety of different structures, such as the parotid glands when considering toxicities such as xerostomia [9, 10]. If a plan contained multiple PTV volumes with different dose levels, each was treated as an independent ROI in the correlation analysis. The evaluation PTV contours (PTV_EVAL), as calculated via taking the Boolean subtraction of sequentially higher dose PTV volumes from the current PTV volume, were utilised as these are the volumes that undergo DVH assessment during treatment planning.

To further evolve the ROI projection mask, one can consider the overlap between the open field of the MLC configuration and the projection of the structure of interest. Thus, the DICOM plan file was also used to extract these coordinates on the EPI to create a 'fluence projection' mask. EPI pixels that lay within the open field projection were given a value of 1, and those outside the open field were given a value of 0. The mask could then further be weighted by the monitor units (MU's) delivered to the open field region for a given control point through multiplying the mask through by the cumulative meterset value and beam MU's found in the DICOM RT plan file as shown in Fig. 2b. The resulting mask could then be integrated along each control point to obtain a final intra-angle projection mask as shown in Fig. 2e, which highlights the regions within the EPI for which dose was delivered to a particular structure of interest, weighted by the structure's volume and MU's delivered.

DVH parameters

Change in transit fluence alone cannot be used as a reliable trigger for ART without first understanding how this quantity relates to dosimetric differences within the patient. Current workflows at the Royal Adelaide Hospital involve an on-course dosimetry monitoring program making use of RayStation's CBCT dose calculation functionality. Evaluations are performed to ensure target coverage does not diminish by a certain amount and that serial organs at risk, such as the spinal cord, do not exceed tolerance values. Replanning thresholds are assessed on a case-by-case basis

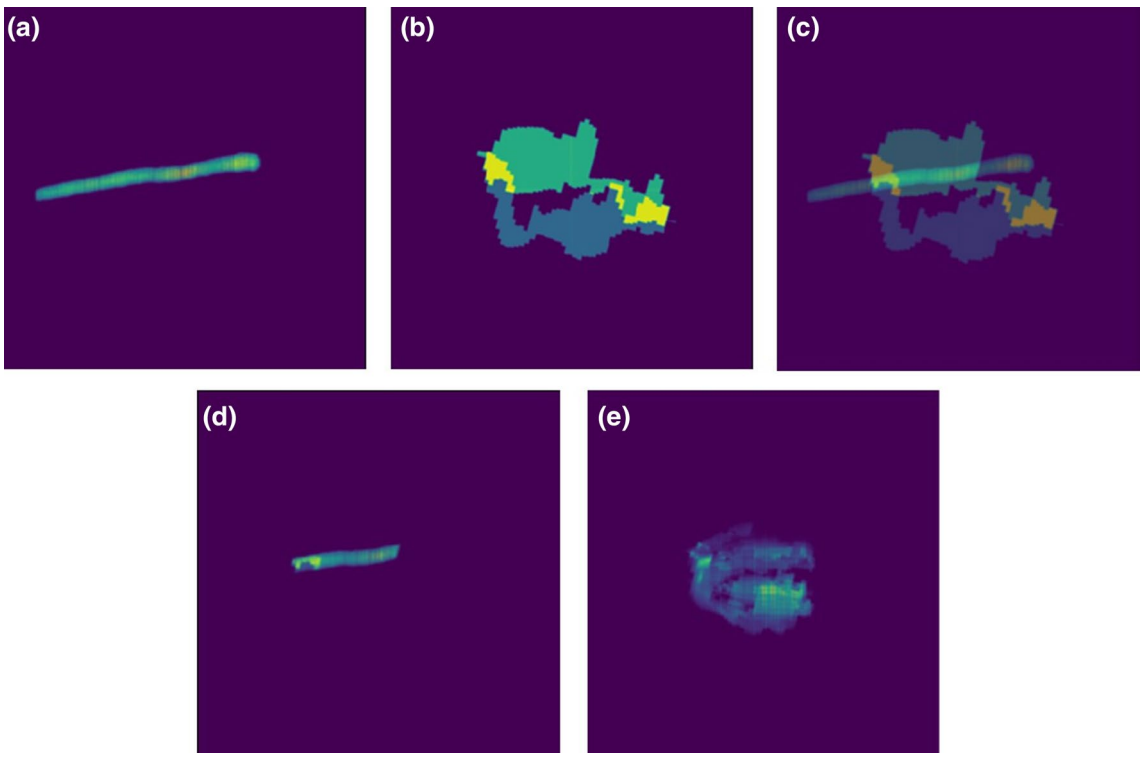

Fig. 2 Process used to derive an intra-angle ROI and fluence projection mask. For each control point, **a** the structure projection mask and **b** MU-weighted fluence projection from each beam is used to obtain **d** the overlap between the two, as visualised by **c**. This process is repeated for each control point to achieve **e** the final intra-angle ROI and fluence mask

by the consulting Radiation Oncologists with a major consideration being the number of remaining fractions. In this study DVH metrics considered for the spinal cord and PTV_EVAL structures relate to the near maximum and minimum doses received by the volumes, being the D0.03cc and D98 metric respectively. In this work, the change in these metrics over the two CT datasets (original planning CT and rescan CT) was considered and any correlation between them and change in transit fluence was explored.

Correlation

As previously mentioned, a correlation between change in transit fluence and change in D0.03cc or D98, for the spinal cord and PTV's respectively, would show that change in transit fluence can be used as a trigger for ART. There have been multiple approaches in quantifying this change in transit fluence to be used as a trigger for ART, where gamma parameters are commonly utilised such as γ_{max}, γ_{mean}, and $\gamma_{1\%}$. One disadvantage of this approach is that gamma values are always positive and thus give no information regarding the direction of such change. A second fraction EPI that has received a greater amount of dose than the baseline may show similar corresponding gamma parameters to a second fraction EPI that has received less dose than the baseline. It was thus decided that the mean percentage difference between the two EPIs should be calculated, relative to the baseline, as this will also provide directional information. It should be noted, however, that signed percentage differences in a region of interest of an integrated image may cancel over multiple control points and lead to lower-than-expected mean values. Care should thus be taken when interpreting these values via first assessing the 2D percentage difference map.

A correlation between the change in D0.03cc and D98, for the spinal cord and PTV_EVAL's, and mean fluence percentage difference with and without the respective masks applied was then explored. Noting that with no mask applied, the entire 40 × 40 cm EPIs were utilised, whilst disregarding doses < 10% of local maximum so that summary statistics are not skewed by clinically irrelevant small doses. Statistical analysis was conducted through considering Pearson's correlation coefficient (R), Spearman's rank correlation coefficient (ρ), and a linear regression with a 95% confidence interval. The statistical significance of the correlation coefficients was also calculated for the given sample size, where the difference between the correlation with and without the projection masks applied was also considered to explore any improvements in sensitivity that the mask may supply.

Results

EPID model

Non-transit verification

The EPID model used in this work was developed through consideration of beam profiles, output factors, and gamma analysis between predicted and measured EPIs. Figure 3 shows beam profiles from Linac-measured and RayStation calculated EPIs after delivering 2.0 × 2.0, 3.0 × 3.0, 4.0 × 4.0, 5.0 × 5.0, 10.0 × 10.0, and 20.0 × 20.0 cm^2 jaw-defined square fields with the EPID positioned at 150 cm SDD. The output factors of these square fields were also obtained, as shown in Fig. 4, showing percentage differences all less than 0.8%.

EPID model validation

The EPID model developed was first validated through simulating change in patient anatomy via anteriorly removing 2.0 cm of a solid water slab between two deliveries of a VMAT plan. Changes in the Linac-measured EPIs were compared to changes in the TPS-calculated EPIs through comparing percentage differences,$\Delta\phi_{\%}$, in beam profiles

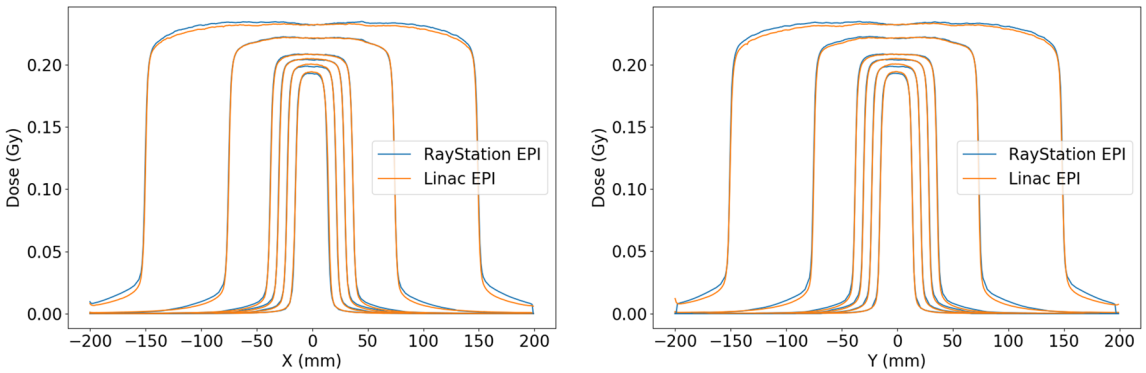

Fig. 3 True (Linac) and predicted (RayStation) non-transit beam profiles with EPID positioned at 150 cm

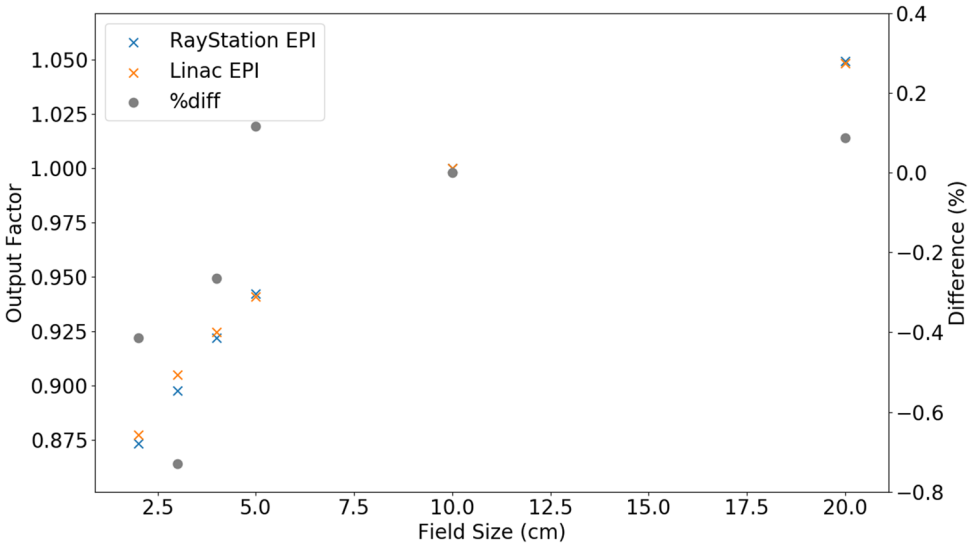

Fig. 4 True (Linac) and calculated (RayStation) output factors from square fields, with percentage difference

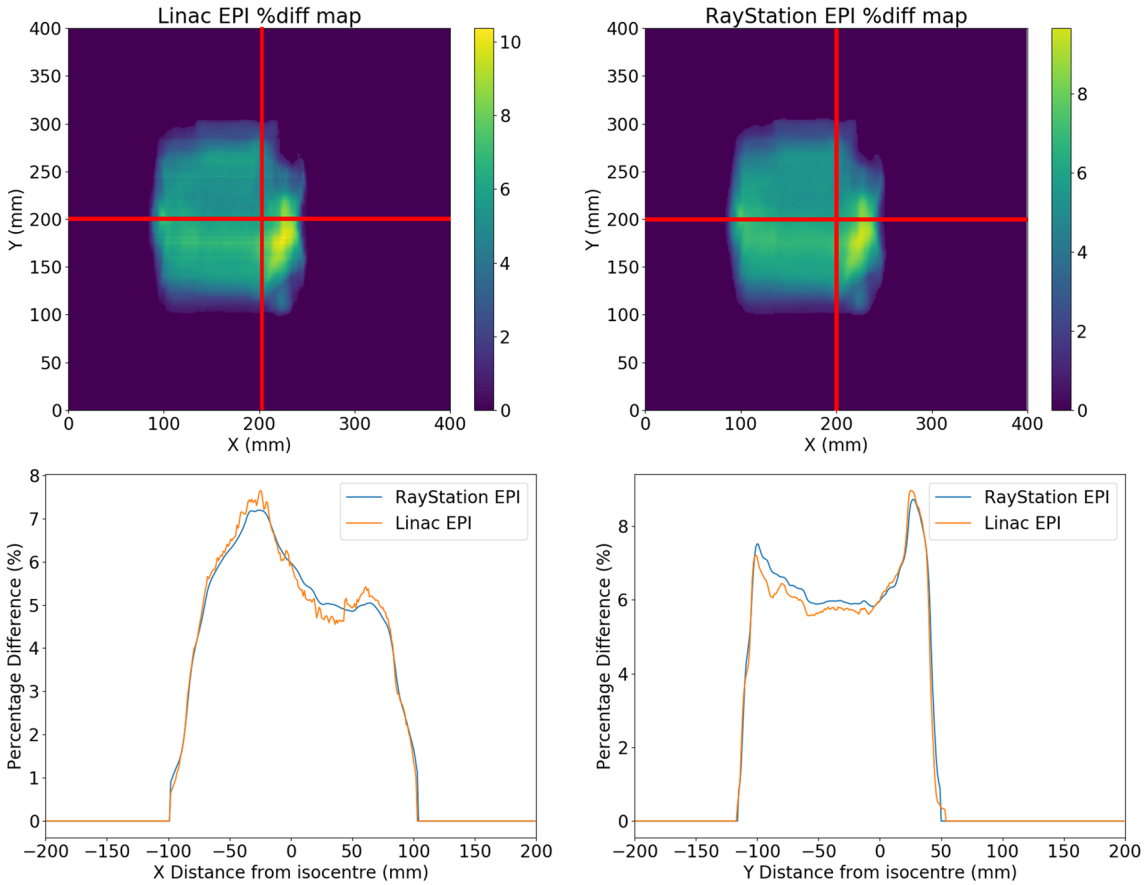

Fig. 5 True (Linac) and calculated (RayStation) 2D percentage difference maps used for model validation, with x and y-profiles

between the two exposures as shown in Fig. 5. In the x-profiles shown, a maximum percentage difference of 7.2% and 7.7% was observed for the predicted and true changes in EPIs, respectively.

Similarly, for the y-profiles, a maximum percentage difference of 8.7% and 9.0% were observed for the predicted and true change in EPIs. The mean percentage error between the true and predicted percentage differences across the whole image was 1.49%, ranging between a maximum of

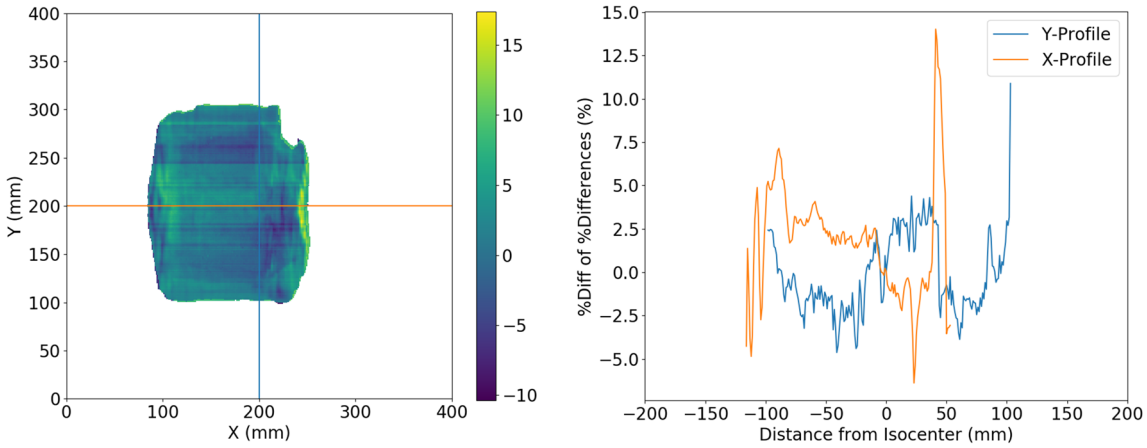

Fig. 6 2D percentage error map of the 2D percentage difference maps used for EPID model validation, with x- and y-profiles

17.4% and a minimum of < 0.01%. The 2D percentage error map between the two percentage differences is shown in Fig. 6. The TPS simulation was thus considered as a good indicator of what one would measure on a Linac MV imager in the corresponding situation.

Correlation of change in transit fluence and change in DVH metrics

No weighting mask applied

The correlation between change in transit fluence and change in DVH metrics for the eight patient datasets was explored. D98 PTVs and D0.03cc for the spinal cord was first explored with no weighting masks applied—utilising the entire 40 × 40 cm EPIs whilst disregarding doses < 10% of local maximum. Figure 7a shows the relationship between mean transit fluence percentage difference and change in D98 for the PTVs, with a linear regression band fitted to a 95% confidence interval. Pearson's and Spearman's correlation coefficients were determined to be 0.79 and 0.82 respectively, indicating a strong correlation exists. Similarly, Fig. 7b shows the relationship between change in D0.03cc for the spinal cord and mean transit fluence percentage difference, also with a linear regression band fitted to a 95% confidence interval. Pearson's correlation coefficient of 0.53 indicates a moderate correlation exists between the two parameters, as well as Spearman's correlation coefficient of 0.32.

Weighting masks applied

ROI projection mask To observe the individual benefits of various contributions to the overall weighting mask applied, the effects of projecting the ROIs onto the EPIs were first considered. Figure 7c d show the correlation between change in D98 and D0.03cc with mean weighted fluence percentage difference, respectively. Pearson's and Spearman's correlation coefficients suggest that strong and moderate correlations exist for the PTVs and spinal cords, respectively, yielding values of 0.70 and 0.67 for the PTVs and 0.41 and 0.32 for the spinal cords. The slope of the linear regression fit for both the PTVs and spinal cords increase when utilising the ROI projection mask, in comparison to no weighting mask applied. This result suggests that the weighting mask applied increases the overall sensitivity of the fit, as expected.

Intra-angle ROI and fluence projection mask The final level of complexity added to the weighting projection mask includes an intra-angle convolution between a fluence projection mask, through considering the MLC leaf configuration, and ROI projection mask, through considering the position of some ROI on the EPI. By considering the overlap between the fluence and ROI projections, one is able to consider the regions on the EPI for which some structure received dose at any point during the treatment delivery.

Figure 7e and f show the correlation between change in D98 and D0.03cc with mean weighted fluence percentage difference for the PTVs and spinal cords, respectively. Pearson's and Spearman's correlation coefficients of 0.69 and 0.72 for the PTVs, and 0.35 and 0.21 for the spinal cords, suggest that a strong correlation exists for D98 and mean weighted percentage difference, and a weak correlation exists with D0.03cc and mean weighted percentage difference. In comparison to the correlation data with the ROI projection masks applied, Pearson's and Spearman's correlation coefficients increase for the cases of the PTV projections and decrease in the case of utilising the spinal cord projections. All correlation coefficients decreased relative to the correlation data with no mask applied, however the sensitivity of the correlation with the intra-angle

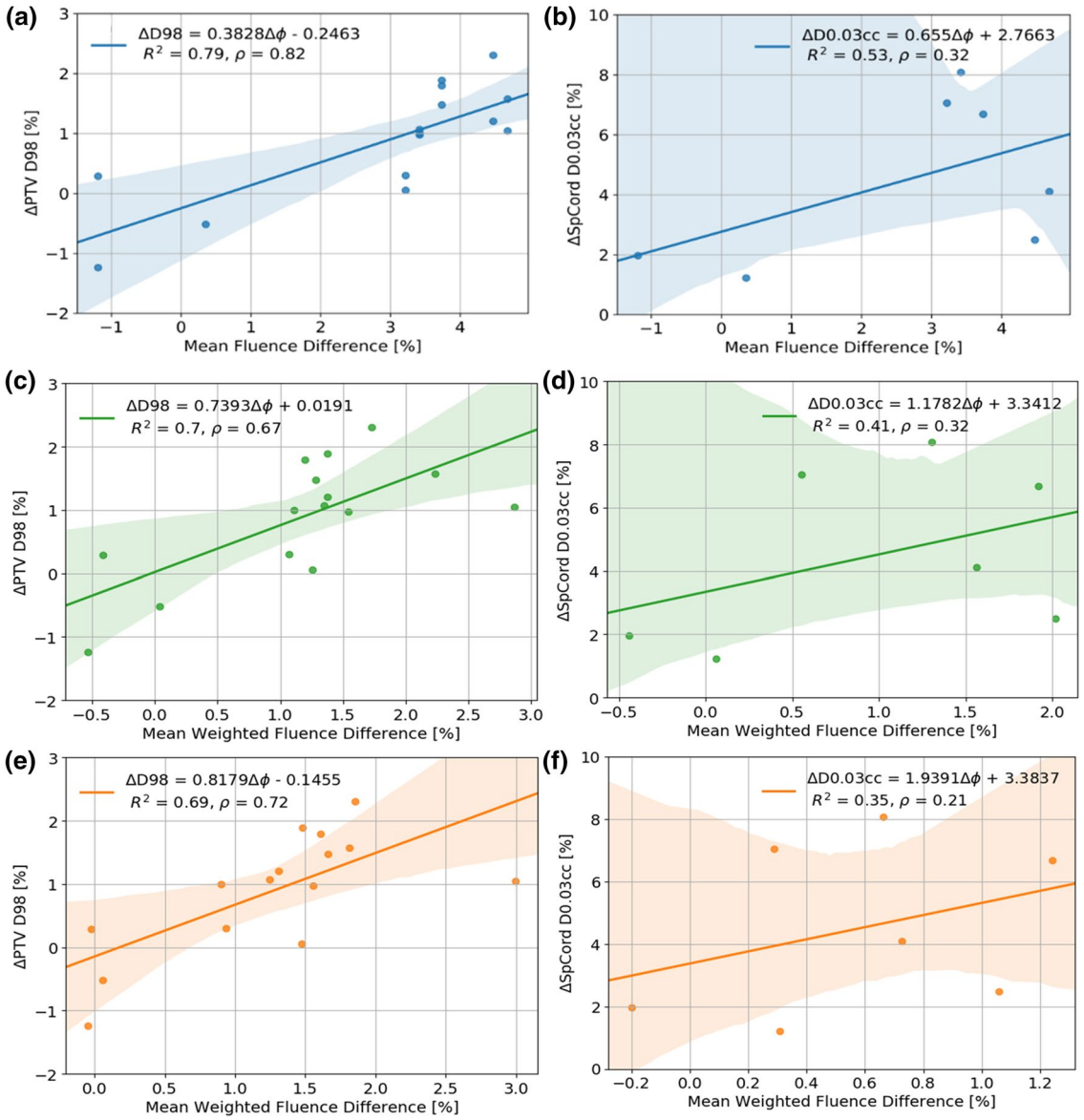

Fig. 7 Correlation between change in D98 and D0.03cc with change in mean fluence percentage difference with no mask applied for **a** the PTV(s) and **b** spinal cord, with the projection mask applied for **c** the PTV(s) and **d** spinal cord, and with the intra-angle fluence projection mask applied for **e** the PTV(s) and **f** spinal cord

ROI and fluence projection mask applied significantly increased, as shown by the steeper slopes.

Discussion

Change in transit fluence, as measured via mean percentage difference, was found to be strongly correlated with change in PTV D98 and moderately correlated with change in spinal cord D0.03cc with no weighting mask applied. Pearson's and Spearman's correlation coefficients were found to decrease when applying a ROI projection mask to the predicted EPIs, however still yielding strong and moderate correlations, respectively. No statistically significant difference between the correlation coefficients was observed between the two sets ($p_{PTV} = 0.32$ and $p_{SpCord} = 0.41$), however the slope of the regression was found to increase by 93% and 80% for the PTVs and spinal cords, respectively. Taking the weighting mask through another layer of complexity via an intra-angle convolution with the MLC fluence projections also resulted in no statistically significant difference in the correlation coefficients calculated, relative to no weighting mask applied. The slope of the linear regression fit, however, increased by 113% and 196% for the PTVs and spinal cords,

respectively; greatly improving the sensitivity of change in transit fluence to a change in key DVH metrics. Future work should consider the specificity of the model, through evaluating some threshold value to trigger the need for plan adaptation, via a receiver operating characteristic (ROC) curve.

This study is consistent with past literature on improving sensitivity via projecting PTVs onto the EPI. For comparison, Piron et al. [6] explored V95% with mean gamma values across the entire EPI as well as by projecting PTV's. Via a meta-analysis of this study, it was found that the correlation between V95% and mean gamma increased from ~ 0.55 to ~ 0.70 when projecting the PTV, as well as the slope of the trend line increasing by ~ 270%. Overall, projecting the PTVs onto the EPI was found to be beneficial to both the correlation coefficient and sensitivity, which agrees with the results presented.

In this work, patient data was selected on the basis that plan adaptation occurred due to significant morphological changes within the patient, such as tissue shrinkage, resulting in some regions receiving greater than anticipated dose and others lesser. One of the eight patients used for this research, however, was replanned due to significant changes in neck tilt; resulting in poor patient alignment in the clinic. In this scenario, there was poor agreement in the position of PTV's and Spinal Cord between the pCT and rCT and as a result led to unreliable ΔD98 and ΔD0.03cc values being calculated for the PTV's and spinal cord, respectively. For this reason, the patient data was omitted from the correlation analysis as the change in datasets reflected an intentional change in patient positioning which would not be encountered when delivering the same plan at different fractions. The poor agreement of this dataset with the proposed correlation does however indicate that the model may also be useful in identifying patient setup errors.

When exploring the correlation between change in transit fluence and ΔD0.03cc for the spinal cords, it was observed that a much poorer correlation was found. The sensitivity, however, of the spinal cord DVH metric was drastically improved with the implementation of the weighting mask derived, as demonstrated by the 196% slope increase in Fig. 7f relative to Fig. 7b. The y-intercept of the linear regressions, however, pose another issue likely due to the small sample size used. y-Intercepts of up to 3.38% were observed for the spinal cord D0.03cc correlations, suggesting that patients showing a mean (weighted) fluence percentage difference of zero still have some change in dosimetry. Moreover, the 95% confidence interval of the linear regression fit for all three correlations explored do not include the origin of the graph—suggesting some systematic error is present within the data obtained. In the future, more datapoints, particularly for the spinal cord results, should be obtained to yield more reliable results. A forced y-intercept could also be explored, however addressing the systematic error would be the preferential approach to minimising this issue. Furthermore, analysing change in EPIs obtained in portal dosimetry mode has some inherent limitations in that the intra-angle differences may cancel out in the final integrated image. Conducting analysis in the continuous *cine* mode may thus improve correlation in the future, however it should be noted further work would be required to validate this acquisition mode. In relation to current limitations of the EPID model, it is hypothesised that discrepancies between change in measured and calculated EPIs lies in the beam hardening that occurs when a phantom is placed in the beam path in conjunction with the strong energy dependence of amorphous silicon detectors; this effect is not included in our current EPID model within the TPS.

It is important to note that the DVH metric considered for the spinal cord, D0.03cc, considers the near-maximum dose received by the spinal cord and is thus derived from very few voxels. The mean percentage difference, on the other hand, considers the entire volume. D0.03cc is thus much more sensitive to slight changes in the position of the structure, and as a result is unlikely to be well correlated with mean percentage difference. The pCT and rCT's utilised are registered as close as possible, however there are still some slight discrepancies in the anatomy between the two—giving rise to somewhat unreliable D0.03cc values. When considering DVH metrics that utilise the entire volume of the structure, such as mean dose and D98, it is reasonable to expect a good correlation. Future work should thus explore the correlation between mean weighted percentage difference and mean dose received by the parotid glands to explore side effects associated with high parotid gland dose from H&N radiotherapy such as xerostomia.

For the purposes of this study, pCT's were utilised to avoid any uncertainties associated with deformable image registration of the pCT to CBCT, and dose calculation uncertainty on CBCT. This, however, introduces a sample size limitation, as one patient plan will only yield one data point per adaptation to be used in the correlation study. In the future, the use of CBCT's would improve the overall sample size obtained, where the gradual change in patient anatomy could also be explored. This has the added benefit in that data points early into the treatment plan would likely include fractions which do not necessarily require adaptation, thus enabling us to explore various action threshold values for deciding when to replan. The sensitivity and specificity of each threshold value could be explored through consideration of a ROC curve and the area under the curve (AUC). The simulation toolkit developed would ensure that all changes in transit fluence are a direct result of change in patient anatomy, rather than incorrect positioning, and thus still be of use in assessing a critical threshold value. The toolkit can also be applied to multiple regions of interest within a treatment plan, and can be modified to the clinic's

specific tolerance values of, for example, dose to the spinal cord or parotid glands for H&N cancer plans. The intra-angle convolution mask between the ROI and fluence projections showed to drastically improve the sensitivity of any regression fits and is thus deemed to be useful in assessing organs at risk.

Conclusion

The simulation toolkit developed provides a useful method to explore the correlation between change in transit fluence and change in dosimetry for particular regions of interest. The toolkit was capable of predicting change in transit fluence accurately, where a weighting mask allows the user to consider particular regions on the EPID to improve sensitivity. Change in D98 was strongly correlated with change in mean weighted percentage fluence when considering the PTV's, however change in D0.03cc was only moderately correlated for the spinal cord OARs investigated in this study.

Funding No funding was received for conducting this study.

Data availability Not applicable.

Code availability Not applicable.

Consent for publication Not applicable.

Declarations

Conflict of interest The authors have no relevant financial or non-financial interests to disclose.

Ethical approval Approval was obtained from the Central Adelaide Local Health Network Human Research Ethics Committee (CALHN HREC). The procedures used in this study adhere to the tenets of the Declaration of Helsinki.

Informed consent Each participant has given consent to participate, via the statement "I do approve the use of my radiation therapy records for retrospective medical auditing and/or research".

References

1. Brouwer CL, Steenbakkers RJHM, Langendijk JA, Sijtsema NM (2015) Identifying patients who may benefit from adaptive radiotherapy: does the literature on anatomic and dosimetric changes in head and neck organs at risk during radiotherapy provide information to help? Radiother Oncol 115(3):285–294. https://doi.org/10.1016/j.radonc.2015.05.018
2. Castelli J et al (2015) Impact of head and neck cancer adaptive radiotherapy to spare the parotid glands and decrease the risk of xerostomia. Radiat Oncol. https://doi.org/10.1186/s13014-014-0318-z
3. Belshaw L, Agnew CE, Irvine DM, Rooney KP, McGarry CK (2019) Adaptive radiotherapy for head and neck cancer reduces the requirement for rescans during treatment due to spinal cord dose. Radiat Oncol. https://doi.org/10.1186/s13014-019-1400-3
4. van Elmpt W, McDermott L, Nijsten S, Wendling M, Lambin P, Mijnheer B (2008) A literature review of electronic portal imaging for radiotherapy dosimetry. Radiother Oncol 88(3):289–309. https://doi.org/10.1016/j.radonc.2008.07.008
5. Piron O, Varfalvy N, Archambault L (2015) MO-F-CAMPUS-J-05: using 2D relative gamma analysis from EPID image as a predictor of plan deterioration due to anatomical changes. Med Phys. https://doi.org/10.1118/1.4925466
6. Piron O, Varfalvy N, Archambault L (2016) EP-1818: using ROIs projected on EPID as a predictor of plan deterioration due to anatomical changes. Radiother Oncol 119(1):S852–S853
7. Piron O, Varfalvy N, Archambault L (2018) Establishing action threshold for change in patient anatomy using EPID gamma analysis and PTV coverage for head and neck radiotherapy treatment. Med Phys 45(8):3534–3545. https://doi.org/10.1002/mp.13045
8. Cilla S et al (2016) Initial clinical experience with EPID-based in vivo dosimetry for VMAT treatments of head-and-neck tumors. Phys Med 32(1):52–58. https://doi.org/10.1016/j.ejmp.2015.09.007
9. Lim SB et al (2019) Investigation of a novel decision support metric for head and neck adaptive radiation therapy using a real-time *in vivo* portal dosimetry system. Technol Cancer Res Treat. https://doi.org/10.1177/1533033819873629
10. You SH et al (2012) Is there a clinical benefit to adaptive planning during tomotherapy in patients with head and neck cancer at risk for xerostomia. Am J Clin Oncol. https://doi.org/10.1097/COC.0b013e31820dc092
11. Panchal A et al (2019) dicompyler/dicompyler-core v0.5.5. https://doi.org/10.5281/ZENODO.3236628

Publisher's Note Springer Nature remains neutral with regard to jurisdictional claims in published maps and institutional affiliations.

6. Conclusions and Future Work

Inter-fractional anatomical variations in H&N cancer patients can lead to clinically significant dosimetric changes. Adaptive re-planning can mitigate over-dosage to OARs, as well as potential under-dosage to target lesions. Utilising an EPID has previously shown to be a useful means of verifying treatment plans, both pre- and on-treatment. The latter may provide a tool to assist with deciding *when* to re-plan.

Comparative analysis between measured and calculated EPIs, using the Varian aS1200 EPID and RayStation TPS respectively, was thus explored in Chapter 4 to develop an in-house toolkit to verify treatment delivery, and predict change in transit fluence between fractions. In the non-transit dosimetry configuration, square and rectangular fields all yielded (2.0 %, 2.0 mm) gamma pass rates above 97.83% at 100 cm SID, and 99.98% at 150 cm SID. In the transit dosimetry configuration, however, the model's agreement worsened significantly - generating gamma pass rates as low as 8.37%, with an average of 27.2%. Future work should thus aim to better validate the transit dosimetry results, where one likely source of error includes the poor energy dependence of *a*-Si EPIDs, which is particularly problematic for transit dosimetry due to presence of more scattered photons. Applying an additional correction factor could thus be developed to help simulate this energy dependence into the EPID model, ideally utilising *a priori* patient thicknesses and densities via planning CT or on-the-day CBCT scans.

Prediction of *change* in transit fluence relative to some baseline was however validated for one extreme case (5cm reduction in patient thickness), and two moderate cases (2 cm reduction) – showing that the toolkit developed could be useful as a tool for indicating when to consider adaptive replanning. Percentage differences within the field were <5% for all square field sizes for the extreme case and <2% for both moderate cases.

Once the model was validated for change in transit fluence, the script was applied in a treatment simulation environment to explore the correlation between relative change in EPID measured transit dose and relative change in DVH metrics to the PTV and spinal cord over the course of H&N VMAT treatments. A weighted projection mask was also developed for PTV and spinal cord structures through considering the intra-angle overlap between fluence and structure contours projected onto the EPID.

The sensitivity of the correlation between change in transit fluence with PTV D98 and spinal cord D0.03cc subsequently increased by 113% and 196% respectively when applying this weighted projection mask. Overall, there was a strong correlation between change in transit fluence and PTV D98, and a weak correlation between change in transit fluence and spinal cord D0.03cc. Future work could explore the use of on-treatment CBCTs rather than pCT and rCTs, as this would improve the overall sample size obtained. The gradual change in patient anatomy could also be explored, as well as various action threshold values for deciding when to replan. Moreover, the sensitivity and specificity of each threshold value could be explored.

Overall, the simulation toolkit developed in this work provides a useful means to investigate the relationship between change in transit fluence and change in key dosimetric parameters for H&N cancer patients.

Appendix A – Graphical User Interface

The graphical user interface (GUI) developed allows users to conduct comparative analysis between predicted and measured EPIs without the need for background knowledge in programming. The following proposed workflow, as shown in Fig. ***24***, underpinned the overall design of the developed GUI, to allow for a seamless comparison between predicted and measured EPIs in the clinic.

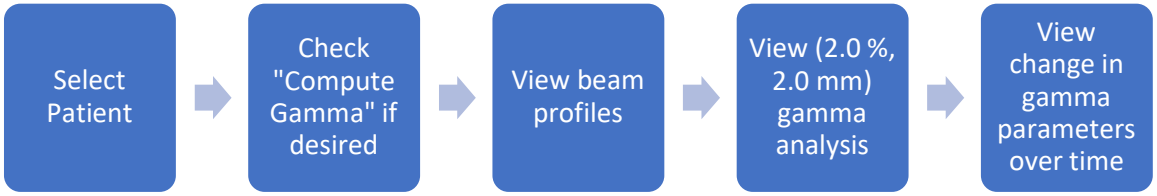

Fig. 24 Proposed workflow for clinical interface

The following figures have been taken from a preliminary version of the GUI, which was tailored towards comparison of square and rectangular fields rather than patient attenuated VMAT EPIs. Small adjustments, however, can be made to convert the GUI into a clinically useful application, as per its original purpose. As a result, the entirety of the parameters to be entered along the top row will be removed when used clinically, as well as the addition of entering a Patient ID. The general process to load the data, however, will be identical.

1. The user should select the ‘Compute Gamma’ checkbox if they wish to conduct a gamma analysis on all EPIs, or fractions, loaded. Leaving this checkbox unticked allows for a quick visual comparison between each fraction. Quick visual comparisons, however, should not be used when making clinical decisions.
2. The user should then press the ‘Load Patient’ button, which will open the corresponding directory depending upon the parameters chosen in the top row. Future changes, as previously mentioned, will include a ‘Patient ID’ entry in which the load patient button will then open the corresponding folder containing the predicted EPIs.
3. The user can then select the fractions for which they would like to conduct their comparative analysis, where multiple fractions can be selected at a time as shown in Fig. ***25***.

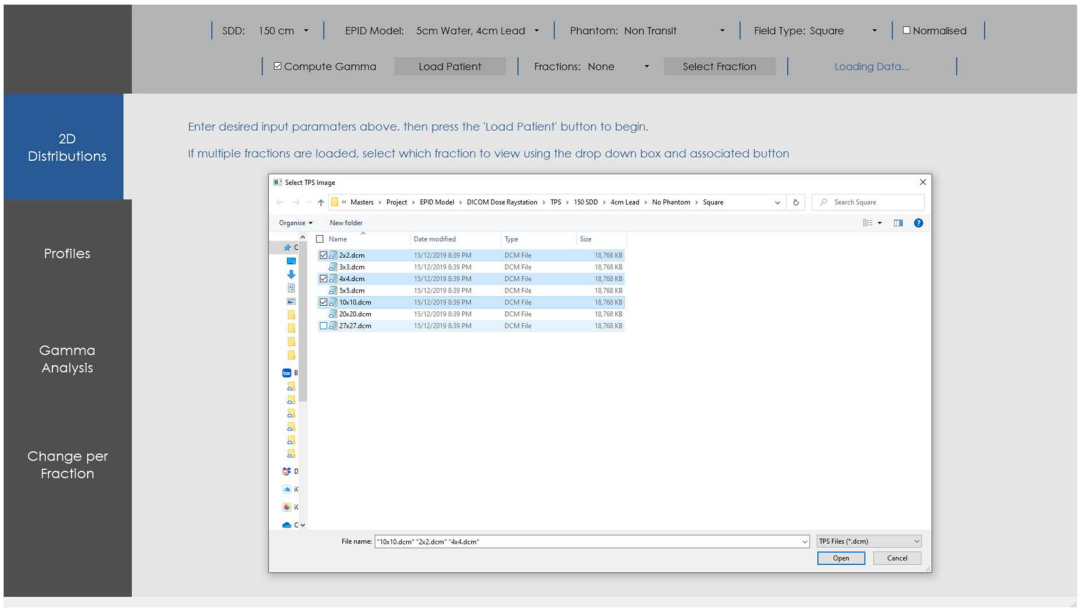

Fig. 25 Developed GUI showing selection of predicted EPIs to be analysed.

4. The GUI will then plot all 2D dose distributions, beam profiles (x, y, and diagonal), and conduct gamma analysis for all files selected. Each figure is plotted behind the background except for the data corresponding to the last file chosen. The 'Fraction:' drop down box allows the user to select the fraction for which they would like to conduct their analysis, where all corresponding figures are then brought to the foreground as shown in Fig. ***26***.

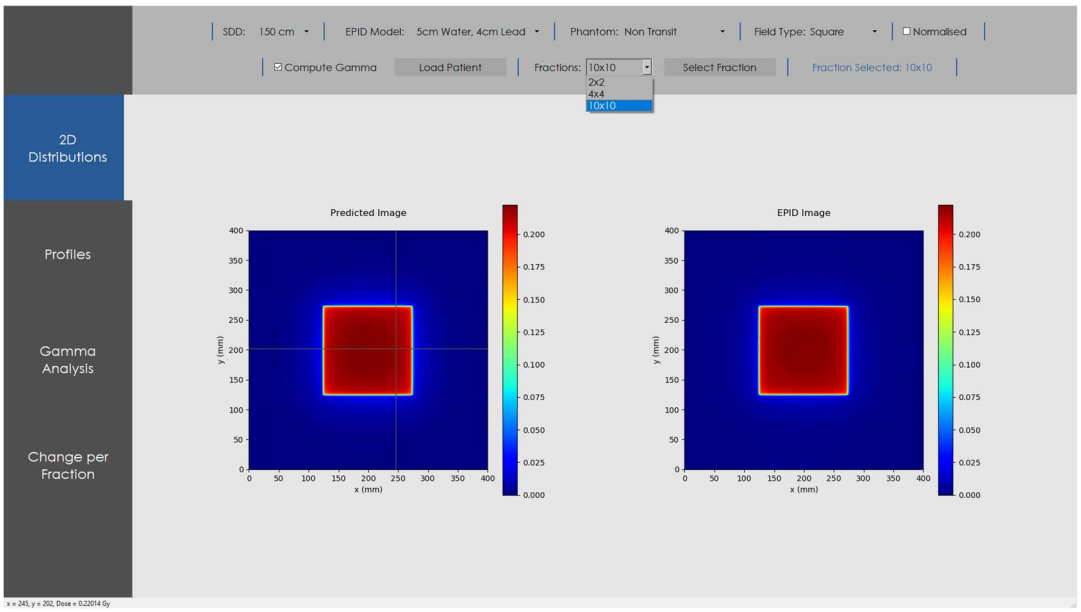

Fig. 26 Developed GUI showing corresponding figures in the foreground when a fraction has been selected.

The purpose and features of each vertical tab will be discussed, namely '2D distributions', 'Profiles', 'Gamma Analysis', and 'Change per fraction'. As shown in Fig. ***26***, the 2D Distribution tab shows the user the predicted and measured EPI from the corresponding fraction, along with a hover cursor which displays the (x,y) coordinates and dose value. This tab should only be used as visual confirmation that the correct fraction or patient has been selected as well as assessing if any unusual artifacts are present within the EPIs. The 'Profiles' tab shows the x, y and diagonal profiles comparing the predicted and measured EPI, as shown in Fig. ***27***. The percentage difference between measured and predicted EPIs is also shown in the plots, with values corresponding to the secondary axis. The purpose of this tab is to allow the user to more closely assess the comparison between measured and predicted EPIs, however this is done more quantitatively in the 'Gamma Analysis' tab.

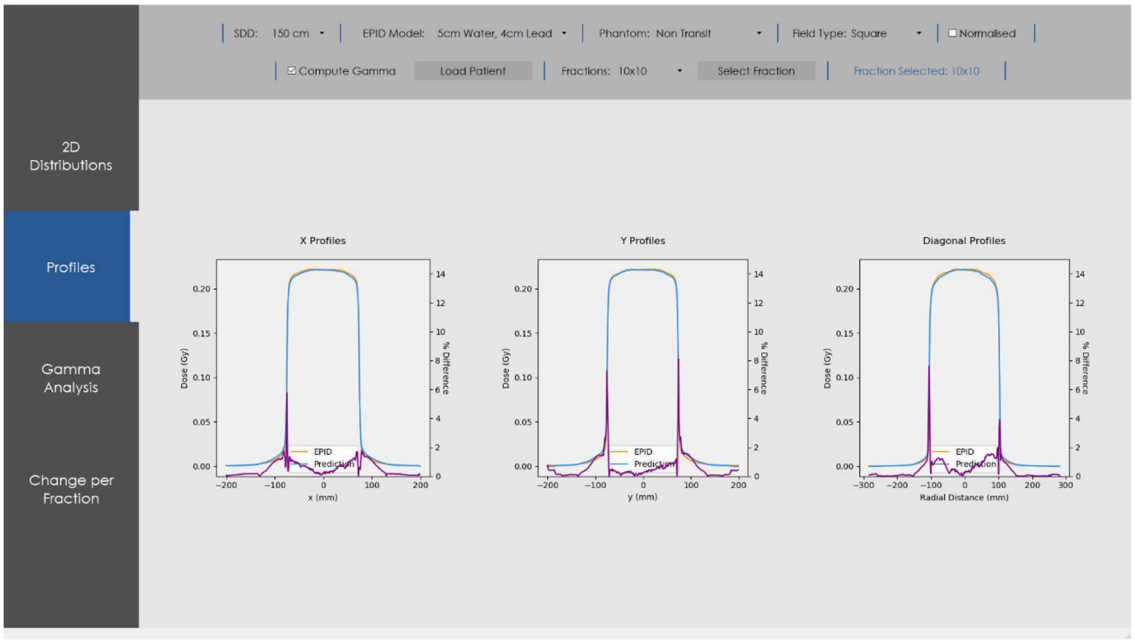

Fig. 27 Profiles tab within developed GUI, showing the x, y, and diagonal beam profiles along with percentage difference between measured and predicted profiles.

The 'Gamma Analysis' tab allows the user to alter the acceptance criteria and low-dose threshold of the conducted gamma analysis, as well as conducting gamma analysis for a single fraction if the checkbox was not ticked.

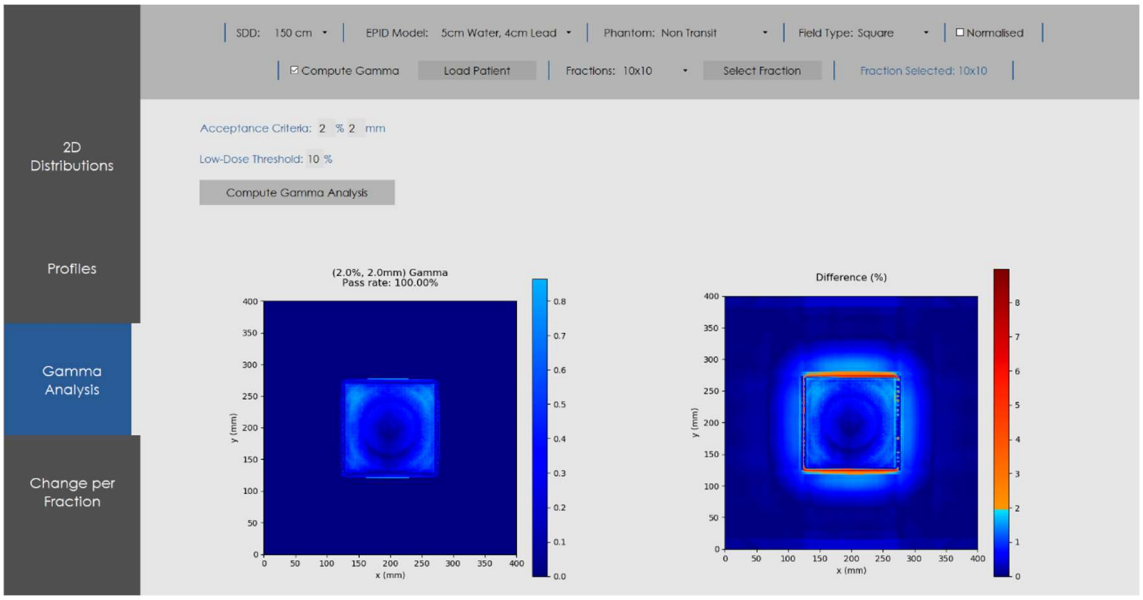

Fig. 28 Gamma Analysis vertical tab, showing the resultant 2D gamma map, gamma pass rate, and 2D percentage difference map.

Finally, a vertical tab allowing the user to observe the change in treatment delivery over multiple fractions for a given patient is also included. Pressing the 'plot metrics over time' button autofill's the table with gamma parameter information, which must first be obtained by ticking the 'Compute Gamma' checkbox when loading the fractions. It should be noted that placeholder dates and plan ID's have been added while the tool is being used for research purposes. The gamma parameters chosen to be monitored include the mean gamma, gamma pass rate, and maximum gamma values, as shown in **Fig. *29***.

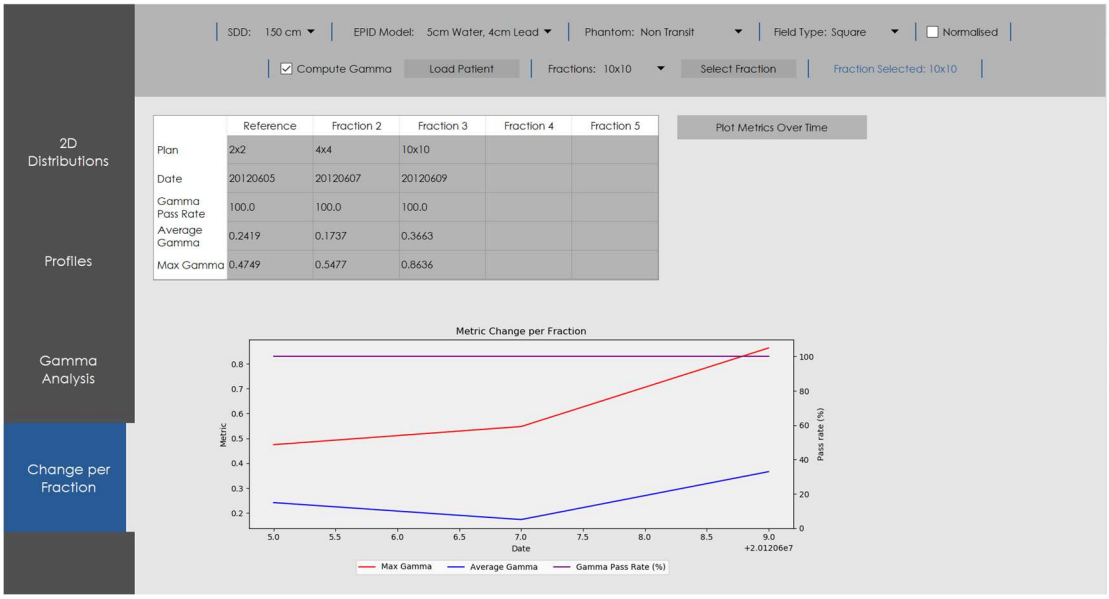

Fig. 29 Change per fraction vertical tab, showing change in gamma parameters over time.

7. References

[1] Australian Institute of Health and Welfare 2018, "Cancer in Australia: Actual incidence data from 1982 to 2013 and mortality data from 1982 to 2014 with projections to 2017," *Asia-Pacific Journal of Clinical Oncology*, vol. 14, no. 1, pp. 5–15, Feb. 2018, doi: 10.1111/ajco.12761.

[2] M. Palmer, "The current & future state of particle therapy," *The MD Anderson Proton Therapy Center - Houston, Available at: http://www.protonpals.org*, 2017.

[3] J. Krayenbuehl *et al.*, "Planning comparison of five automated treatment planning solutions for locally advanced head and neck cancer," *Radiation oncology (London, England)*, vol. 13, no. 1, p. 170, Sep. 2018, doi: 10.1186/s13014-018-1113-z.

[4] S. Ishikura, "Quality assurance of radiotherapy in cancer treatment: Toward improvement of patient safety and quality of care," *Japanese Journal of Clinical Oncology*, vol. 38, no. 11. Oxford Academic, pp. 723–729, Nov. 01, 2008. doi: 10.1093/jjco/hyn112.

[5] K. Jabbari, F. Pashaei, M. R. Ay, A. Amouheidari, and M. B. Tavakoli, "Evaluating the Impact of Various Parameters on the Gamma Index Values of 2D Diode Array in IMRT Verification," *Journal of Medical Signals and Sensors*, vol. 8, no. 1, pp. 31–38, Jan. 2018, doi: 10.4103/jmss.jmss_15_17.

[6] H. H. Li *et al.*, "Patient-Specific Quality Assurance for the Delivery of 60 Co Intensity Modulated Radiation Therapy Subject to a 0.35-T Lateral Magnetic Field Radiation Oncology," *Int J Radiation Oncol Biol Phys*, vol. 91, no. 1, pp. 65–72, 2015, doi: 10.1016/j.ijrobp.2014.09.008.

[7] C. K. Mcgarry, C. E. Agnew, M. Hussein, Y. Tsang, A. R. Hounsell, and C. H. Clark, "The use of log file analysis within VMAT audits," *Br J Radiol*, vol. 89, 2016, doi: 10.1259/bjr.20150489.

[8] S. L. Berry, R. D. Sheu, C. S. Polvorosa, and C. S. Wuu, "Implementation of EPID transit dosimetry based on a through-air dosimetry algorithm," *Medical Physics*, vol. 39, no. 1, pp. 87–98, Jan. 2012, doi: 10.1118/1.3665249.

[9] W. van Elmpt, L. Mcdermott, S. Nijsten, M. Wendling, P. Lambin, and B. Mijnheer, "A literature review of electronic portal imaging for radiotherapy dosimetry," *Radiotherapy and Oncology*, vol. 88, pp. 289–309, 2008, doi: 10.1016/j.radonc.2008.07.008.

[10] I. Sumida *et al.*, "Intensity-modulated radiation therapy dose verification using fluence and portal imaging device," *Journal of Applied Clinical Medical Physics*, vol. 17, no. 1, pp. 259–271, 2016, doi: 10.1120/jacmp.v17i1.5899.

[11] P. B. Greer, "Correction of pixel sensitivity variation and off-axis response for amorphous silicon EPID dosimetry," *Medical Physics*, vol. 32, no. 12, pp. 3558–3568, Dec. 2005, doi: 10.1118/1.2128498.

[12] B. Warkentin, S. Rathee, and S. Steciw, "2D lag and signal nonlinearity correction in an amorphous silicon EPID and their impact on pretreatment dosimetric verification," *Medical Physics,* vol. 39, no. 11, pp. 6597-6608, Nov 2012, doi: 10.1118/1.4757582.

[13] N. Miri, P. Keller, B. J. Zwan, and P. Greer, "EPID-based dosimetry to verify IMRT planar dose distribution for the aS1200 EPID and FFF beams," *Journal of Applied Clinical Medical Physics*, vol. 17, no. 6, pp. 292–304, 2016, doi: 10.1120/jacmp.v17i6.6336.

[14] A. Reilly, A. van Esch, and A. Carver, "PD-0381: Evaluation of a new Electronic Portal Imaging Device (EPID) for pre-treatment and in vivo dosimetry - ClinicalKey," *Radiotherapy and Oncology*, vol. 115, pp. S182–S183, 2015, Accessed: Jul. 02, 2021. [Online]. Available: https://www-clinicalkey-com-au.proxy.library.adelaide.edu.au/#!/content/playContent/1-s2.0-S0167814015403779?returnurl=null&referrer=null

[15] C. L. Brouwer, R. J. H. M. Steenbakkers, J. A. Langendijk, and N. M. Sijtsema, "Identifying patients who may benefit from adaptive radiotherapy: Does the literature on anatomic and dosimetric changes in head and neck organs at risk during radiotherapy provide information to help?," *Radiotherapy and Oncology*, vol. 115, no. 3. Elsevier Ireland Ltd, pp. 285–294, 2015. doi: 10.1016/j.radonc.2015.05.018.

[16] J. Castelli *et al.*, "Impact of head and neck cancer adaptive radiotherapy to spare the parotid glands and decrease the risk of xerostomia," *Radiation Oncology*, vol. 10, no. 1, Jan. 2015, doi: 10.1186/s13014-014-0318-z.

[17] L. Belshaw, C. E. Agnew, D. M. Irvine, K. P. Rooney, and C. K. McGarry, "Adaptive radiotherapy for head and neck cancer reduces the requirement for rescans during treatment due to spinal cord dose," *Radiation Oncology*, vol. 14, no. 1, Nov. 2019, doi: 10.1186/s13014-019-1400-3.

[18] W. van Elmpt, L. McDermott, S. Nijsten, M. Wendling, P. Lambin, and B. Mijnheer, "A literature review of electronic portal imaging for radiotherapy dosimetry," *Radiotherapy and Oncology*, vol. 88, no. 3. Elsevier, pp. 289–309, Sep. 01, 2008. doi: 10.1016/j.radonc.2008.07.008.

[19] O. Piron, N. Varfalvy, and L. Archambault, "MO-F-CAMPUS-J-05: Using 2D Relative Gamma Analysis From EPID Image as a Predictor of Plan Deterioration Due to Anatomical Changes," *Medical Physics*, vol. 42, no. 6Part30, Jun. 2015, doi: 10.1118/1.4925466.

[20] O. Piron, N. Varfalvy, and L. Archambault, "EP-1818: Using ROIs projected on EPID as a predictor of plan deterioration due to anatomical changes," in *Radiotherapy and Oncology*, 2016, vol. 119, no. 1, pp. S852–S853.

[21] O. Piron, N. Varfalvy, and L. Archambault, "Establishing action threshold for change in patient anatomy using EPID gamma analysis and PTV coverage for head and neck radiotherapy treatment," *Medical Physics*, vol. 45, no. 8, pp. 3534–3545, Aug. 2018, doi: 10.1002/mp.13045.

[22] S. Cilla *et al.*, "Initial clinical experience with Epid-based in-vivo dosimetry for VMAT treatments of head-and-neck tumors," *Physica Medica*, vol. 32, no. 1, pp. 52–58, Jan. 2016, doi: 10.1016/j.ejmp.2015.09.007.

[23] J. L. Bedford, I. M. Hanson, and V. N. Hansen, "Comparison of forward- and back-projection in vivo EPID dosimetry for VMAT treatment of the prostate," *Physics in Medicine & Biology*, vol. 63, no. 2, p. 025008, Jan. 2018, doi: 10.1088/1361-6560/AA9C60.

[24] M. Wendling, L. N. McDermott, A. Mans, J.-J. Sonke, M. van Herk, and B. J. Mijnheer, "A simple backprojection algorithm for 3D in vivo EPID dosimetry of IMRT treatments," *Medical Physics*, vol. 36, no. 7, pp. 3310–3321, Jul. 2009, doi: 10.1118/1.3148482.

[25] A. Mans *et al.*, "3D Dosimetric verification of volumetric-modulated arc therapy by portal dosimetry," *Radiotherapy and Oncology*, vol. 94, no. 2, pp. 181–187, Feb. 2010, doi: 10.1016/J.RADONC.2009.12.020.

[26] A. Mans *et al.,* "Catching errors with *in vivo* EPID dosimetry," *Medical Physics,* vol. *37*, no. 6(2), pp. 2638-2644, June 2010, doi: 10.1118/1.3397807.

[27] Sun Nuclear Corporation, "On the matter of forward and back projection for radiotherapy 3D dose reconstruction," Melbourne, FL, 2016. [Online]. Available: https://www.sunnuclear.com/uploads/documents/whitepapers/PF_ForwardBackward_012119.pdf

[28] T. R. McNutt, T. R. Mackie, P. Reckwerdt, N. Papanikolaou, and B. R. Paliwal, "Calculation of portal dose using the convolution/superposition method," *Medical Physics*, vol. 23, no. 4, pp. 527–535, Apr. 1996, doi: 10.1118/1.597810.

[29] P. Reich, E. Bezak, M. Mohammadi, and L. Fog, "The prediction of transmitted dose distributions using a 3D treatment planning system," *Australasian Physical & Engineering Sciences in Medicine*, vol. 29, 2006, doi: 10.3316/informit.456842596521713.

[30] M. Mohammadi, E. Bezak, and P. Reich, "Comparison of two-dimensional transmitted dose maps: evaluation of existing algorithms," *Australasian Physical & Engineering Sciences in Medicine*, vol. 29, 2006, doi: 10.3316/informit.451960758052064.

[31] K. Chytyk-Praznik, E. Vanuytven, T. A. Vanbeek, P. B. Greer, and B. M. C. McCurdy, "Model-based prediction of portal dose images during patient treatment," *Medical Physics*, vol. 40, no. 3, p. 031713, Mar. 2013, doi: 10.1118/1.4792203.

[32] J. L. Bedford, I. M. Hanson, and V. N. Hansen, "Portal dosimetry for VMAT using integrated images obtained during treatment," *Medical Physics*, vol. 41, no. 2, p. 021725, Feb. 2014, doi: 10.1118/1.4862515.

[33] R. Nilsson, "Development of an EPID image prediction algorithm for treatment verification in photon radiation therapy," 2016.

[34] S. B. Lim *et al.*, "Investigation of a Novel Decision Support Metric for Head and Neck Adaptive Radiation Therapy Using a Real-Time *In Vivo* Portal Dosimetry System," *Technology in Cancer Research & Treatment*, vol. 18, Jan. 2019, doi: 10.1177/1533033819873629.

[35] S. H. You *et al.*, "Is There a Clinical Benefit to Adaptive Planning During Tomotherapy in Patients with Head and Neck Cancer at Risk for Xerostomia?," *American Journal of Clinical Oncology*, vol. 35, no. 3, Jun. 2012, doi: 10.1097/COC.0b013e31820dc092.

[36] D. A. Low, "Gamma dose distribution evaluation tool," in *Journal of Physics: Conference Series*, Nov. 2010, vol. 250, no. 1, pp. 349–359. doi: 10.1088/1742-6596/250/1/012071.

[37] M. Sabet, F.W. Menk, and P.B. Greer, "Evaluation of an a-Si EPID in direct detection configuration as a water-equivalent dosimeter for transit dosimetry," *Medical Physics,* vol. 37, no. 4, pp. 1459-1467, Apr 2010, doi: 10.1118/1.3327456.

[38] C. Kirkby, and R. Sloboda, "Consequences of the spectral response of an a-Si EPID and implications for dosimetric calibration," *Medical Physics, vol.* 32, no. 8, p. 2649-2658, Aug 2005, doi: 10.1118/1.1984335.

[39] C. Yeboah, and S. Pistorius, "Monte Carlo studies of the exit photon spectra and dose to a metal/phosphor portal imaging screen," *Medical Physics, vol.* 27, no. 2, p. 330-339, Feb 2000, doi: 10.1118/1.598835.

[40] S.M.J.J.G. Nijsten *et al.,* "A global calibration model for *a*-Si EPIDs used for transit dosimetry," *Medical Physics,* vol. 34, no. 10, p. 3872-3884, Oct 2007, doi: 10.1118/1.2776244.